Project Title	Virtual Presence in Moving Objects through 5G
Project Acronym	PriMO-5G
Grant Agreement No	815191
Instrument	Research and Innovation Action
Topic	The PriMO-5G project addresses the area of “a) Focus on mmWave and super broadband services” in the call “EUK-02-2018: 5G” of the Horizon 2020 Work Program 2018-2020.
Start Date of Project	01.07.2018
Duration of Project	36 Months
Project Website	https://primo-5g.eu/

D3.1 - INTERMEDIATE REPORT ON ENHANCED 5G RADIO ACCESS TECHNOLOGIES

Work Package	WP3, mmWave radio technologies
Lead Author (Org)	Sang-Hyun Park (YU)
Contributing Author(s) (Org)	Sang-Hyun Park (YU), Gee-Yong Suk (YU), Soo-Min Kim (YU), Chan-Byoung Chae (YU), Yeosun Kyung(YU), Seunghwan Kim (YU), Sejin Seo (YU), Seong-Lyun Kim (YU), Sanghwa Lee (YU), Dong Ku Kim (YU), Kwanghoon Lee (YU), Jungseop Lee (YU), Kwang Soon Kim (YU), Dong-Yeon Ko (KAIST), Jae-Young Song (KAIST), Hyo-Seung Kang (KAIST), Kyung-Rak Son (KAIST), Hee-Kang Song (KAIST), Wan Choi (KAIST), Yonggu Lee (GIST), Euiseok Hwang (GIST), Jinho Choi (GIST), Vincent Kotzsch (NI), Achim Nahler (NI), Markus Ullmann (NI), Ursula Challita(Ericsson), Ki Won Sung (KTH), Woong-Hee Lee (KTH), Nicolas Malm (Aalto), Estifanos Menta (Aalto), Muhammad Sheikh (Aalto), Fayezeh Ghavimi (Aalto), Riku Jäntti (Aalto), Giuseppe Destino (KCL), Toktam Mahmoodi (KCL)
Due Date	30.04.2019, M10
Date	30.04.2019
Version	10.0 (Submitted)

Dissemination Level

The work described in this document has been conducted within the project PriMO-5G. This project has received funding from the European Union’s Horizon 2020 research and innovation programme under grant agreement No 815191. The project is also supported by the Institute for Information & communications Technology Promotion (IITP) grant funded by the Korea government (MSIT) (No.2018-0-00170, Virtual Presence in Moving Objects through 5G). The dissemination of results herein reflects only the author’s view, and the European Commission, IITP and MSIT are not responsible for any use that may be made of the information it contains.

X	PU: Public
	PP: Restricted to other programme participants (including the Commission)
	RE: Restricted to a group specified by the consortium (including the Commission)
	CO: Confidential, only for members of the consortium (including the Commission)

Disclaimer

PriMO-5G has received funding from the European Union's Horizon 2020 research and innovation programme under grant agreement No 815191. The project is also supported by the Institute for Information & communications Technology Promotion (IITP) grant funded by the Korea government (MSIT) (No.2018-0-00170, Virtual Presence in Moving Objects through 5G). The dissemination of results herein reflects only the author's view, and the European Commission, IITP and MSIT are not responsible for any use that may be made of the information it contains.

Table of Contents

List of Tables

List of Figures

Executive Summary

The title of Deliverable D3.1 is the *Intermediate report on enhanced 5G Radio Access Technology*. This deliverable is the first report from *WP3 mmWave radio technologies*, which aims to investigate important radio technology concepts for 5G NR. To that end, D3.1 includes research and development of new innovative transmission concepts using 5G mmWave frequencies. This intermediate report focuses on developing radio technologies that contribute meet operational, functional and technical requirements inspired by the PriMO-5G firefighting use cases (specified previously as part of work in *WP1 Scenarios, architecture, economic and regulatory analysis*).

Therefore, in addressing those use case requirements, this deliverable reports on initial research in PriMO-5G on enhanced 5G radio access technologies that could be classified into four thematic areas, namely: seamless connectivity, mobility management, interference management and security management. These thematic areas are described briefly below and are presented in more detail in this report in chapter 3, 4, 5 and 6, respectively.

- Seamless connectivity aims to offer seamless video streaming services to high-mobility drones in safety-of-life applications. This enables safe, remote inspection using augmented and virtual reality (AR/VR) technologies. Specifically, we focus on cell free architecture, initial access delay reduction, fast beam searching and channel estimation technologies.
- Mobility management for fast moving objects is essential to provide reliable immersive video services. Remote and real-time control for drone wireless networks can support reliability and low latency. Under limited communication resources, coordinated transmission and efficient resource allocation are required for high mobility vehicles, in which mobility caching and resource management are investigated to reach these goals.
- Interference management focuses on immersive video streaming at the uplink and downlink between the BSs and UEs, which are in most scenarios, drones. Furthermore, we investigate on the interference issue in multi-cell full duplex system and channel characteristics of mmWave full-duplex system.
- Security management focuses on unified approach for both compression and authentication in 5G systems to prevent impersonation attacks while sending the sampled signals at a high rate.

List of Acronyms

Acronym	Definition
5G	Fifth-Generation Mobile Network
3GPP	3rd Generation Partnership Project
ADC	Analog-to-Digital Converter
AFE	Analog Front-End
AGL	Above Ground-Level
AoA	Angle of Arrival
AR	Augmented Reality
AUC	Area Under the Curve
BS	Base Station
CE	Coverage Extension
CQI	Channel Quality Indicator
CR	Compression Ratio
CS	Compressive Sensing
CSI	Channel State Information
CSI-RS	Channel State Information Reference Signal
D2D	Device-to-Device
DAC	Digital-to-Analog Converter
DL	Downlink
DoA	Description of Action
DT	Decision Tree
eMBB	Enhanced Mobile Broadband
FAPI	Femto Application Platform Interface
FFT	Fast Fourier Transform
FPR	False Positive Rate
FR	Frequency Range
FTP	File Transfer Protocol
gNB	Next Generation Node B
HARQ	Hybrid Automatic-Repeat-Request
HO	Handover
HOF	Handover Failure
I/O	Input and Output
IoT	Internet of Things
ITU	International Telecommunication Union

Acronym	Definition
LFSRs	Linear Feedback Shift Registers
LOS	Line-of-Sight
FPGA	Field-Programmable Gate Array
LR	Logistic Regression
LTE	Long Term Evolution
MAC	Medium Access Control
MBSFN	Multicast-Broadcast Single-Frequency Network
MCL	Maximum Coupling Loss
MCS	Modulation and Coding Scheme
MEC	Multi-access Edge Computing
MIMO	Multiple Input Multiple Output
MTC	Machine type communications
OAI	Open Air Interface
OFDM	Orthogonal Frequency Division Multiplexing
OP-map	Opportunity map
PBCH	Physical Broadcast Channel
PDCCH	Physical Downlink Control Channel
PDSCH	Physical Downlink Shared Channel
PHY	Physical Layer
PL	Pathloss
PRS	Positioning Reference Signal
PUSCH	Physical Uplink Shared Channel
PXI	PCI eXtensions for Instrumentation
QAM	Quadrature Amplitude Modulation
QoS	Quality of Service
RAN	Radio Access Network
RLC	Radio Link Control
RLF	Radio Link Failure
RLM	Radio Link Monitoring
RMa	Rural-Macro
ROC	Receiver Operating Characteristic
RRC	Radio Resource Control
RSRP	Reference Signals Received Power
RSSI	Received Signal Strength Indicator

Acronym	Definition
RT	Real-Time
RU	Resource Utilization
RX	Receive
SCH	Synchronization Channel
SDR	Software Defined Radio
SFN	System Frame Number
SIM	Subscriber Identity Module
SINR	Signal-to-Interference-and-Noise Ratio
SIR	Signal-to-Interference Ratio
SISO	Single-Input and Single-Output
SRS	Sounding Reference Signal
SSB	Synchronization Signal Block
STD	Standard Deviation
TDD	Time Division Duplex
TPC	Transmit Power Control
TRP	Transmission-Reception Point
TTT	Time-to-Trigger
TX	Transmit
UAV	Unmanned Aerial Vehicle
UDN	Ultra-Dense Network
UE	User Equipment
UHD	USRP Hardware Driver
UL	Uplink
UMa	Urban-Macro
URLLC	Ultra-Reliable Low Latency Communication
USRP	Universal Software Radio Peripheral
V2X	Vehicle-To-Everything
VR	Virtual Reality

1 Introduction

1.1 Purpose and Scope

The title of Deliverable D3.1 is the *Intermediate report on enhanced 5G Radio Access Technology*. This deliverable is the first report from *WP3 mmWave radio technologies*, which aims to investigate important radio technology concepts for 5G NR. To that end, D3.1 includes research and development of new innovative transmission concepts using 5G mmWave frequencies. This intermediate report focuses on developing radio technologies that contribute meet operational, functional and technical requirements inspired by the PriMO-5G firefighting use cases (specified previously as part of work in *WP1 Scenarios, architecture, economic and regulatory analysis*). These PriMO-5G firefighting use cases create need to support high data-rates for immersive services (e.g. AR/VR) that enhance operational efficiency and safety of firefighting operations. From the radio access technologies perspective, this suggests, among other developments, the need for support of high data-rate mmWave connectivity to fast moving objects.

Therefore, in addressing the challenges presented by PriMO-5G use cases, this deliverable reports on initial research in PriMO-5G on enhanced 5G radio access technologies that could be classified into four thematic areas, namely: seamless connectivity, mobility management, interference management and security management.

1.2 PriMO-5G Use Case

The main PriMO-5G use case is about smart firefighting using mobile unmanned aerial vehicles (UAV). There are two main firefighting scenarios identified that will be investigated in the project specifically:

- Fires in rural areas with mobile infrastructure only partially available but less spectrum competition
- Fires in urban areas with mobile infrastructure available but competition in spectrum usage

Figure 1-1 shows a basic illustration of the network setup and involved entities.

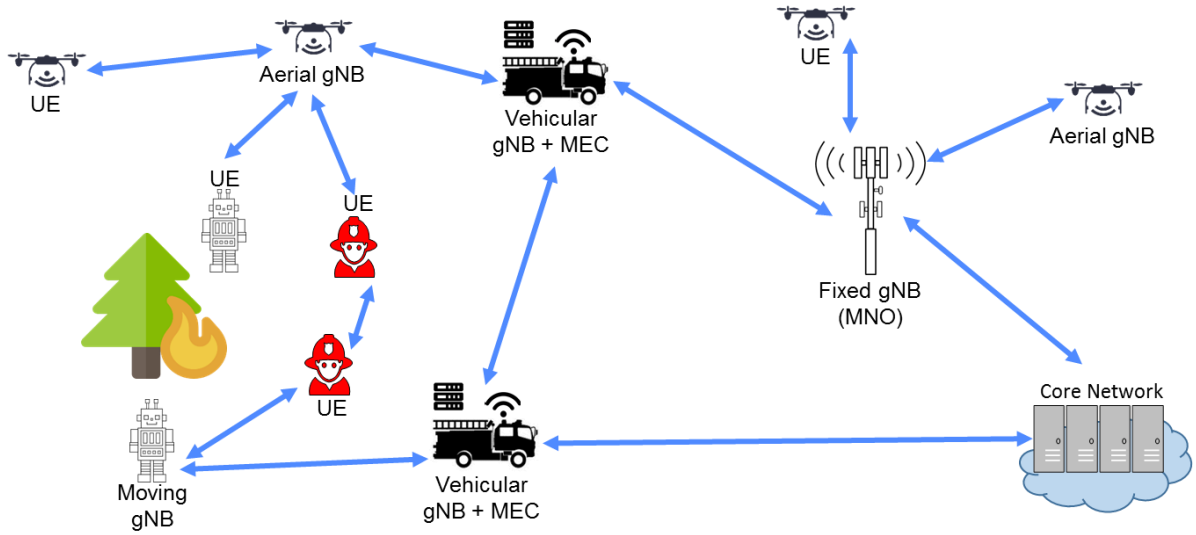

Figure 1-1 : Illustration of drone-assisted smart robot firefighting (from D1.1)

The firefighting use cases involves multiple mobile users that can be a firefighter person, a robot assistant as well as drones each with specific tasks. All the involved users are controlled by an incident commander, who will be located in a control centre and oversees that entire operation. For the rural (forest fire or wildfire) scenario, the control centre can be mobile, to be closer to the incident. The mobile control centre is equipped with a vehicular Next Generation Node B (gNB) and multi-access edge computing (MEC) infrastructure. In order to provide the required coverage for all mobile users due to natural features in rural areas the use of an aerial gNB can be beneficial as a line-of-sight connection to the mobile control centre could be assumed. Some mobile users can produce several hundreds of megabits per second of data, e.g. when streaming high-resolution video for immersive video applications. This requires a capable mobile backhaul between the control centre and the aerial gNB. For this purpose, a high bandwidth mmWave link is beneficial due to its capability of providing a high throughput and low latency data connection.

To overcome the high path loss at mmWave carrier frequencies and to cover larger distances between the control centre and the aerial gNB antenna arrays have to be used to exploit a high possible beam directivity. When using beam-tracking algorithms, the aerial gNB may move also dependent on the channel condition for the mobile access links. For the communication between the aerial gNB and the mobile users on the ground a line-of-sight link cannot necessarily be. Therefore, mmWave with its required beamforming may not be useful and the use of sub-6 GHz frequencies is more suitable which have better propagation properties but are limited in bandwidth. More details about the PriMO-5G use case scenario and the corresponding key performance indicators are described in Deliverable D1.1.

1.3 Structure of the document

This report is structured as follows. Section 2 discusses the first concept for mmWave links in terms of 5G Radio Access technology. After that, section 3, 4, 5 and 6 elaborate on four branches: seamless connectivity, mobility management, interference management and security management respectively. These four branches are composed of technical challenges that need to be accomplished for implementing PriMO-5G scenario. Section 3, 4, 5 and 6 present an overview of each item and describe each solution. Section 7 presents the conclusion and outlook for WP3.

1.4 Relationship to other project outcomes

This deliverable is inspired by the challenges derived from the use cases specificied PriMO-5G WP1. Specifically, deliverable *D1.1 PriMO-5G use case scenarios* includes use cases that considered the high-data rate radio connectivity to both fixed and moving objects in different firefighting contexts. Furthermore, D3.1 has strong links to WP4 research on the use of Artificial Intelligence (AI) and machine learning improved networking (including radio access networks) for PriMO-5G use cases. The early results for WP4 are outlined in more detail in *D4.1 Intermediate report on AI-assisted networking and edge computing*. Finally, deliverable 3.1 will provide input on the planned demonstration activities in *WP5 Testbed and demonstration*, which will include some of experimental implementation of the enhanced radio access technologies and concepts introduced in this document.

2 Initial Overview about mmWave Link

2.1 Motivation for mmWave Link

The mmWave link developed in this work package shall be used for work package 5 demonstrations. The mmWave link is realized with a mmWave transceiver system consisting of gNB and UE. Section 2.2 gives a short overview of the 3GPP 5G NR standard with focus on the physical layer aspects related to operating in mmWave frequency bands and how mmWave systems can help to address challenges of enhanced mobile broadband (eMBB) and low latency use cases. eMBB addresses the immersive video application, while drone control requires wireless low latency connections. Beam steering and beam tracking capabilities are key features for mmWave transceivers. Section 2.3 gives an introduction into this topic. The architecture of the mmWave transceiver system is covered in section 2.4.

2.2 3GPP 5G NR Standard Overview for Radio Access Network

In this section, an overview about the 5G NR standardization for the Radio Access Network (RAN) is given with focus on mmWave capabilities. A summary of the new 3GPP 5G NR standardization status as of March 2019 is shown in Figure 2-1 for frequencies above 6 GHz. In phase 1 (Release 15), important new features have already been included, such as a new frame structure and numerology [1] serving the needs for future anticipated services like eMBB and ultra-reliable low latency communication (URLLC). Furthermore, there are two frequency ranges (FR) specified:

- FR1: 450 MHz – 6000 MHz
- FR2: 24250 MHz – 52600 MHz

In the upper part of Figure 2-1, the discussed frequency bands in the different regions like Europe and Korea are shown. As one can observe, at the moment there is in particular consensus in using the frequency bands between 24.25-29.5 GHz. In October 2019 the next World Radiocommunication Conference organized by the ITU takes place with the goal to evaluate the studies of frequency bands in the range of 24.25-86 GHz (Agenda Item 1.13 [2]). Furthermore, in the 3GPP specification 38.104 [3] for FR2 the following bands have been already included for the operation in TDD:

Table 2-1: 5G NR FR2 Operating Bands [3]

NR *operating band*	Uplink (UL) and Downlink (DL) *operating band*
n257	26500 MHz – 29500 MHz
n258	24250 MHz – 27500 MHz
n260	37000 MHz – 40000 MHz
n261	27500 MHz – 28350 MHz

Therefore, first 5G NR mmWave deployments are already taking place in these frequency bands mainly to address eMBB use case. In particular band n257 will also be adopted by the PriMO-5G project demonstrator for showcasing the mmWave backhaul links.

The lower part of Figure 2-1 gives also an outlook on what can to be expected in the 3GPP 5G NR Rel-16. The RAN1 specifications for this release will be due end of 2019. 3GPP put emphasis on specification support for additional features such as side link, enhanced URLLC and improved beam management as well as on specification support for applications like V2X, NR in unlicensed, integrated access and backhaul and positioning.

In the 3GPP 38.913 technical report[1] , potential deployment scenarios are also provided. For example, in the urban macro scenario for FR2 inter site distances of approx. 500m are considered that has to be taken into account for the PriMO-5G firefighting use case.

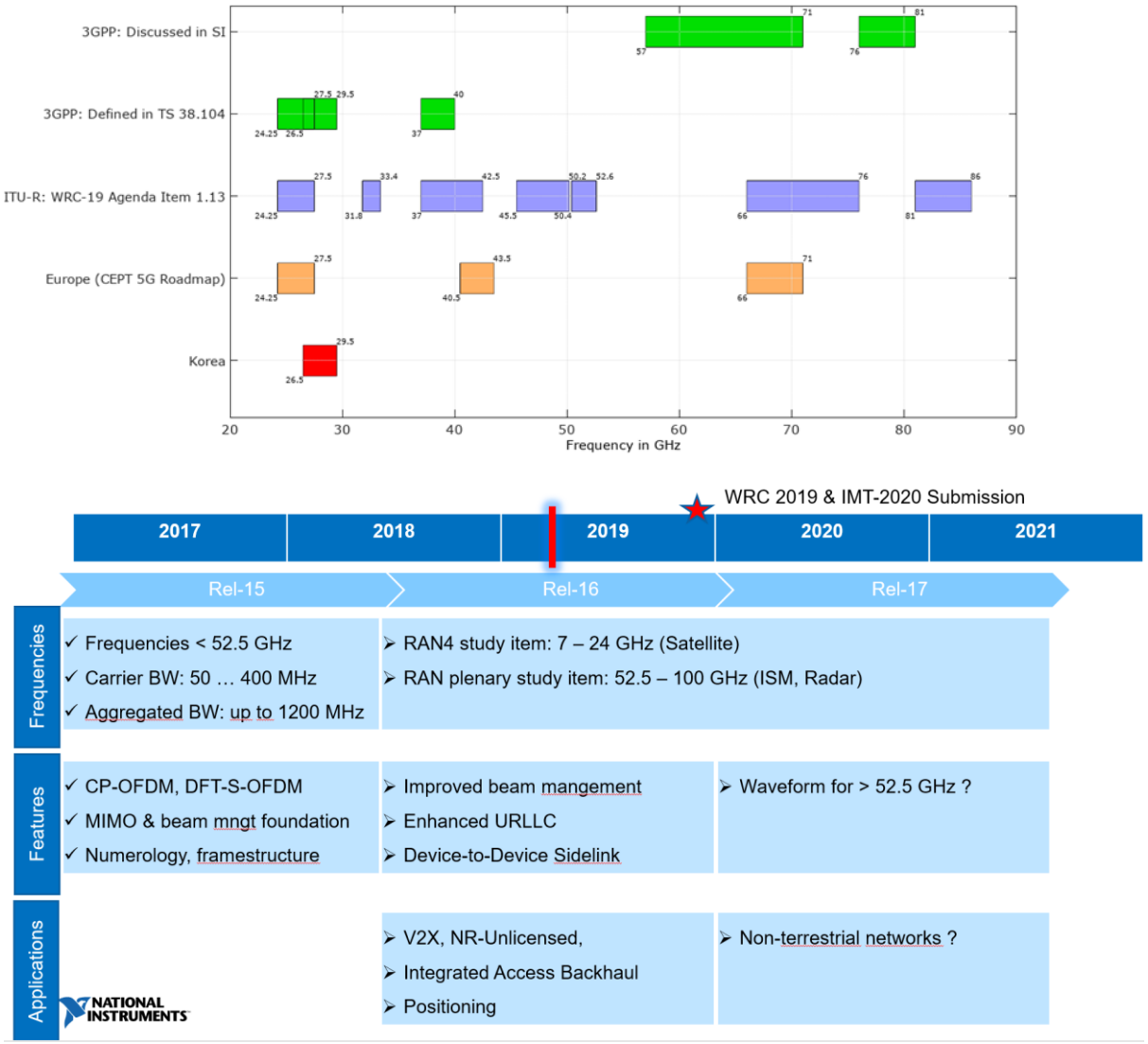

Figure 2-1: 3GPP 5G NR Standardization Status for frequencies above 6 GHz as of Mar 2019

As mentioned above, the 5G NR specification supports a variety of different numerologies and frame structures allowing the use in heterogeneous deployment scenarios. For FR2 the bandwidth modes given in the table below are possible.

[1] 3GPP TR 38.913, Study on Scenarios and Requirements for Next Generation Access Technologies, V15.0.0

Table 2-2: 5G NR Bandwidth Configurations [3]

μ	SCS (kHz)	50 MHz (61.44 Msps)	100 MHz (122.88 Msps)	200 MHz (245.76 Msps)	400 MHz (491.52 Msps)
		N_{SC}/ N_{FFT}	N_{SC}/ N_{FFT}	N_{SC}/ N_{FFT}	N_{SC}/ N_{FFT}
2	60	792/1024	1584/2048	3168/4096	N/A
3	120	384/512	792/1024	1584/2048	3168/4096

Depending on the FFT size for each bandwidth a certain subcarrier bandwidth with a corresponding symbol duration can be derived. As each slot consists of 14 symbols for normal cyclic prefix [5], for each subcarrier spacing a specific slot duration can be derived. As the subframe length is defined as 1 ms there is a varying number of slots within a subframe possible depending on the numerology index μ, which is directly related to the subcarrier spacing.

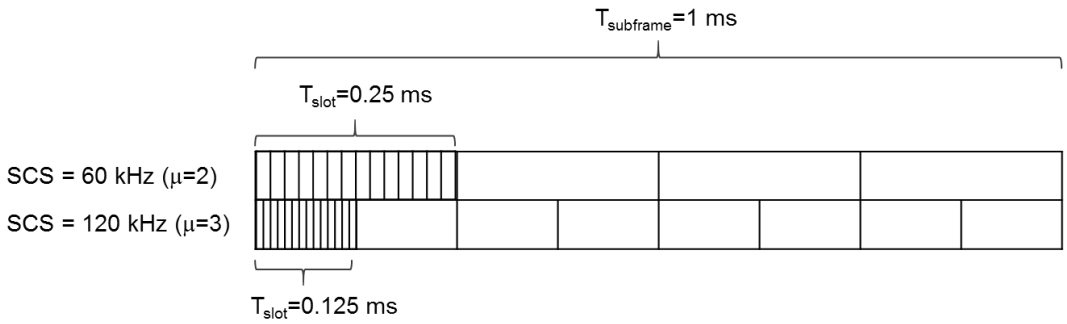

Figure 2-2: 3GPP 5G NR Slot Structure

For mmWave frequencies, operating bands provide larger chunks of contiguous bandwidth compared to operating bands for frequencies below 6 GHz. Considering this and the option to use carrier aggregation, overall achievable data rate could become much higher on operating bands above 6 GHz compared to operating bands below 6 GHz.

Depending on the values like number of subcarriers and the subcarrier spacing mode a maximum achievable throughput [6] can be calculated. For some of the configuration parameters typical throughput values are provided in the table below. The default parameters here are to transmit with 64-QAM modulation using one MIMO layer and one component carrier. If one of these values change this would impact the throughput value. For example, when increasing the number of component-carriers the throughput values would scale up accordingly.

Table 2-3: Maximum Throughput Values for Selected 5G NR Configurations

Parameters	Max throughput in Mbps
SCS=120 kHz, N_{SC}=3168	3232
SCS=120 kHz, N_{SC}=1584	1616
SCS=120 kHz, N_{SC}=792	808
SCS=120 kHz, N_{SC}=384	391

As shown in Figure 2-2, the higher the subcarrier spacing the shorter the slot length which directly impacts the achievable latency in the system. In 5G NR, also other methods for reducing latencies have

been introduced, namely the concept of mini-slot transmission, the concept of configurable HARQ response times and the concept of configurable duration between reception of an UL grant and the related PUSCH transmission. In order to flexibly use each slot for downlink and/or uplink transmission in the 3GPP 38.213 specification [7] various slot formats are defined supporting different TDD schemes, which are based on symbol-level TDD DL/UL configurations. Some selected slot formats are shown in the table below:

Table 2-4: Selected Slot Formats [7]

Format	OFDM symbol number in a slot													
	0	1	2	3	4	5	6	7	8	9	10	11	12	13
0	D	D	D	D	D	D	D	D	D	D	D	D	D	D
1	U	U	U	U	U	U	U	U	U	U	U	U	U	U
2	F	F	F	F	F	F	F	F	F	F	F	F	F	F
:														
19	D	F	F	F	F	F	F	F	F	F	F	F	F	U
20	D	D	F	F	F	F	F	F	F	F	F	F	F	U
21	D	D	D	F	F	F	F	F	F	F	F	F	F	U
22	D	F	F	F	F	F	F	F	F	F	F	F	U	U
23	D	D	F	F	F	F	F	F	F	F	F	F	U	U
24	D	D	D	F	F	F	F	F	F	F	F	F	U	U
:														
46	D	D	D	D	D	F	U	D	D	D	D	D	F	U
47	D	D	F	U	U	U	U	D	D	F	U	U	U	U
48	D	F	U	U	U	U	U	D	F	U	U	U	U	U
49	D	D	D	D	F	F	U	D	D	D	D	F	F	U
50	D	D	F	F	U	U	U	D	D	F	F	U	U	U
51	D	F	F	U	U	U	U	D	F	F	U	U	U	U
52	D	F	F	F	F	F	U	D	F	F	F	F	F	U
53	D	D	F	F	F	F	U	D	D	F	F	F	F	U
:														

Starting from downlink only or uplink only slots (format 0 and 1), self-contained subframes have been defined including downlink (D) and uplink OFDM symbols (U) that repeat every half-slot length. Furthermore, flexible OFDM symbols (F) have been also defined that can be used either for dynamic allocation (e.g. for mini-slots) or guard symbols but also for downlink or uplink symbols. For example, for slot format 53 there are two OFDM symbols with downlink data followed by 4 flexible symbols as well as one OFDM symbol containing uplink data. Given the large number of subcarriers in the 400 MHz bandwidth mode with a subcarrier bandwidth of 120 kHz in particular for mmWave frequency bands (FR2) this will allow to ultra-low latencies.

However, the achievable time between the reception of downlink data to the HARQ acknowledgment via uplink as well as the time between the reception of an uplink grant to the start of an uplink data

transmission depends also on the UE processing capabilities and the length of the PDSCH/PUSCH. A general overview about the HARQ features is given in 3GPP 38.912 specification[2]. A general notion is that the UE will indicate the gNB its minimum HARQ processing time during connection setup. Furthermore, in 3GPP 38.214 specification[9] the UE PDSCH as well as the UE PUSCH processing times are specified that are shown below specifically for the FR2 configurations:

Table 2-5: PDSCH and PUSCH Processing Times [9]

μ	PDSCH decoding time in OFDM symbols		PUSCH preparation time in OFDM symbols
	No Additional DM-RS Symbols configured	Additional DM-RS Symbols configured	
2	17	20	23
3	20	24	36

For example, for the PDSCH processing time using a subcarrier spacing of 120 kHz this leads to a latency of approx. 0.18 ms [10]. Furthermore, it has also been shown that with the 5G NR configuration options round trip latencies in the sub-ms region can be achieved [3].

2.3 Beam Management

While in the previous section an overview about the 5G NR standard with focus on the configuration options available for mmWave frequency bands is given, in this section the beam management shall be discussed as this is of particular importance for the PriMO-5G project.

In general, communication over mmWave mobile radio channel faces mainly the following challenges: First, it needs to be considered that the pathloss is proportional to the square of frequency. This is nothing mmWave-specific but shows clearly its impact on higher frequencies. Second, due to short wavelength, mobile radio channel becomes much more vulnerable to slight changes in the environment like motions of the UE, reflections or blockage.

The effect of higher pathloss for higher frequencies can be overcome by utilizing [12]

- Multiple TX antennas to direct energy and
- Multiple RX antennas to effectively increase aperture size.

To overcome these limitations, the task of beam management is to establish and maintain a beam pair consisting of transmit beam and receive beam as shown below in Figure 2-3.

[2] 3GPP TS 38.912, Study on New Radio (NR) access technology, V15.0.0

[3] Shehzad Ali Ashraf, Torsten Dudda, 5G for latency-critical IoT applications, https://www.ericsson.com/en/blog/2017/7/5g-for-latency-critical-iot-applications

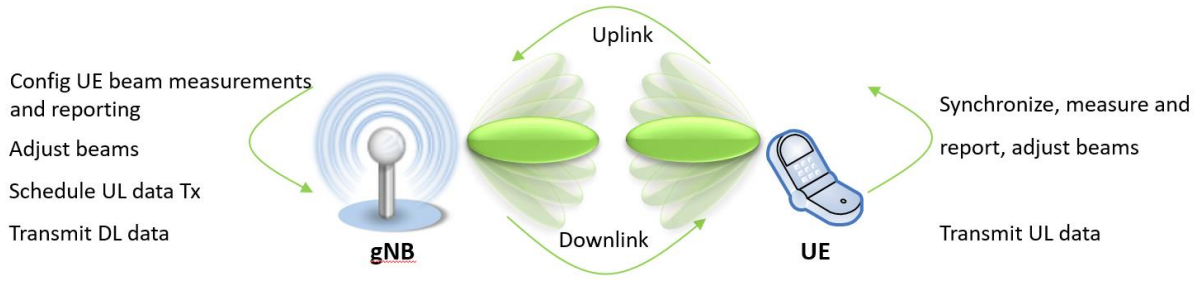

Figure 2-3: Beam management overview

According to the 5G NR specification the beam management consists of three main procedures [10]:

1. Initial beam establishment
2. Beam adjustment and
3. Beam recovery.

Beam management functionality spread to MAC and PHY layer, respectively. Beam management control is a functionality of the MAC layer whereas the PHY layer needs to have all the necessary functions to cope with beam management procedures. During beam management, the gNB has full control over UE. For the different procedures mentioned above, the gNB configures measurements and measurement reporting schemes for UE and based on measurement reports sent from the UE, the gNB does beam-management-related decisions.

It is worth to note that 3GPP standardization body specified only a framework for measurements and measurement reporting. This beam management framework allows different suppliers to come up with different implementations that might address the beam management related challenges in different manners.

Beam-management-related challenges are the following topics but are not limited to these topics listed below:

- Initial beam establishment: Find not necessarily best beam but as quick as possible the beam that is good enough for the targeted service.
- Beam adjustment: Avoid interruption of service during beam adjustment (beam change)
- Beam recovery: Keep service interruption as short as possible

Initial beam establishment includes procedures and functions by which a beam pair is initially established for downlink and uplink. Initial beam establishment is part of the initial access procedure and mainly consists of beam sweeping functionality carried out at gNB and UE. Beam sweeping for initial beam establishment is based on Synchronization Signal Block (SSB).

Device mobility and/or blocking effects might raise the need for re-selection of beam directions. Beam adjustment functionality consists of means for re-evaluation and possible re-selection of beam directions either on transmitter- and/or receiver-side. Downlink beam adjustment is based again either on Channel State Information Reference Signal (CSI-RS) or SSB, whereas uplink beam adjustment is based on Sounding Reference Signal (SRS).

Sometimes, beam adjustment is not able to cope with rapid-changing environment conditions that degrade significantly the quality of established beam pairs. This requires beam recovery which consists of four steps:

- *Beam failure detection*: Beam failure is detected by the UE, based on - measurements of a periodic CSI-RS/SSB. Those CSI-RS/SSB-based measurements are used to calculate link quality. The link quality decrease below a threshold is considered as a beam-failure instance

and beam failure is declared once the number of consecutive beam-failure instances surpassed a configured threshold.

- *Beam candidate identification*: UE receives a set of reference signals within a set of corresponding downlink candidate beams. L1-RSRP is measured on those reference signals. If it exceeds a configurable threshold, the corresponding beam is assumed to be able to restore the connectivity.
- *Beam recovery request*: After beam failure detection and beam candidate detection, UE is ready to inform the network about the beam failure which may also include information about new found suitable beam pair. The beam failure recovery request is essentially a contention-free random access procedure having the same principles of association of reference signals with candidate beams.
- *Network response to the recovery request*.

2.4 PriMO-5G mmWave Radio Transceiver Architecture

In this section an overview about the planned PriMO-5G mmWave transceiver architecture is given that is part of the experimentation system to demonstrate the main PriMO-5G use case discussed above. A general overview about the system architecture is given in Figure 2-4.

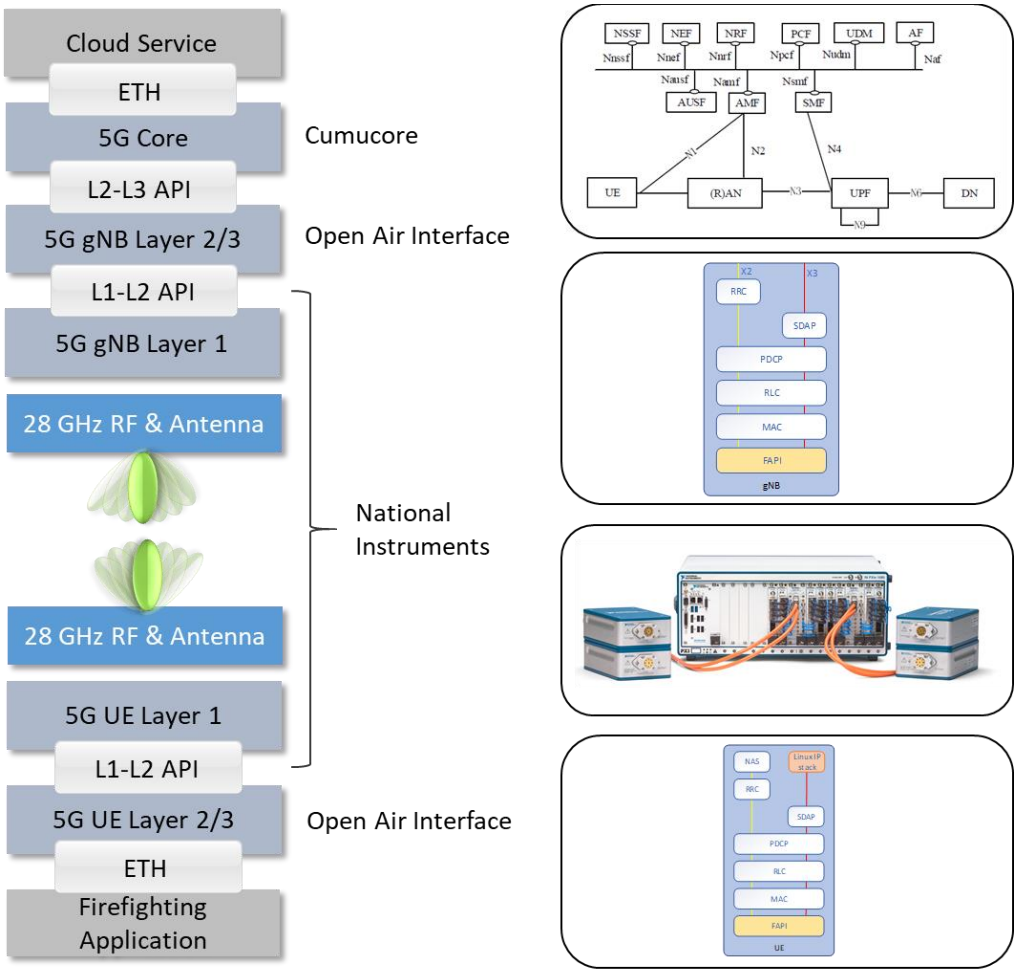

Figure 2-4: PriMO-5G mmWave Link Architecture for WP5 demonstrations

The PriMO-5G mmWave link will be based on the NI 5G NR mmWave node including the radio frequency and antenna part as well as a Layer 1 implementation following the 5G NR standard that allows for high throughput and low latency. An overview about the NI SDR Platform is given on their website [13]. In the project a PXI based system is used for mmWave link. The node consists of FPGA processing modules interconnected in a PXI chassis via a high-performance backplane. In addition to the FPGA modules, an RT controller (CPU) is integrated where an NI Linux RT system is running, which is controlling the PXI system and is running PHY related procedures. A C/C++ based higher layer protocol stack can run on the RT controller or on a separate PC. To connect the NI mmWave platform to external devices a 10Gbit Ethernet interface is available to feed in and out data on high data rates. Furthermore, the NI mmWave system supports DACs and ADCs that can capture up to 2 GHz channel bandwidth [14]. Furthermore, RF and antenna components are available for the required frequency bands at 28 GHz. The NI PXI-based system scales from single input, single output (SISO) to multiple input, multiple output (MIMO) configurations with a fully integrated design flow based on the LabVIEW programming environment.

The NI 5G NR Layer 1 implementation is planned to be connected to the Open Air Interface (OAI) 5G stack [15] specifically to the Layer 2/3 modules. The Open Air Interface platform is a C-based software protocol stack that runs entirely on Linux based CPU systems. For the radio frequency part among others the NI/Ettus USRP platform [16] is supported making use of the UHD driver.

The OAI 4G stack is Release 8.6 compliant and includes also a subset of Release 10 features. A complete overview about the OAI 4G stack features is given on the organization website [17]. A system diagram is shown in Figure 2-5.

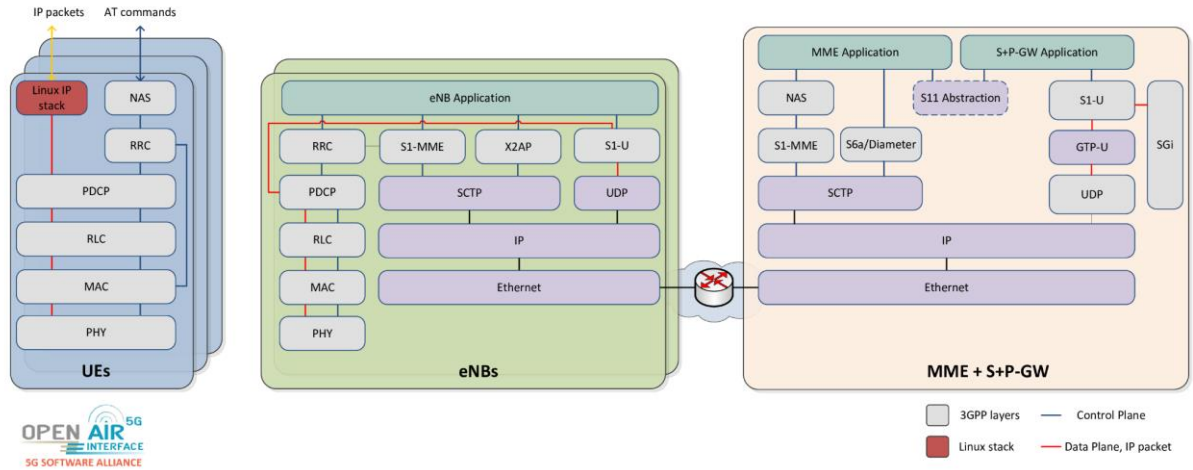

Figure 2-5: Open Air Interface System Diagram [17]

One main feature of the OAI platform is the availability of complete implementation of the core network, the base station as well as the user terminal. Each component can run separately on an independent node. The development of the OAI 5G stack in currently ongoing and it is expected that the overall system is comparable to the OAI 4G system. In order to allow very high throughput and very low latency values using the OAI stack the NI FPGA based PHY implementation would be beneficial which is targeted in the PriMO-5G mmWave transceiver.

As interface between the OAI Layer 2 as well as the NI Layer 1 the Femto Application Platform Interface (FAPI) is selected that represents a specification of procedures and messages for the MAC-PHY split

of base station. A FAPI specification is already available for 4G/LTE and is planned to have also a 5G version[4].

One main feature of the PriMO-5G testbed is the availability of the Cumucore 5G core network as central element to connect the 5G mmWave link with the existing testbed infrastructure as well as the EU-Korea testbed interworking. Therefore, the OAI core network implementation is not used in the project context. As interface between the OAI Layer 2 stack and the Cumucore 5G core network standard N1, N2 and N3 interfaces as described in the 3GPP 23.501 specification [19] are planned to be used.

[4] Industry can take its cue from SCF as it seeks to define the open RAN [18]

3 Seamless Connectivity

PriMO-5G aims to offer seamless video streaming services to high-mobility drones in safety-of-life applications. This enables safe, remote inspection using AR/VR technologies. Autonomous vehicles can provide capabilities complementary to those of human personnel. Accomplishing this level of immersion requires seamless connectivity for the drones. The traditional/legacy connectivity approach is insufficient for the targeted use cases due to high signalling overhead, especially when there are high-speed users traversing small cells. This may result in slow and unreliable handover procedures. Moreover, the legacy network deployment options primarily cater to ground-based users, and this option does not suit the targeted use-case as the drones are flying at high altitude with elevation as a new dimension to consider for aerial UE mobility. Legacy network design does not scale well to enable efficient 3D position and mobility management of flying drones at high altitude and high velocity.

Achieving the project's vision will be accomplished using two complementary approaches: 1) optimizing and enhancing 5G NR and 2) beyond 5G cell-free architectures. 5G NR introduces the concept of beams to the air interface. Beamforming provides enhanced coverage by directing transmission power in the most useful directions. This, however, presents a challenge in terms of initial access and mobility. The network must be able to decide accurately and rapidly with which beams to serve each UE in order to avoid interruptions and provide seamless connectivity.

One approach is to exploit network density to provide more beam candidates, more quickly. Instead of attempting to find the best beam that one BS can provide, the network will consider all beams of BSs within range and select the first acceptable one. This network-oriented approach enables a reduction in access time by trading off optimality of selection for speed of acquisition.

Another approach to provide seamless connectivity is to exploit location information of drones from the exchanged uplink pilots. Localization of drones is carried out utilizing a beam-based positioning approach in 5G NR technology. In this approach, positioning can be done at a single base-station (gNB) with fixed beams and UAV with or without multiple antennas.

In parallel, the PriMO-5G consortium is also investigating an alternative network design known as a cell-free user centric ultra-dense network [20]-[22]. The aim is to further obviate the need for beam searching by continuously tracking UEs' positions. Provision of seamless service to aerial UEs will require the development of elevation-aware positioning, channel estimation techniques adapted for flying UEs and appropriate interference management techniques for uplink beacons.

The following sections present in detail the various technology components contributed by partners. These components provide the building blocks for a network offering the envisioned seamless connectivity.

3.1 Reducing Initial Access Delay in Dense mmWave Networks

This section is concerned with the initial access phase of mmWave communications. Particularly, we consider an environment with densely deployed mmWave BSs, and we focus on how to exploit the dense network deployment in reducing the initial access delay. This section is based on [23]-[25]. Interested readers are directed to the references for further details.

It is well known that mmWave bands are subject to high propagation and penetration loss. To compensate for the loss, wireless systems in mmWave usually rely on directional transmissions with antenna array, i.e. beamforming, at both the transmitter and the receiver sides. Despite the advantages of beamforming in the coverage extension and interference management, the use of narrow beam causes complicated initial cell search and random access procedure. Unlike conventional cellular systems which employ omnidirectional or sectored antenna for initial access, mmWave systems may need to apply directional transmission and reception even at the cell search and random access phase, which would induce significant initial access delay.

The most popular cell search methods in the mmWave communication can be divided into two categories: exhaustive search and iterative search [26]. Exhaustive search refers to the sweeping of

the beam in all directions at both the transmitter and the receiver so that the transceiver pair can find the best direction for transmitting and receiving. Although it is a guaranteed way of finding the best beam direction, it requires substantial time for the initial cell search. In iterative search, also known as hierarchical search, a coarse-grained sector matching is followed by a refined narrower beam sweeping within the direction identified at the first search. Such hierarchical or iterative refinement reduces the search delay, but it may suffer from a lack of coverage during the coarse-grained search phase. Figure 3-1 illustrates the two cell search methods.

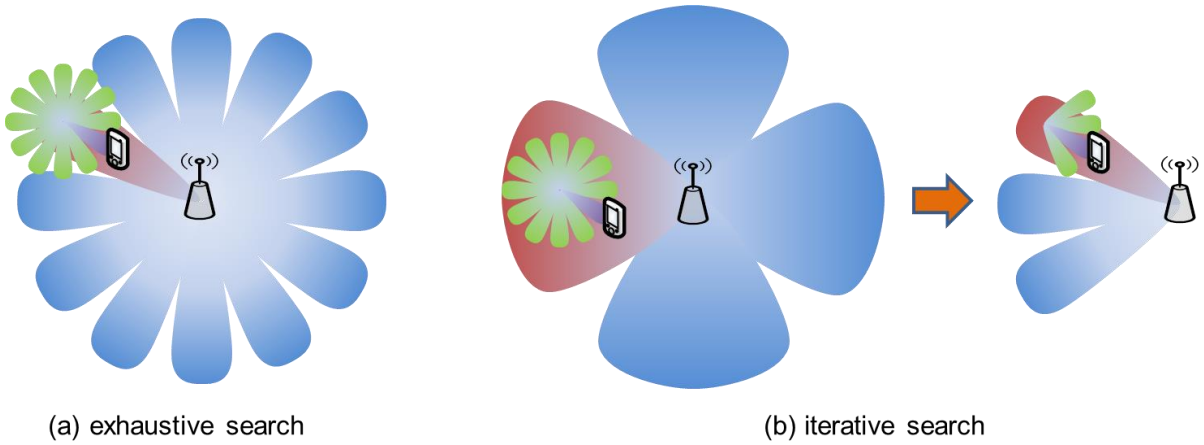

Figure 3-1: An illustration of exhaustive search and iterative (hierarchical) search

We notice that the aforementioned cell search methods basically aim to find the *best* (or strongest) BS among the surrounding BSs. In a dense network, it is likely that several BSs with *acceptable* link quality exist, and thus it would be beneficial to associate with one of them rather than to keep searching the best BS. It is particularly the case when the traffic is short and bursty such that the data transmission ends quickly after the connection is established. Therefore, our idea is **to find the acceptable BS and stop cell search to reduce the initial access delay** when BSs are densely deployed.

To demonstrate the effectiveness of our idea, we consider a simple *random beamforming* for the cell search. Note that we do not claim the random beamforming is an elaborated cell search method. Rather, our objective is to show that our idea can be implemented by such a simple scheme and yet with reasonably good performance.

Let us explain the random-beamforming-based initial access in detail. Consider a dense deployment of homogeneous BSs. Then, UEs are also assumed to be of a same type. Our working assumption is that both BS and UE employ beamforming. Let N_{BS} be the number of beams in a BS required for spanning 360 degrees, and let N_{UE} be that of a UE. We define a scan cycle as the time period that each BS sends N_{BS} cell-search pilots. We say that BSs employ random beamforming in the sense that each BS independently selects a random beam sweeping pattern. For simplicity, we assume that each UE fixes its antenna to a random direction during a scan cycle. UE moves to another random direction in the next scan cycle.

The random beamforming is not different from the exhaustive search if the cell search continues until N_{UE} scan cycles, i.e. all the $N_{BS}N_{UE}$ possible directions are examined. The major difference of the random beamforming is that only k scan cycles are engaged during the cell search ($k < N_{UE}$). This allows UEs to select a BS of an acceptable link quality instead of exploring all the combinations. One can intuitively figure out that denser deployment of BSs will reduce k required for finding an acceptable BS. Figure 3-2 depicts how the random beamforming operates.

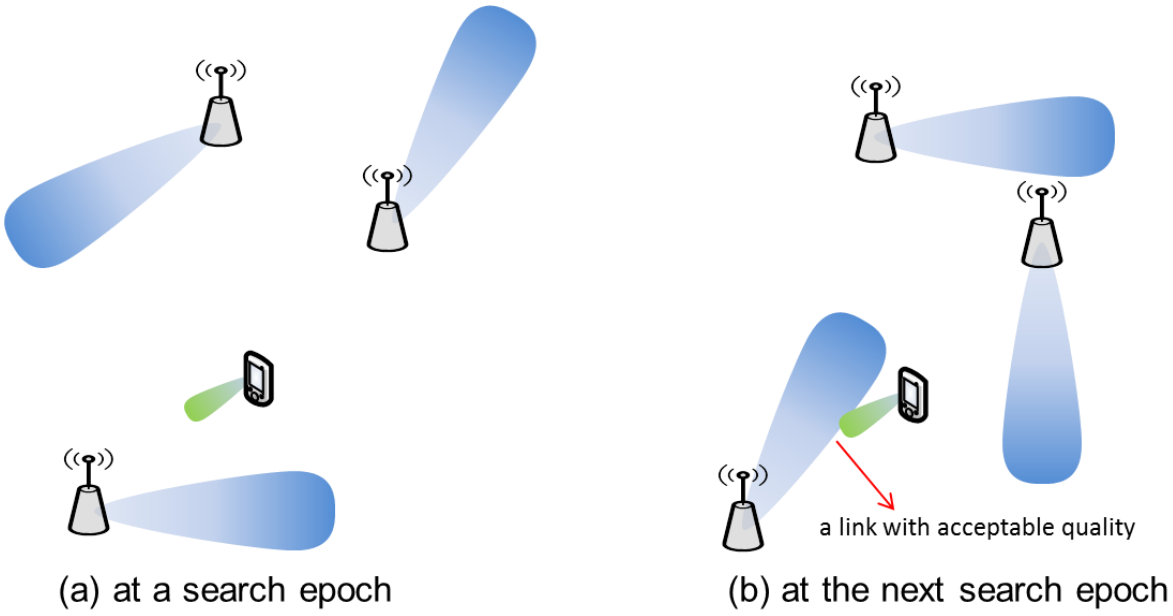

Figure 3-2: Cell search based on random beamforming

A thorough performance analysis has been conducted in [24] by employing the tool of stochastic geometry and Monte Carlo simulations. Key results are summarized below.

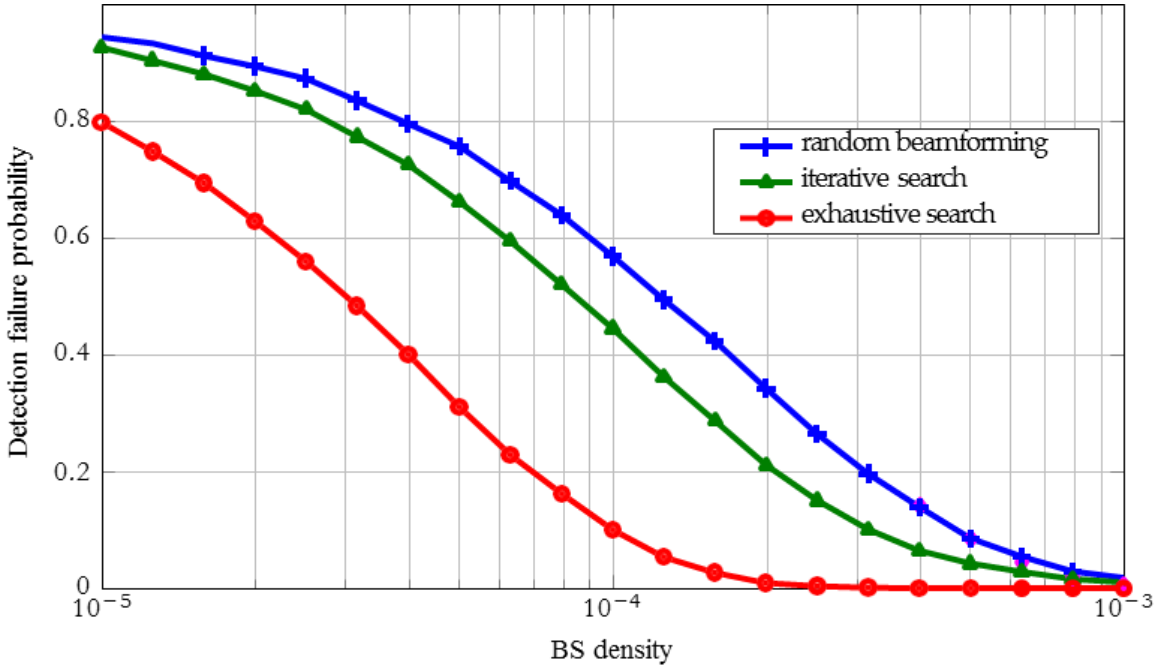

Figure 3-3: Detection failure probability of cell search schemes as a function of BS density

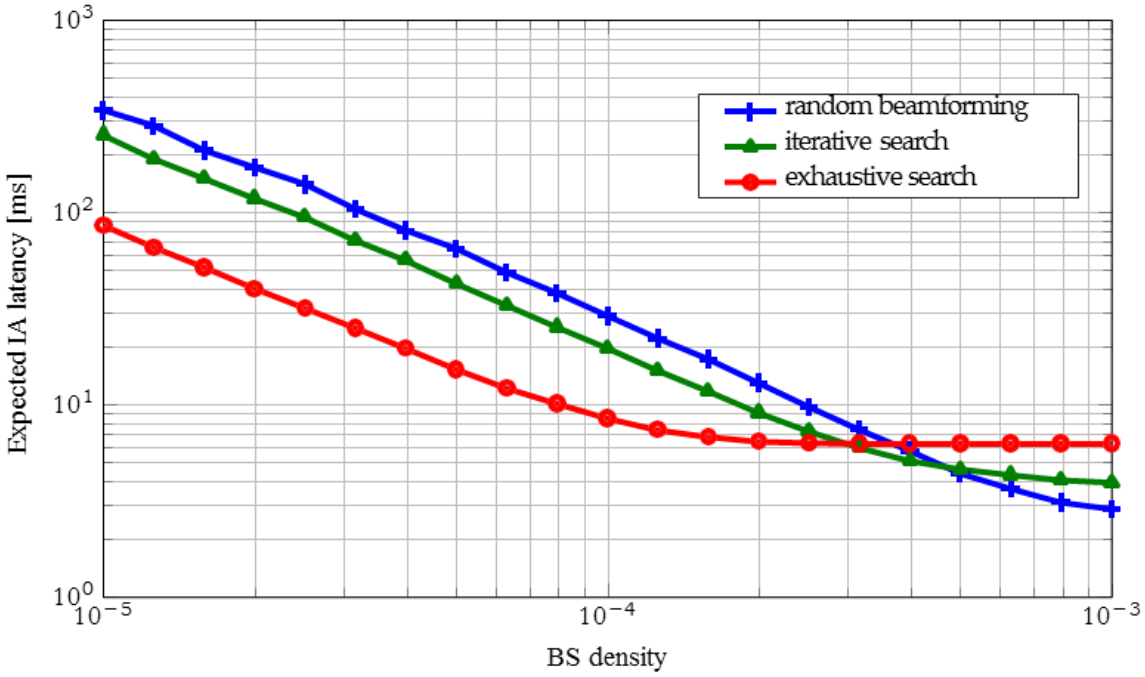

Figure 3-4: Initial access latency of cell search schemes as a function of BS density

Figure 3-3 and Figure 3-4 show the detection failure probability and the expected initial access latency, respectively as a function of the BS density. The unit of BS density is the number of BSs per m^2. Detection probability is defined as a probability that the UE is not detected by any BS within the scan cycle. It is obvious that the exhaustive search always gives the lowest detection failure. However, the difference in the detection performance diminishes quickly as the BS density increases. On the other hand, initial access latency has a cross point where the random beamforming starts to perform better than the other two. As expected, it happens in a dense deployment regime.

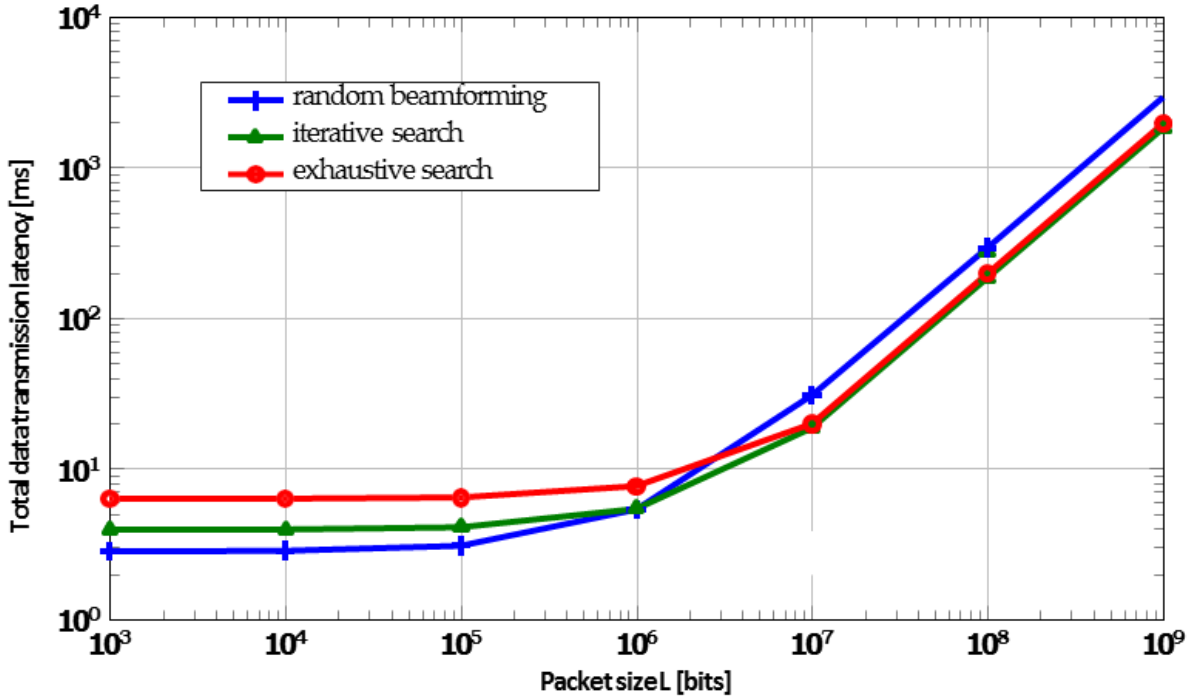

Figure 3-5: Total packet transmission latency as a function of packet size

Selecting an acceptable BS in terms of RSRP certainly reduces the initial access delay, but it may result in lower data rate compared to the association with the strongest BS. Therefore, it is expected that the random beamforming would work better for shorter packets, which would be particularly useful when a standalone mmWave system is used. The conjecture is numerically corroborated in Figure 3-5, where the impact of packet size on the total data transmission latency is illustrated. Here, the total latency is defined as the sum of initial access latency and the transmission time for one packet. The random beamforming achieves the lowest total data transmission latency when a packet is small. However, it becomes even worst for the large packet size. Note that the beam refinement is not considered in this experiment.

As a final remark, we emphasize that the random beamforming is a simple cell search scheme demonstrating the effectiveness of ***network-oriented thinking*** in the initial access of mmWave systems. Further enhancement of the network-oriented initial access remains as an interesting research area.

3.2 Beam-based Positioning

In this Section we focus on the problem of UAV positioning with NR technology. Figure 3-6 shows the basic system model, which consists of a single base-station (gNB) with beamforming capability, LOS channel condition and a UAV with or without multiple antennas. The transmission scheme is based on OFDM and positioning is performed at the gNB based on the reception of up-link reference signal.

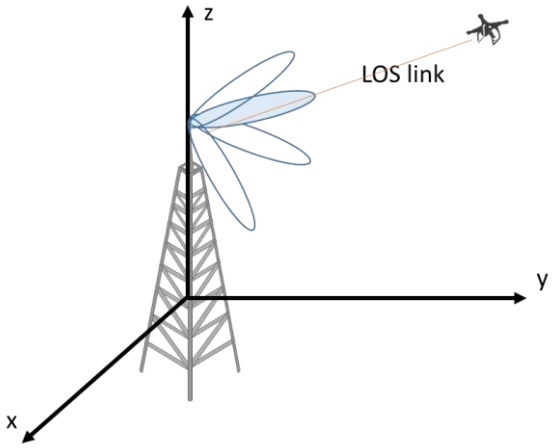

Figure 3-6: UAV positioning

The technique proposed in this work is hereafter referred to as *Direct positioning* and it is developed with the aim of eliminating bearing and ranging measurements. In other words, UE location estimates are obtained directly from pilot symbol processing (similarly to channel estimation).

The fundamental relationship between signal and position is given by

$$\mathbf{y}(t) = \sqrt{P}\mathbf{W}^H\mathbf{H}(a,\mathbf{x})x_p(t-\tau(\mathbf{x})) + \mathbf{W}^H\mathbf{n}(t) \quad (1)$$

where **x** is the coordinate vector of the UE's location[5], **W** is the receive beamforming matrix with M beamforming vectors, **H**() is the complex-channel matrix parameterized by the location, τ() is a function returning the path-delay, P is the transmit power and **n**(t) is a vector modelling the noise at each antenna element.

Rewriting equation (1) in the frequency domain, two key aspects can be noted. First, location parameter appears only in the received signal phase, which includes a beamforming and subcarrier rotation. Also, and more importantly, the signal model shows a sparse Kronecker structure in frequency-spatial domain. In other word, there is a form of common sparse model across frequency and beamspace domain.

More specifically, for n-th subcarrier, the frequency model of the received signal can be written as

$$\mathbf{y}_n = \mathbf{g}_r(\mathbf{x})\rho_1(n,\mathbf{x},a)x_{p,q} + \tilde{\mathbf{n}}_n \quad (2)$$

where $\rho_1(\mathrm{n},\mathbf{x},\mathrm{a})\mathrm{x}_{\mathrm{p,q}}$ is a complex coefficient including subcarrier phase-delay, channel coefficient and pilot symbol and $\boldsymbol{g}_r(\boldsymbol{x})$ is the position signature in the beamspace domain, which is common across subcarriers. Thus, by writing $\boldsymbol{g}_r(\boldsymbol{x})$ as the product of a frame-matrix and a sparse vector, we obtain a sparse model equation (2), with a dominant component corresponding to a sector including the location **x.** This operation can be also understood as a linear match-filter, which yields a sparse signal. Figure 3-7 shows the spatial sector detected by the filter.

[5] The location of UE is relative to the gNB position, which is defined as the origin.

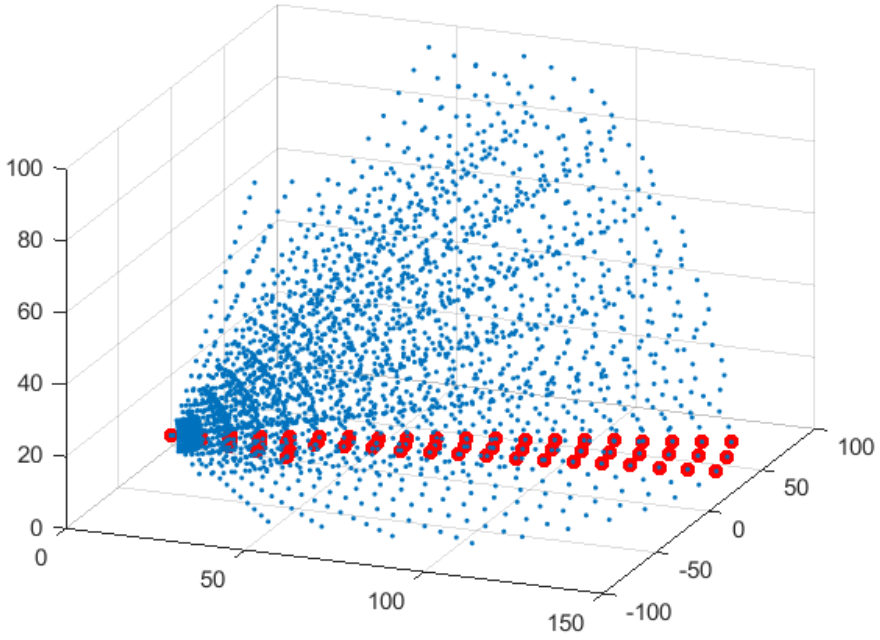

Figure 3-7: Spatial filtering: blue circle indicates the candidate particle and the red ones are those selected by the filter.

On the other hand, the received signal by the m-th beamformer (signal combined by the m-th beamforming vector) contains a frequency signature of **x.** This can be noted by rewriting equation (1) as

$$\mathbf{y}_m = \mathbf{g}_d(\mathbf{x})\rho_2(m, \mathbf{x}, a) \odot \mathbf{x}_p + \tilde{\mathbf{n}}_m \quad (3)$$

where $\rho_2(\mathrm{m}, \mathbf{x}, \mathrm{a}) \odot \mathbf{x}_\mathrm{p}$ is a complex coefficient including the m-th beamformer phase, channel coefficient and pilot symbols and $\boldsymbol{g}_d(\boldsymbol{x})$ is the position frequency-signature, which is common across beamformers.

As before, we consider $\boldsymbol{g}_d(\boldsymbol{x})$ as a linear combination of a location-based frame matrix and a sparse vector. which detect a partial sphere including the location **x.** Figure 3-8 exemplifies this decomposition

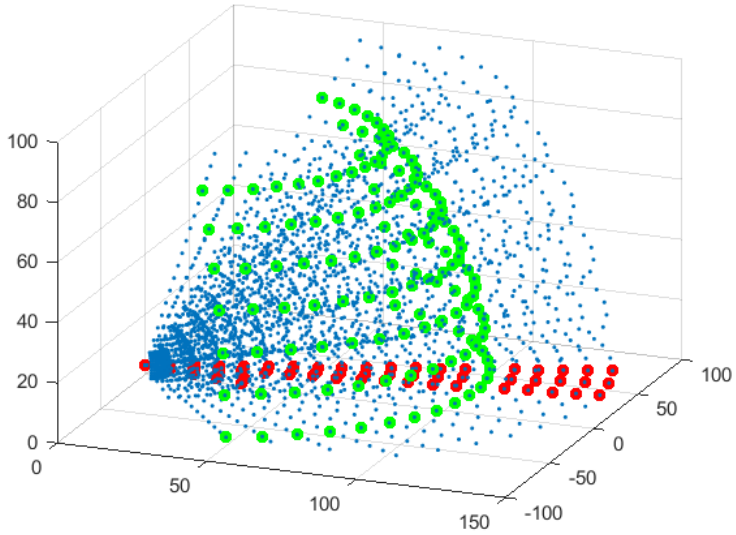

Figure 3-8: Overlap of sector and distance filter: blue circle indicates the candidate particle, the red and the green ones are those selected by the spatial and distance filters, respectively.

In light of the above results, the proposed positioning algorithm can be developed as an iterative process where sector and distance filters are alternated and adapted.

Figure 3-9 shows the flow-chart as well as an illustration of the sector-angle refinement.

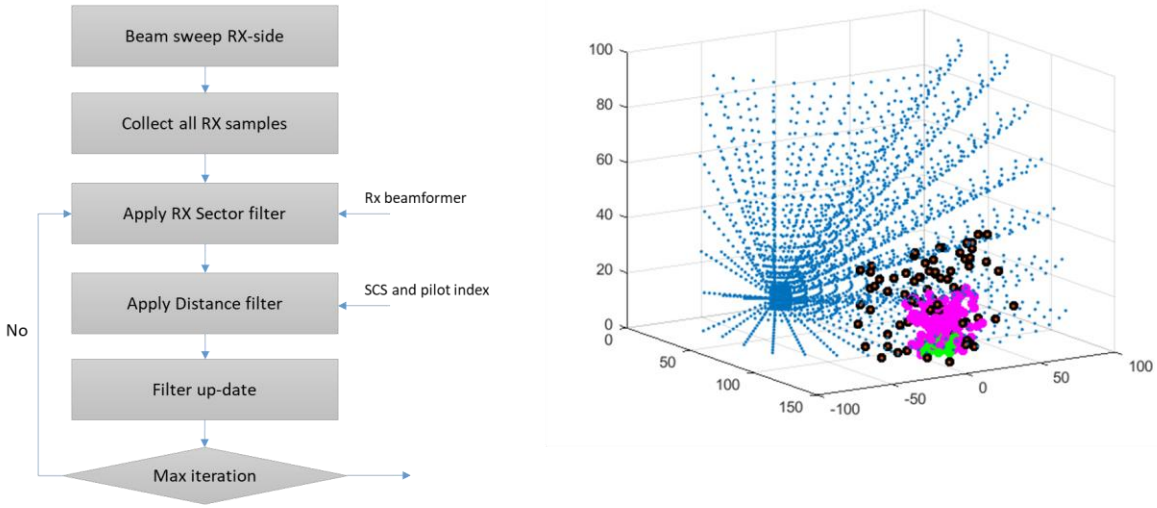

Figure 3-9: Positioning algorithm

In what follows we evaluate the proposed method for a typical outdoor LOS scenario. Relevant simulation details are provided in Table 3-1. We use the UMi street-canyon LOS channel model in [27] to compute the path-loss as a function of the distance.

Table 3-1: Simulation details for positioning testing

Parameter	Value
FFT	2048
SCS	60 KHz
Pilot	Combo 4, 128
Carrier	30 GHz
Path-loss model	ABG model ()
gNB height	3 m
UE height	20 m
UE-gNB distance	(3, 120) m
UE-gNB (az x el)	(-45, 45) x (0, 45)deg
gNB antenna	URA 8x8
gNB Sector	(-180,180)x(-90,90)
gNB Element gain	0 dBi
gNB RF codebook	2D-DFT, sequential
gNB RX noise	5 dB
UE antenna	single
Element gain	0 dBi
UE TX power	-10 dBm

The performance of Direct positioning algorithm is evaluated in terms of the 3D position error. More specifically, we are interested in the characterization of the cumulative distribution function of the error as well as in the average error as function of the SNR As benchmark, we utilize the position error bound [28].

In Figure 3-10 and Figure 3-11, both results are shown and, it is readily noted, that the proposed method can closely achieve the theoretical bound. More quantitively, the expected localization error is about 40 cm with a 95-percentile of 127 cm.

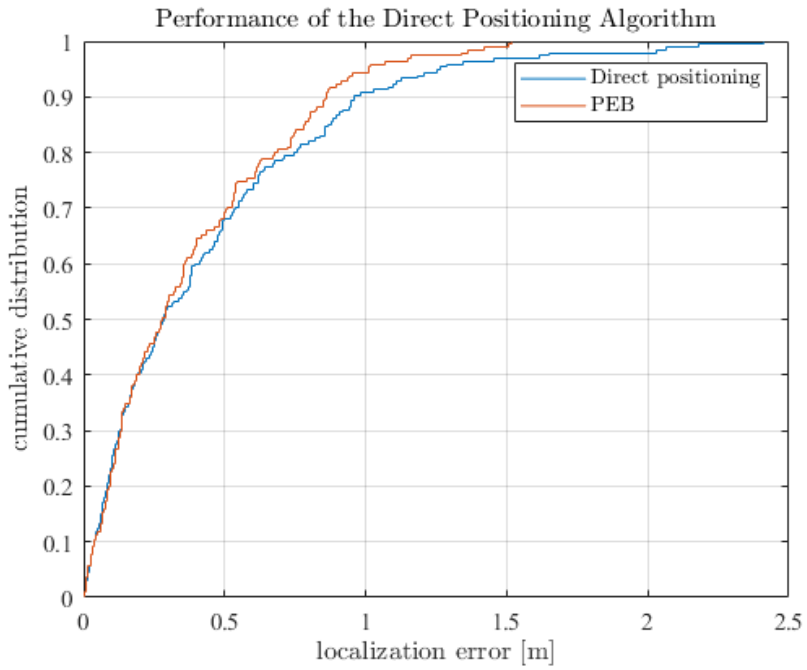

Figure 3-10: CDF of the 3D localization error in LOS channel conditions

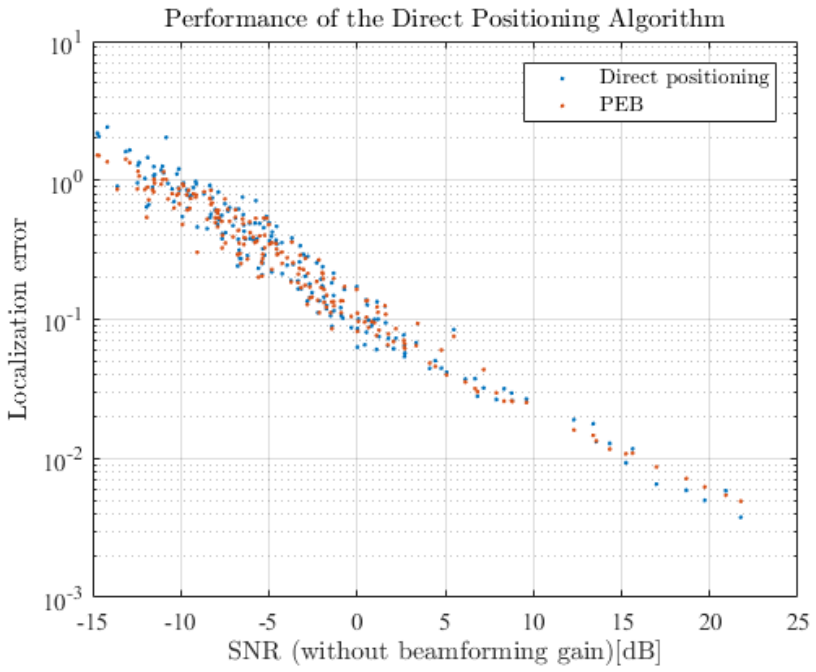

Figure 3-11: 3D positioning error as a function of the SNR

3.3 Cell-free Architecture

3.3.1 Network Densification and Handover Management

Fifth generation (5G) cellular systems aim to provide 1000 times increased system capacity, about 10 times decrease in the end-to-end latency, and always-on connectivity for users with varying mobility. Cellular systems have coped with exponentially increased traffic demand by decreasing cell sizes. Network densification is a promising solution in order to provide the possibility for cellular operators to cope with the increasing traffic demands. It is expected that cellular operators will cater for a big chunk of requirements for 5G cellular systems through network densification.

In 5G ultra-dense networks (UDN), intra-cell distances around tens of meters are expected. As cell sizes have been shrinking, the number of handovers (HOs) within the same area has been increasing correspondingly. Figure 3-12: The number of handovers in different mobile network generations vs cell size normalized to 1 km^2 area. Smaller cell sizes increase the number of handovers UEs must perform per distance unit travelled. illustrates how the number of HOs per unit area has increased over generations of cellular networks. As a user is moving in the network, the number of cell border crossings is a function of the cell radius. In Figure 3-12: The number of handovers in different mobile network generations vs cell size normalized to 1 km^2 area. Smaller cell sizes increase the number of handovers UEs must perform per distance unit travelled., a classical hexagonal site layout has been used, with each site divided into three sectors. Users are moving along straight lines in the network, and the number of handovers are normalized to 1 km^2 area. HO procedures have developed according to the service requirements of cellular generations. 5G networks are also expected to have a thousand times more users than the previous network generations. One can predict that in 5G UDN networks there will be so many HOs that the traditional HO procedure will have difficulty in coping with them. The HO management problem becomes especially challenging, when fast moving mobiles such as vehicles and drones are to be served using UDNs.

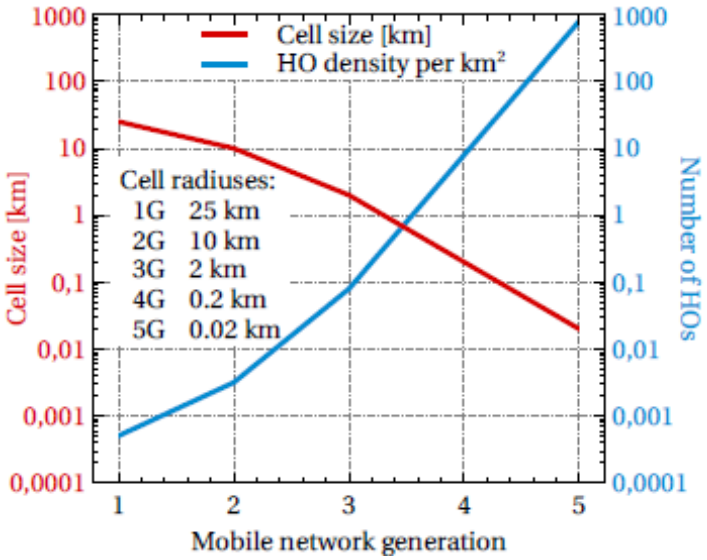

Figure 3-12: The number of handovers in different mobile network generations vs cell size normalized to 1 km^2 area. Smaller cell sizes increase the number of handovers UEs must perform per distance unit travelled.

3.3.2 Cell-free architecture for efficient HO management

Cell-free architectures present a departure from previous generations. Traditional cellular architectures rely on the concept of individual cells to provide wide-area network coverage. Each cell is responsible for a geographic area defined by the prevailing channel conditions as perceived by UEs. The latter

perform measurements of the serving, and neighbouring cells' signal levels. Results are reported to the serving BS for mobility decision-making. When a neighbouring cell is deemed more suitable for serving a given UE, the serving BS instructs it to perform a handover. Connection to the new cell is accomplished through an initial access procedure by the UE while state is transferred by the network from BS to BS. A mobile user will thus be handed over from cell to cell along its trajectory according to the measured channel conditions.

The emergence of the cell-free concept stems from the densification of networks. As cell sizes shrink, so do the cell dwelling times. In UDNs, this may result in inter-handover times in the order 10 seconds. For example, in a cell of radius 50 m, a UE moving at 50 km/h (13.9 m/s) will cross the entire cell (100 m) in ~7.2 s. Such high rates impose an excessive signalling overhead burden on the network. Similarly, the need to perform measurements continuously imposes a burden on the UE as well. Cells need to be measured and results reported to the network. Data transmission interrupts also results from the measurement gaps. This proves particularly problematic vis-à-vis the 5G aims of providing reliable, low-latency and ubiquitous service to devices.

A cell-free architecture aims to solve the above-mentioned issues. The structure of the network gains an additional layer of organization granularity below the cell: transmission-reception points (TRP). The role of cell is taken over by gNBs, which are an evolution of the eNB in LTE. Each gNB, however, controls a group of TRPs. gNBs can therefore co-ordinate TRPs operation to provide high-quality service to UEs. One example is interference mitigation between neighbouring TRPs. UEs anchor their sessions to the gNB as in previous generations. Each gNB can then use any of its TRPs to serve the user. This enables much larger cells for handover purposes while retaining the benefits of small cells in terms of placing BS transmitters close to users. A switchover from TRP to TRP does not constitute a fully-fledged handover. Thus, the air interface signalling overhead between network and UE is removed. The switchover from one TRP to another is transparent to the UE. Figure 3-13: Cell-free user-centric architecture presents an illustration of the Aalto Radio Framework cell-free positioning-based mobility architecture. The figure shows an urban drone-assisted firefighting scenario, which is extracted from the generic use case illustrated in Figure 1-1.

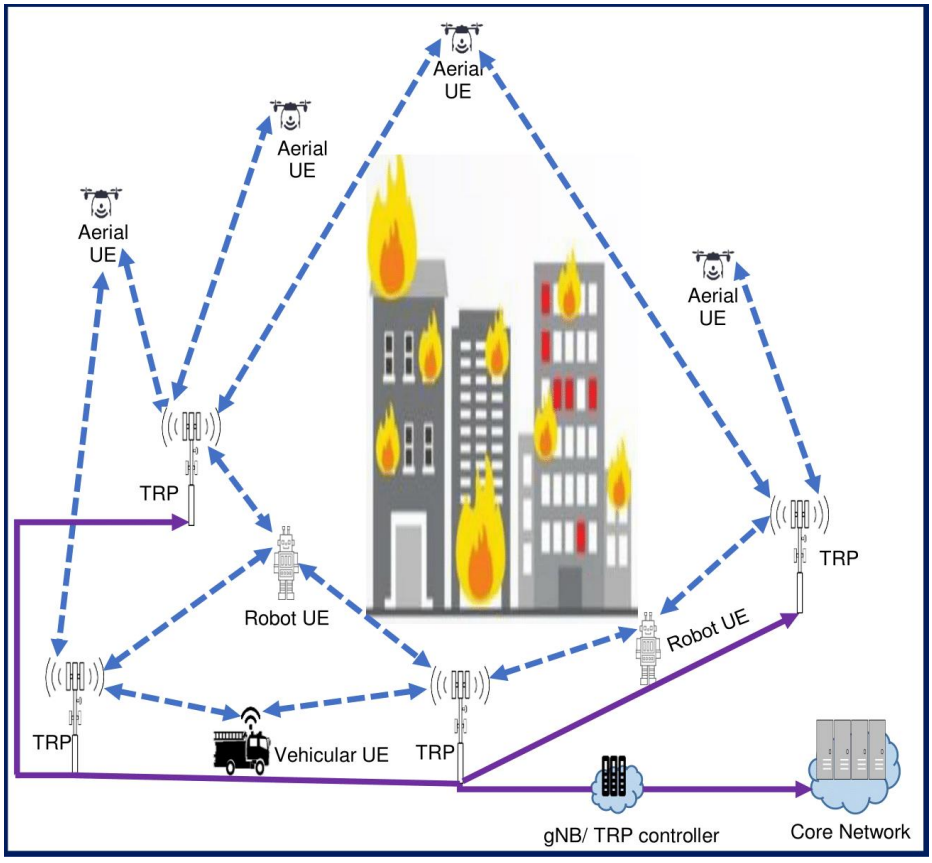

Figure 3-13: Cell-free user-centric architecture

In a cell-free UDN, a gNB constructs a virtual cell for a UE anchored to it and the TRPs serve the targeted UE in a user-centric manner under the gNB's control. The gNB also determines when switchover from one TRP to another should take place. This is achieved by using the UE's position, which is obtained in a user-centric manner. In a cell-free user-centric UDN architecture, a given UE periodically transmits UL beacon signals to connected TRPs. These beacon signals are used for channel parameter estimation, which form the basis for user positioning. Using uplink measurements is preferable to using downlink ones as the latter would need to be reported back to the network. Doing so would increase the signalling burden a cell-free approach aims to reduce. In this document, acquiring users' location is based on the angle-of-arrival (AoA) estimate of the line-of-sight (LoS)-path between the UE and multiple TRPs under the serving gNB. The AoA estimates from multiple TRPs are fused into position estimates at the gNB [29].

A properly designed and dimensioned cell-free network possesses greater flexibility than previous generations of cellular systems. One way in which this can be exploited is to provide handover types. Instead of a break-then-make handover, the gNB can decide to serve the UE from two, or more, TRPs simultaneously. Doing so enables different profiles for different users. For instance, in the URLLC case, both the source and target TRPs could send the same information on different frequency resource to maximise the probability of successful reception.

Another advantage of cell-free networks lies in the extra information provided by UE location data. By combining RSRP, SINR and position, gNB can form a Radio Environment Map (REM). A REM describes the typical channel conditions experienced in the area served by the gNB. By comparing to such a baseline, the network can distinguish between temporary worsening of channel conditions and areas shadowed by permanent obstructions. This information can be taken into account when making switch over and handover decisions. For example, a gNB could anticipate a UE moving behind a

building's corner. The resulting RSRP drop at mmWave frequencies could be significant and difficult to recover from using a traditional measurement-based approach.

One constraint in the UL beaconing approach of the cell-free architecture is the availability of orthogonal beacon sequences due to all TRPs operating on the same frequency band. In order to locate each user individually, each UE's beacon must be uniquely identifiable. However, in practice, there is only a limited set of beacon sequences with good orthogonal cross-correlation properties, which can be assigned to each UE so that each UE's beacons are uncontaminated. Therefore, this necessitates reuse of the available orthogonal beacon sequences after a certain spatial distance to serve a large number of users. Another way to tackle the aforementioned UE beaconing problem is to use increased time-frequency resources for beacon transmission. This increases the number of available orthogonal pilots, but at the cost of data resources. In network level design, one has to keep the right balance between pilot and data resource by finding the optimum amount of pilot resources needed. This is particularly important in UDNs as the small cell sizes mean therefore many potentially neighbouring TRPs.

3.3.3 Drone Classification and Handover Optimization

Providing service to drones introduces mobile airborne users as a targeted device for the first time in cellular networks. As such, network deployment models must be updated. Doing so requires an understanding of the behaviour of cell-free networks at scale. The first target is to analyze the system performance of a cell free network considering drone UEs and ground UE in terms of handover realization and other Quality of Service (QoS) parameters. We are targeting to perform two separate sets of simulations. In the first set of simulations, a simplified 19 site regular hexagonal grid will be considered with flat terrain (without actual building data), and a 3GPP specified models will be used to model the propagation related matters. The performance metrics considered for the analysis will be received power, SINR, handover performance related parameters. One of the targets is to use machine learning for improving the performance of handover for ground UE and drone UE. In the initial part, it also involves the classification of users as drone UE and ground UE using ML algorithm. In the second set of simulations, a more realistic 3D building data will be used for making a cell free network architecture. Radio propagation simulations will be performed using a sophisticated 3D ray tracing tool for finding the propagation paths between the TRP and the UEs. Later, that data will be used for optimizing a HO performance in a cell free architecture. In this way, we will analyze the system performance using two different approaches.

4 Mobility Management

In PriMO5G, mobility management for fast moving objects is essential to provide reliable immersive video services. Remote and real-time control for drone wireless networks can support reliability and low latency. Under limited communication resources, coordinated transmission and efficient resource allocation are required for high mobility vehicles. Additionally, the caching techniques based on vehicle mobility features can increase data rate of overall mobile communication systems.

The targeted user-case is challenging for following reasons. First of all, to support safety control and operation of drone mobility management, connection reliability of UAVs becomes challenging problem, since the cell association pattern of UAV becomes more complicated depending on the heights. Secondly, in the case of D2D mobility caching, which deals about the caching system reflecting user mobility in D2D environments, finding the optimal caching strategies is challenging problem, because user cache and mobility pattern should be jointly optimized. Moreover, in the case of joint association and resource management for fast moving object, providing reliable services is a problem since these services require quickly converting appropriate resource for moving objects.

For each mentioned category, the traditional approach is insufficient and defective. Firstly, real time drone control, drone identification and regulation, and high precision drone positioning should be supported for drone mobility management. Secondly, for the case of D2D mobility caching, temporal and spatial features, which reflects the user's mobility patterns, should be delicately modelled. Finally, in the case of joint association and resource management for fast moving object, association procedure for fast varying trajectory or topology is lacking.

Partners will contribute technologies including caching or resource allocation strategies capturing mobility pattern of moving object and clarify desirable mobility pattern reflecting position and velocity of drone. For Ericsson that is in charge of drone mobility management, results to develop the mobility performance of cellular-connected UAVs is derived and potential enhancements for improving mobility performance in the sky for existing cellular networks that have been optimized for terrestrial coverage are proposed. For KAIST concentrating on D2D mobility caching, temporal feature is elaborately modelled by how many neighboring users cache the requested content. Also, spatial feature is modelled by how long the neighboring users stay inside the communication range. YU proposes the joint association and resource management for minimizing the required bandwidth and reducing computational complexity while guaranteeing QoS requirements to fast moving objects.

4.1 Performance Assessment for Mobility Support of Cellular-connected UAVs

Ensuring reliable connections during the UAVs' mobility is important for the safety control and operations of such unmanned aerial vehicles (UAVs). Nevertheless, using current terrestrial cellular networks to provide connectivity to the UAVs faces new challenges. In particular, the radio environment changes with increasing height above the ground thus affecting the UAVs' mobility performance. Figure 4-1 provides an example for the cell association vector of the UAVs at different heights from the ground level. From this figure, it can be seen that at the ground level, the strongest site is in general the closest one. However, this is not the case at higher altitudes, where the expected fragmentation is observed, and a pattern created by the lobe structure of the BS antennas appears.

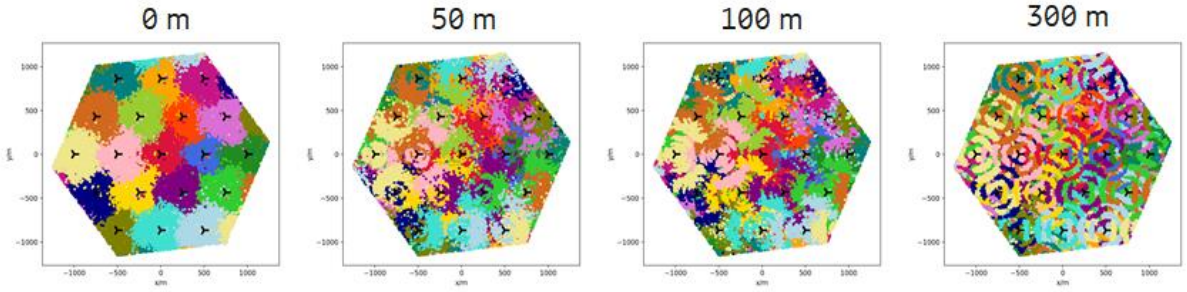

Figure 4-1: Cell association patterns for the UAVs at different heights from the ground level [30]

That said, in this subsection, we summarize some of the findings in the context of mobility support for cellular-connected UAVs. In particular, we present evaluation results to shed light on the mobility performance of LTE connected UAVs and discuss potential enhancements for improving mobility performance in the sky for existing cellular networks that have been optimized for terrestrial coverage.

4.1.1 Performance Metrics

For performance evaluation, we adopt the radio link failures (RLF) and the number of successful and failed handover (HO) for studying the mobility performance of cellular-connected UAVs. Next, we describe the network conditions during which RLF and HO situations can happen.

A RLF occurs when the UE cannot establish or maintain a stable connection to the serving cell. According to the 3rd generation partnership (3GPP) LTE radio resource control (RRC) specification [31], the UE declares RLF upon indication from the radio link control (RLC) layer that the maximum number of retransmissions has been reached, or upon expiry of the timer T310 that is started when physical layer problems are detected, or upon indication from medium access control (MAC) layer on random access problems.

the user equipment (UE) declares RLF upon indication from the radio link control (RLC) layer that the maximum number of retransmissions has been reached, or upon expiry of the timer T310 that is started when physical layer problems are detected, or upon indication from medium access control (MAC) layer on random access problems.

For mobility evaluations, RLF triggered upon the expiry of T310 is considered in this subsection. In the radio link monitoring (RLM) process, the UE periodically computes a channel quality indicator (CQI) by evaluating the signal quality of a reference signal (CRS for LTE and SSB or CSI-RS for NR) related to the part of the frame from which the UE detects scheduling grants carried in the physical downlink control channel (PDCCH). If the CQI drops lower than a threshold Qout, it is considered “out-of-sync.” Higher layers count subsequent out-of-sync indications. If a maximum number of consecutive out-of-sync indications (denoted by N310) is reached, the UE starts timer T310, whose expiry would trigger RLF. While the timer T310 is running, the UE periodically evaluates the signal quality. If the signal quality recovers such that the CQI is above a threshold Qin, it is considered “in-sync.” Higher layers count subsequent in-sync indications. If a maximum number of consecutive in-sync indications (denoted by N311) is reached, the UE stops the timer T310. In this case, the UE will not declare RLF and will maintain the RRC connection. If the quality of PDCCH does not improve while the timer T310 is running i.e., if N311 consecutive in-sync indications are not reported to higher layers while T310 is running, the UE declares RLF upon the expiry of T310. If RLF is declared, the UE either tries to re-establish the RRC connection or goes back to idle mode and starts the cell search procedure in order to establish a new RRC connection.

Meanwhile, HO failure (HOF) is defined in the context of the HO process, which is initiated by measurements of the reference signals fulfilling certain conditions, so-called events. According to the

3GPP technical report TR 36.839 [32], the HO process can be divided into 3 states, as summarized below:

- State 1: Before the event (e.g. event A3 indicating that a neighbour becomes offset better than the serving cell) entering condition is satisfied, i.e., before the actual HO procedure has started.
- State 2: After the event entering condition is satisfied, but before the HO command is received by the UE, i.e., while the UE is waiting for and expecting the HO command from the BS.
- State 3: After the HO command is received by the UE, but before the HO complete is sent by the UE, i.e., during the HO execution.

In this process, a HOF is counted if any of the following occurs:

- If RLF occurs in State 2, i.e., if the quality of the serving cell drops too fast before the HO to the target cell can be executed.
- If the timer T310 (at whose expiration the UE would declare RLF) is running when the HO command would be received, i.e., if the UE cannot receive the HO command from the source cell due to the poor link quality.
- If a PDCCH failure (using the same criterion as for starting the timer T310) occurs in State 3, i.e., if the target cell signal quality turns out to be too low to establish a connection.

A ping-pong HO is defined as a HO that is followed by another HO back to the original cell, occurring within some time window t. Throughout this subsection, we have used t = 1s in accordance with [33].

4.1.2 Simulation Results and Analysis

For the simulation analysis, we consider a cellular network with a regular hexagonal cell layout. We consider both urban-macro (UMa) and rural-macro (RMa) scenarios. In each simulation, all UAV-UEs are considered to be operating with the same speed and at the same altitude while having random starting points and directions in the x-y plane. Four different heights (ground level, 50m, 100m, 300m) and four different UE speeds (3 km/h, 30 km/h, 60 km/h, 160 km/h) are simulated. The simulations are repeated with two different traffic models: a full-buffer model, where the network is used to full capacity (i.e. 100% resource utilization), and a file transfer protocol (FTP) traffic model with the parameters (FTP object size and reading time) chosen such that an intermediate level of resource utilization is realized. In the simulations, all failure types (HOF and RLF) are logged separately for each state described earlier. Moreover, HOFs and RLFs are counted in a mutually exclusive way: if a RLF occurs in State 2 of the HO process, it is counted as a HOF only and not logged again as part of the final RLF statistics. For the HO rates, these include both the successful and failed HOs.

Table 4-1 summarizes the main evaluation assumptions considered in this subsection.

In the simulations, all failure types (HOF and RLF) are logged separately for each state described earlier. Moreover, HOFs and RLFs are counted in a mutually exclusive way: if a RLF occurs in State 2 of the HO process, it is counted as a HOF only and not logged again as part of the final RLF statistics. For the HO rates, these include both the successful and failed HOs.

Table 4-1: Simulation Assumptions

Parameter	Value	
	UMa	RMa

Cell Layout	Hexagonal grid, 19 sites, 3 sectors per site	
Inter-site distance	500 m	1732 m
BS antenna height	25 m	35 m
Carrier frequency	2 GHz	700 MHz
BS antenna pattern	(M, N, P) = (8, 1, 2) where M denotes the number of rows in the array, N denotes the number of columns in the array, P denotes polarization	
BS antenna down-tilt angle	10 degrees	6 degrees
UE density	15 UAV UEs per cell, no terrestrial UEs	
UE height	{0, 50, 100, 300} m	
UE speed	{3, 30, 60, 160} Km/h	
Traffic model	{Full buffer, FTP} in the downlink	
Event A3 offset	2 dB	
Time-to-trigger (TTT)	160 msec	
T 310	1 sec	

4.1.2.1 UMa Scenario with Full-buffer Traffic

For baseline comparison, we consider in this section the UMa scenario with full-buffer traffic. This scenario represents a worst case due to the high UE density per unit area (compared to the RMa scenario, which features the same number of UEs, but within significantly larger cells), high network load (100% resource utilization), and the resulting high levels of interference.

Figure 4-2(a) and Figure 4-2(b) show the HO rate and RLF rate, respectively, for the different considered UE heights and speed settings. As expected, the HO rate increases with speed since a faster UE passes through more cells than a slower UE during the same time window. An interesting observation is that HO rate and RLF rate are negatively correlated: with increasing height, the UEs perform fewer HOs while the RLF rate increases strongly. The key takeaway is that UAV-UEs often go into RLF instead of initiating the HO process. When the serving cell quality decreases rapidly, the out-of-sync indications due to low PDCCH quality start the timer T310, which expires before a measurement event A3 is triggered meaning that no candidate cell reaches the threshold.

The above phenomenon can be illustrated by Figure 4-2(c), which shows an example of the simulated reference signal receive power (RSRP) and signal-to-interference-and-noise ratio (SINR) traces for a UAV-UE moving for 10 s at a height of 300m and with a speed of 30 km/h. Each coloured line in the RSRP subplot corresponds to the RSRP trace of one cell. The vertical dark green dashed line at the beginning of the simulation marks cell selection of the cell with the corresponding colour. After 3 s, the serving cell RSRP begins to drop. After 5 s, the RSRPs from some neighbouring cells become stronger than that of the serving cell. After 6 s, the RSRPs from all the neighbouring cells become stronger than that of the serving cell. However, the RSRPs of the neighbour cells are all at about the same level and stay relatively low. None of them is at least 3 dB better than the serving cell, which is the A3 threshold in this particular simulation and thus the condition to trigger a measurement report. After 7 s, the UE

declares RLF (marked by the vertical red dashed line) due to poor serving cell SINR, without having even sent a measurement report, which would have been a prerequisite for initiating a HO.

Another example for mobility trace is shown in Figure 4-2(d). Here the UE starts in the light green cell before being successfully handed over to the dark green cell after about 3.5 s. At about 5 s, however, the UE moves through a null between two sidelobes of the same BS antenna. The RSRP of the serving cell drops sharply, about 10 dB within only one second (corresponding to a distance of about 8 m at a speed of 30 km/h). At the bottom of the dip, the UE inevitably declares RLF.

These examples illustrate the two main challenges for providing mobility support for UAV UEs using existing terrestrial cellular networks: (i) the stability of the signal strength of the serving cell and (ii) the interference fluctuation. Sudden drops in signal strength due to the UE moving through antenna nulls between sidelobes might lead to frequent RLFs because the default HO procedure may simply be too slow to be successfully executed. We can see further that the gaps between the serving cell RSRP and the neighbour cell RSRPs are small. The strong interference from neighbour cells results in relatively low throughput from the serving cell.

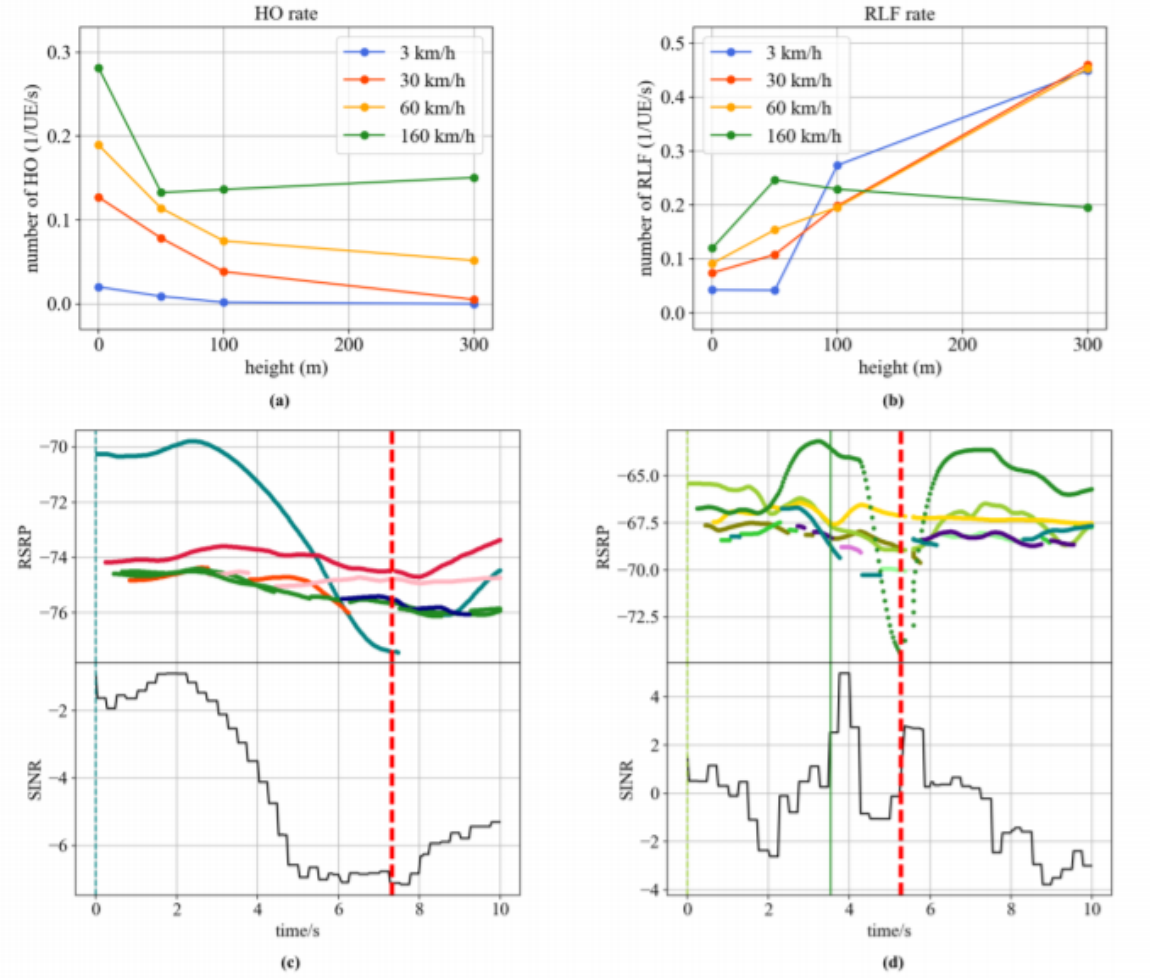

Figure 4-2: UMa scenario with full-buffer traffic: (a) HO rate, (b) RLF rate, (c) an example of mobility trace where different curves correspond to RSRP values from different base stations, (d) another example of mobility trace [34]

4.1.2.2. RMa Scenario with FTP Traffic

In this section, we study the RMa scenario with an FTP traffic model, which is more realistic than the full-buffer traffic condition. The FTP parameters are chosen to result in an intermediate network load level. Because the parameters are kept constant for all speed and height settings, load levels may however change between simulation cases, since the needed radio resources vary with speed and height. The resulting HO and RLF rates are shown in Figure 4-3(a) and Figure 4-3(b), respectively. From these figures, it can be seen that there is a negative correlation between HO rate and RLF rate. In contrast to the UMa scenario with full buffer traffic (and with the notable exception of the 100m height setting), we see quite good mobility performance. Here, the HO rates do not decrease with height, and the RLF rates are low, especially at 300m height. This is due to lower UE density per unit area, lower network load, and larger cell size thus resulting in much lower interference levels.

Another aspect of the mobility performance is the HOF ratio, i.e., the fraction of attempted HOs that fail, either because the quality of the serving cell drops too fast such that the measurement reports or the HO commands are lost during transmission, or because the quality of the target cell turns out to be not good enough such that the UE cannot establish a new connection. The fraction of failed HOs for the RMa scenario with FTP traffic simulation is shown in Figure 4-3(c). Here, we also observe good mobility performance with low HOF rates at all heights except at 100m, where between 40% and 60% (depending on the UE speed) of all attempted HOs (which are already fewer than at other altitudes according Figure 4-3(a)) fail.

The anomalous phenomenon at 100m height, as indicated by the poor HO, RLF, and HOF performance (shown in Figure 4-3(a-c), respectively), is reflected by the observation that at 100m height, we can see an excessively high resource utilization level (above 80%). To understand the anomalous behaviour at 100 m height, we examine the distributions of signal-to-interference ratio (SIR) values for the RMa scenario. Figure 4-3(d) shows the 10th percentile, median, and 90th percentile SIR as a function of height. It can be clearly seen that there exist areas with poor SIR around 100m height with large variance. At larger heights, the variance becomes smaller, and the 10th percentile SIR is much higher than the counterpart at 100m height.

It should be noted that the SIR distribution at a certain height depends on the network deployment and BS antenna patterns. The existence of large regions with very low SIR at a specific height might be a consequence of the regular hexagonal deployment with identical BS antenna patterns that are used in this simulation. Nonetheless, even in more irregular and thus more realistic deployments, we expect the existence of regions in the sky with poor radio conditions, where UAV-UEs might experience disproportionately high rates of RLF and HOF.

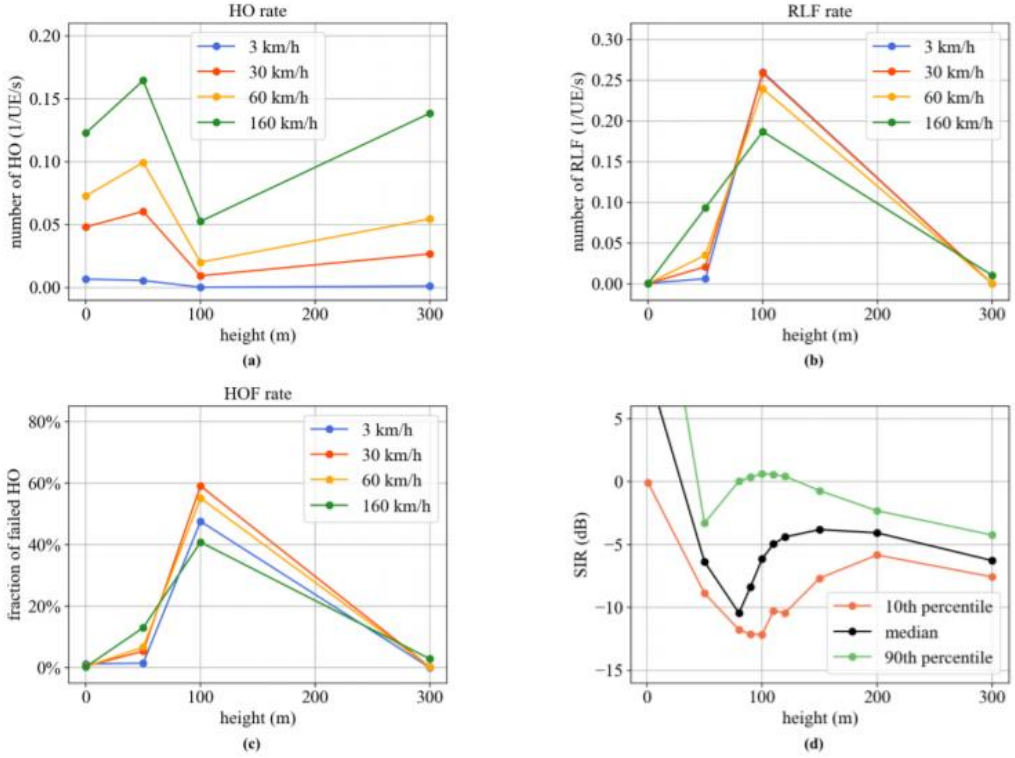

Figure 4-3: RMa scenario with FTP traffic: (a) HO rate, (b) RLF rate, (c) HOF rate (d) 10th percentile, median, and 90th percentile SIR [34]

The results presented in this subsection suggest that the existing terrestrial LTE networks should be able to offer wide-area wireless connectivity with good mobility support to the initial deployment of a small number of UAVs. However, higher UAV densities and/or more difficult radio environments might be challenging. In this context, two main problems have been identified:

- When UAV-UEs move through BS antenna sidelobe nulls, the default mobility procedures might be too slow to be successfully executed. UAV-UEs might declare RLF before a HO to another cell can be completed.
- UAV-UEs experience line-of-sight (LOS) propagation conditions to many neighbour cells, which results in comparably high interference levels. This makes it difficult to establish and maintain connection to the network, which might lead to increased RLF and HOF rates.

A possible solution to the first problem is to reduce the reaction time of the mobility procedures, e.g., by tuning the HO parameters. A more advanced solution is the introduction of a conditional HO procedure, where the network pre-emptively (without the UE having sent a measurement report) sends a HO command to the UE with an added condition. Upon fulfilment of this condition, the UE can immediately initiate the HO, without having to wait for the HO command. Meanwhile, to address the second problem, one could possibly rely on the coverage extension feature introduced for LTE-M, which allows UEs to connect to the network under worse SINR conditions. In addition, careful flight planning might be used to avoid regions of poor SINR in the sky. The positions of such regions could be determined by the network, for example by evaluating the measurement reports of UAV-UEs. The network might then in turn inform UAV-UEs about these regions, so that these UAVs could adapt their flight paths to avoid the coverage holes in the sky. A complementary approach is to reduce the amount of interference generated in the first place, e.g., by using directional antennas at the UE side.

4.2 D2D Mobility Caching & Modelling Temporal and Spatial Features of Mobility

Consideration of mobility becomes necessary as wireless paradigm evolves from the past. In the past, most of wireless traffic was packet for short time-scale such as texts, and images. Hence, communication duration for serving demands of users is shorter than time-scale of user movement. Thereby, wireless system was designed while considering users as stationary.

However, as multimedia services such as Netflix and YouTube shows explosive growth, users are demanding their requests continuously while they are moving. Furthermore, since video streaming which dominates the current wireless traffic shows running time of several minutes up to hours. Hence, wireless caching system which aims for reducing video traffic efficiently should take the effects of mobility into consideration. The most noticeable effect of mobility is limitation of communication time. Since communication is valid only when receivers can sense a signal sent from transmitters. However, signal is attenuated dramatically as the distance between transmitter and receiver increases. Thus, if transmitters and receivers is moving apart, which results the distance between them increases, communication is no longer feasible. Therefore, when we consider mobility of transmitters and receivers, we need to capture how long proximity between transmitters and receivers lasts. In general, communication duration depends on velocity, path and communication protocol.

In addition to temporal effects such as limitation of communication time, there exists a spatial feature of mobility. Considering multiple user communication, a transmitter may transmit to multiple receivers or vice versa. For broadcasting channel and multiple access channel, the number of receiver and transmitter, respectively, affects link capacity. Hence, how many users are located inside of the communication range is important. Suppose there are a single transmitter and multiple receivers, wireless resource such as transmit power, bandwidth, and time is allocated appropriately; hence, the link capacity per user is decreasing as the number of receivers increases. Hence, characterization of number of users participating in communication is of great importance.

As a consequence, in order to analyze mobility-aware caching system, appropriate modelling of mobility is essential. However, to capture both of temporal and spatial features of mobility correctly is challenging. One of conventional modelling of mobility used in many mobility-aware caching system is to assume contact event of transmitters and receivers is Poisson event which makes communication duration is equivalent to inter-arrival time of Poisson process. For example, in D2D caching system meaning that each mobile device has memory which stores data and transmits corresponding data via D2D communication, contact duration between individual pair is given as independent exponential random variable with a given mean rate of contact. Then, average contact duration between user pair is the inverse of mean rate of contact. Also, contact events between users are all independent. Hence, time for receiving the requested content is limited by contact rate between user pairs. In this setting, content placement is affected by the mean contact rate or mean contact duration.

However, assumption of independent contact makes contact between users in far distance feasible. As an example, suppose that user B caches the content which user A requests and is communicating with user A. There exists a user C who also stores the content requested by user A but is located far from user B. In this case, user A cannot communicate with user C although user C has what user A is requesting because user A is close to user B which implies that user A is far from user C. However, independent contact modelling cannot prevent this infeasible event to occur since geographical correlation between users is not reflected. Therefore, accurate modelling which covers both time and space limitation caused by mobility is necessary for wireless caching system.

To capture the characteristic of mobility in both time and space domain for D2D caching system, interpretation of mobility based on relative motion with respect to a receiver or transmitter can be effective. As shown in , there exist an arbitrary user in D2D caching system called a typical user and neighboring users around the typical user. When the typical user requests a content, given the D2D communication range *Z,* the neighboring user within a distance Z can be a transmitter. Also, the communication time between the typical user and a neighboring user can be characterized as a length of stay inside the D2D communication area of the typical user. In other words, how many neighboring

users who caches the requested content can represent a spatial feature of mobility and how long neighboring users stay inside the communication range shows temporal effects of mobility.

Using this model, mobility can be addressed appropriately for D2D caching system. Moreover, based on this modelling, content placements or other important factors in D2D caching system can be optimized under the consideration of mobility and various wireless features including pathloss and fading. Thus, in this situation, we formulate an optimization problem to minimize the average load of the BS for orthogonal multiple access scheme under consideration of randomness of incoming and outgoing users. It is proved that minimization of the average data load of BS can be transformed to maximization of a monotonic submodular function with a matroid constraint, for which a greedy algorithm can find near-optimal solutions.

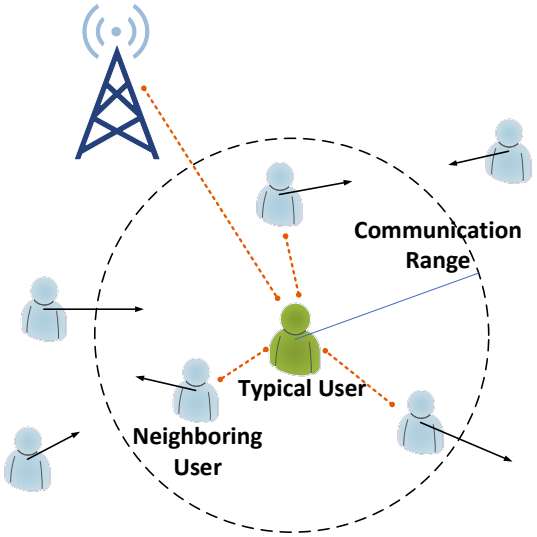

Figure 4-4 : Mobility-aware D2D caching system

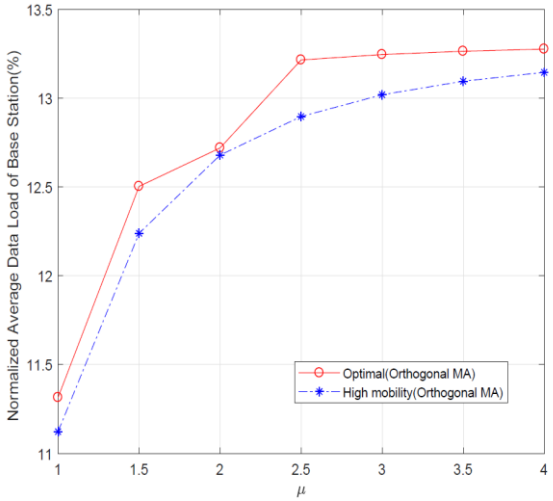

Figure 4-5 : Normalized average data load of base station through orthogonal multiple access when SNR=20dB

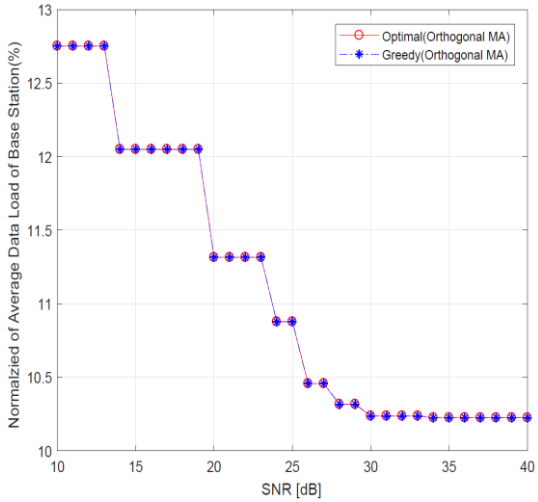

Figure 4-6 : Normalized average data load of base station through orthogonal multiple access when mean of arrival and departure rate is 1, 1, respectively

4.3 Joint Association & Resource Management for Fast Moving Object

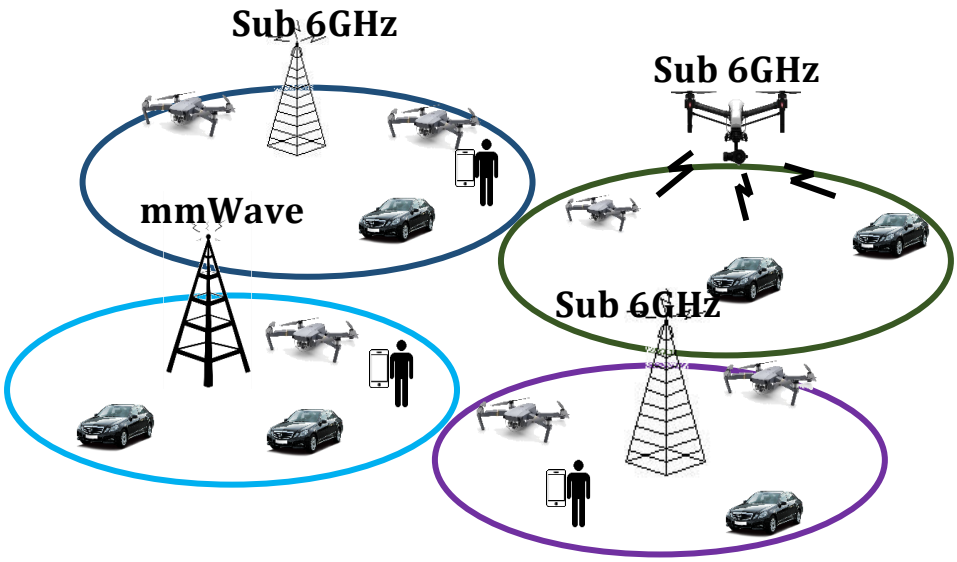

Figure 4-7 : Network Model

In the emergency situations assumed in this study, people, vehicles, and drones are assumed to be terminals as shown in Figure 4-7, and each terminal is expected to be able to use sub-6 and mmWave bands [35]. Each terminal has different mobility according to the characteristics of terminals, and has a positional change with time based on the mobility. Also assume that each base station that can support sub-6 and mmWave bands exists, and that there is a further drone base station. A conventional base station is a fixed base station whose position does not change, and a drone base station is a mobile base station whose position changes with time. When an emergency occurs, each of the terminals generates various types of applications at the same time in order to solve this problem, and the packets generated in each application have different characteristics. The packets generated at this time are expected to have characteristics of eMBB and URLLC [36]. Especially in an emergency situation, URLLC should be given priority service because it needs immediate response to a rapidly changing situation [37]. In this study, we assume the most extreme situation in which nodes have fast mobility, packets have event driven characteristics that do not know when to occur, and at the same time, the packets of relatively large size must be transmitted in a short time and solve that situation. In other words, the proposed technology should be dynamic because it must consider mobility, and should transmit a large number of packets within a short latency, so that spectral efficiency should be high and multiple access should be possible.

To solve this problem, we classify packets according to QoS characteristics as shown in Figure 4-8. This is because the optimal point of cell association and resource management may differ depending on which QoS is used [38]. In other words, by optimizing different optimal points for each QoS, it becomes possible to service various requirements simultaneously. In this study, we will study cell association and resource management for packet QoS that can occur in autonomous mobile or autonomous control mentioned above among the classified packets. The packets we are going to deal with are sporadic packet characteristics, as mentioned above, which must be transmitted in a short time. In conventional cell association and resource management, a cell association was made in such a way that a user associated to an appropriate base station through initial access, and then resource allocation has been performed to the users associated with the base station [39]. However, in this way, resource allocation within the base station can be optimized, but it is difficult to satisfy all the requirements of the packets to be handled because it may not be the optimal point for the entire system resources [40]. In order to solve this problem, joint cell association and resource management, which considers resource allocation in each base station from cell association, is needed and has been studied in our team. In this study, we plan to advance the scheme to solve the problem when users have fast mobility.

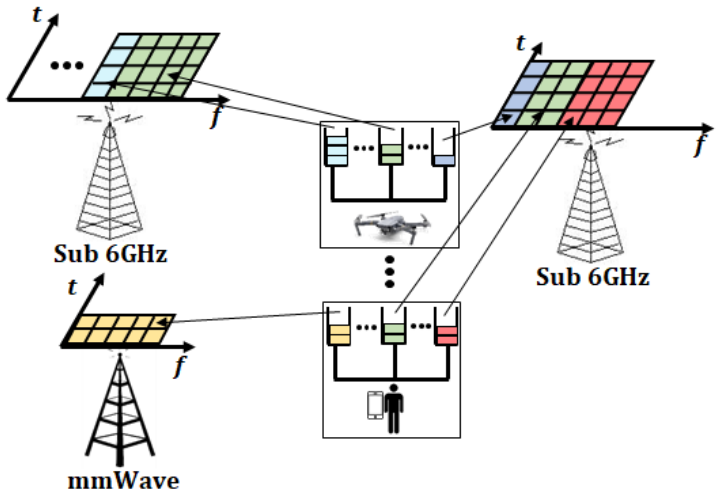

Figure 4-8 : System model

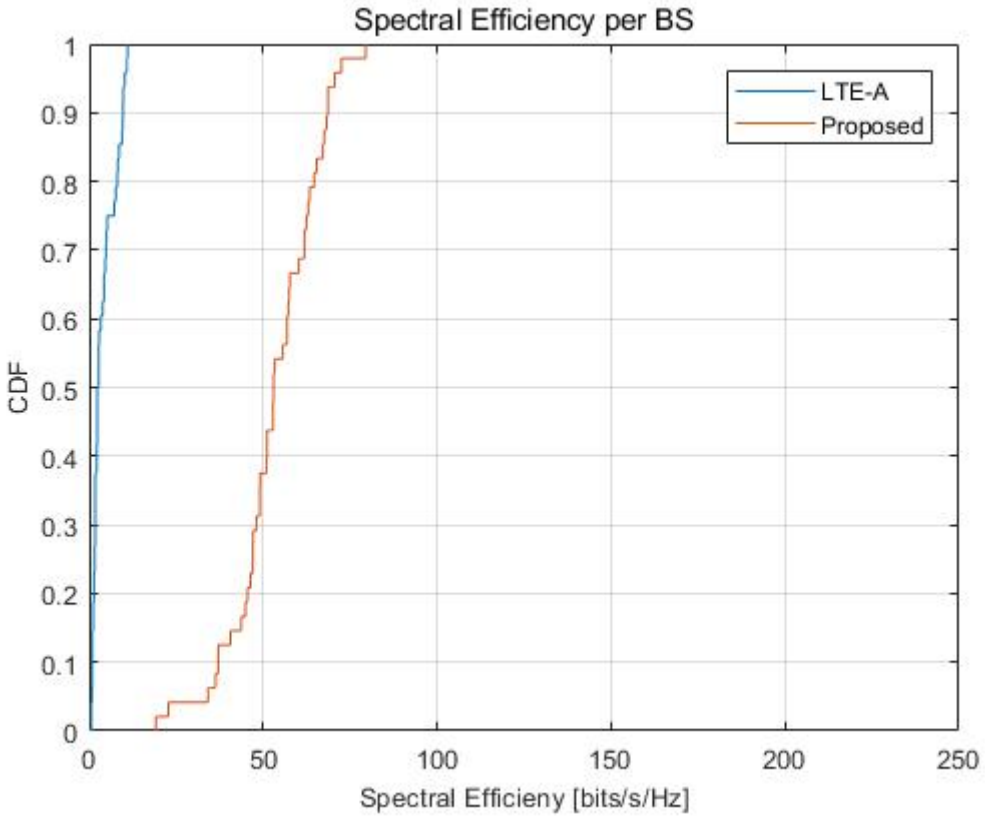

Figure 4-9 : Spectral Efficiency LTE vs propose scheme

Figure 4-9 Spectral efficiency obtained from the existing LTE when only mobility is excluded in the above assumed environment and the proposed spectral efficiency. Through this study, we will study algorithms that can support mobility.

4.4 Mobility Management for Cache-Enabled Network in mmWave Networks

Millimeter wave networks are considered as a key factor of cutting edge wireless mobile communication. This is on the grounds that mmWave network has huge capabilities by using wide bandwidth with respect to the inheritance cellular spectrum bands and its short transmission period enables low latency communication. However, there are some well-known shortages in using mmWave. For example, there is an inevitable loss of signal power caused by high attenuation and blockage vulnerability. These lead to the confined size of cell (i.e., small cell) because the transmitted signal experiences drastic attenuation in the wireless channel especially when a receiver moves in the network. As a result, mobile users in the mmWave network are forced to experience frequent handover. Many methods have been studied to solve this mobility management problem. One of the promising solutions is to use the cache of the base station storing transmitted packet when the channel state is good yielding burst data rate in the radio link. It has been confirmed that TCP protocol has a significant benefit, which is very meaningful considering that most applications transmit data based on TCP. However, the cache-enabled base station suffers from a large overhead for frequent handover, which is another disadvantage of the millimeter wave mentioned earlier. Consequently, to solve the channel problem of mmWave by using the advanced cache, we have to redesign the operation of TCP to enable caching. To this end, we designed an efficient mobility management method based on the framework of dual connectivity (DC) in the 3GPP specifications. The proposed approach overcomes the limitations of TCP caching and we specified the operations in the following subsections. The terms and scenarios are based on 3GPP LTE, thus there would be further extension considering 5G NR protocol stack when the 5G DC specification with mmWave is completed.

4.4.1 Handover Overhead for Cache-Enabled BS

When an individual TCP packet is temporarily stored in the cache in the BS, the degradation of TCP performance decreases due to the gain taken advantage from NLoS period using the packets stored in the cache of the base station. However, such a cache compliant TCP has a disadvantage that a new overhead occurs as the handover procedure is performed. Since packets cached by the BS are only used for specific UEs, other UEs may not utilize them. Furthermore, the new serving BS (or handover target BS) also need the entire TCP packet to guarantee reliable delivery of the whole contents. In other words, if their owner's UE moves to the new BS, all packets in the cache should be forwarded to the new serving BS.

4.4.2 Dual Connectivity Option for Cached mmWave Networks

The main design objectives of DC are to compensate for problems such as mobility management, data traffic offloading and throughput improvement of end user. In DC scenario, two different BSs, the master eNB (or master base station, MBS) and the secondary eNB (or secondary base station, SBS) serve a single UE at the same time. This means that the UE is simultaneously connected to two different BSs linked through a non-ideal backhaul. Although there are several DC options depending on how the data is routed and delivered to the UE between the MBS and the SBS, below two representative options are currently considered for the user plane data split, which are

1. ***DC option 1A**:* This option is promising since the protocol stack of the data bearer is independent and the BS does not need to buffer or process the packet. In addition, the architecture is simple, so it has little impact on existing protocol.

2. ***DC option 3C**:* This option is noticed in 3GPP specifications as all data is moved to the MBS once, so SBS change, delete, and additional events due to user mobility can be hidden from the core network. In addition, MBS RLC processing can be offloaded to SBS.

Despite the fact that DC may be a promising headway to improve the mobility execution, constrained consideration has been paid to the capacity maximization, which is another vital issue not to be neglected. Cache empowered SBS uses mmWave that prompts decrease of the communication coverage. At the point when the UE has high mobility, the associated SBS is changed frequently. In the DC option 1A, the serving SBS ought to send information to a target SBS. In the DC option 3C,

information is streamed that are sent to an MBS and SBS. On the off chance that the data transmission is not completed for quite a while, conveyed information from the serving SBS isn't perceived by a UE's application until the missing information is delivered. A new architecture for a protocol stack M is proposed on this work to improve network performance in a heterogeneous network:

3. ***DC option 2M:*** A new architecture for a protocol stack M is proposed on this work to improve network performance in a heterogeneous network. The proposed method meets two conditions: frequent changes of SBS should be possible to be hidden on the core network by receiving all packets first. Then, a single data bearer should not be transmitted in the both MBS and SBS, because for the divided bearer the terminal has to reassemble the data packets. All packets coming from the core network gathered on an MBS and then the MBS separates one independent bearer into a serving SBS. A transport layer control (TLC), a new layer with a cache, separates the packets. In such an architecture, a new layer TLC is considered, but it has little effect on the existing layers. Moreover, since the TLC is not considered in the protocol stack of the UE, and it means the structure of the existing UE is not affected.

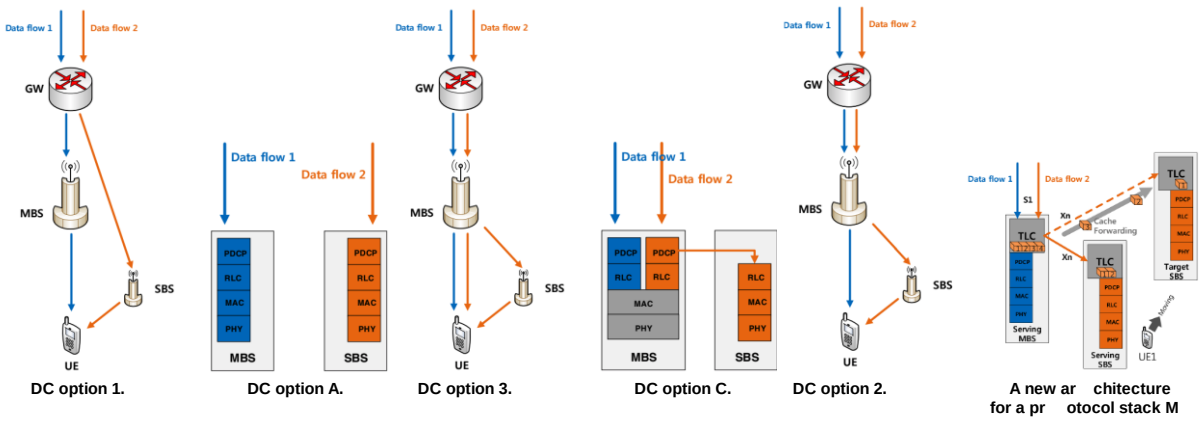

Figure 4-10 : Dual connectivity option 1A, 3C, and proposed cache operation DC option 2M

4.4.3 Hierarchical Cache Architecture

The MBS and SBS are connected via a non-ideal backhaul (X2) link interface, and mmTCP [41] is installed in each BS (M-cache, S-cache). Each cache operates hierarchically, which means that M-cache recognizes S-cache as UE and S-cache as M-cache server. Two scenarios are considered:

1. **Non-handover scenario**: When handover does not occur, the operations of the M-cache and the S-cache are similar, but the M-cache operation does not support batch retransmission of mmTCP. Since the batch retransmission is triggered by the expiration of the retransmission timer or three consecutive duplicated Acks, the batch retransmission does not occur because of the early-Ack or Ack discarding operation at the S-cache.

2. **Handover scenario**: When the UE moves to another SBS coverage, all packets in the S-cache of serving SBS must be forwarded to target SBS. At this time, the link usage between MBS and SBSs can be reduced by forwarding packets from a serving MBS. In this case, only packets corresponding to the capacity of the cache can be forwarded, so overflow can be prevented in the target SBS. Such consideration for this situation increases the stability of mobility control of the cache.

4.4.4 Numerical Results

One MBS, two SBSs, three buildings, and one UE are deployed in virtual 500 meter by 500 meter rectangular space. The SBSs and MBS are configured with dual connectivity option 2M. Since the UE

moves around the buildings with constant velocity of 1.42m/s along a straight path, it experiences both LoS and NLoS link environments.

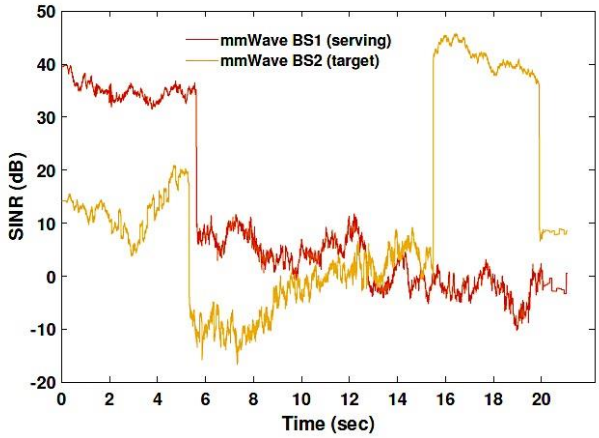

Figure 4-11: Average of signal to noise plus interface ratio (SINR) corresponding mmWave SBSs

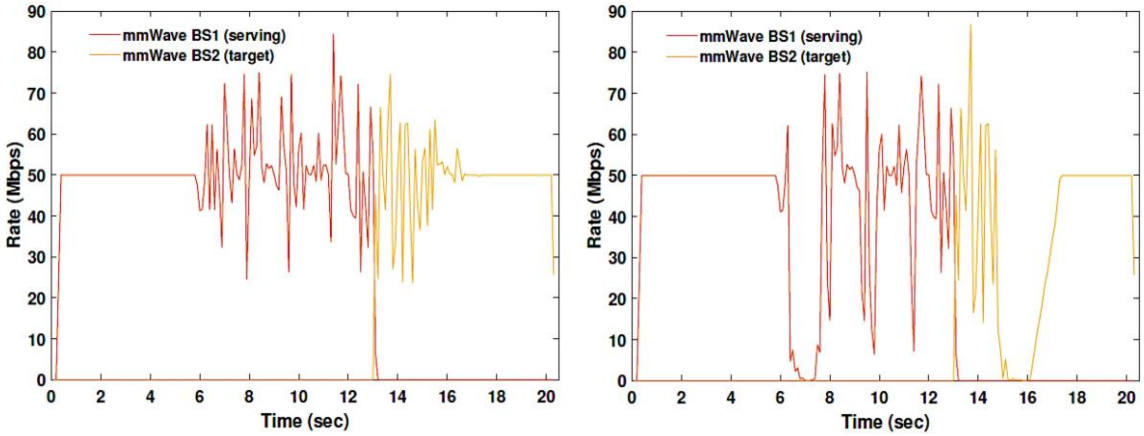

Figure 4-12: Average rates of TCP traffic with/ without caching scheme

Figure 4-11 shows the variety of signal to noise plus interference ratio (SINR) relating to mmWave SBSs experienced while the UE moves a straight way during the simulation period. As shown in the figure, when t began, SBS 1 is a serving BS. Around 6 seconds after the event, the UE is situated in the NLoS state from both SBSs, which causes the sharp SINR drop from the both cells. Notwithstanding, since the signal from SBS 1 is generally more grounded, the SBS 1 is a serving cell until 16 seconds. From that point forward, since channel state for the SBS 2 is superior to serving SBS 1, then SBS 2 turns into a serving cell for the UE.

Figure 4-11 illustrates the end-to-end TCP performance of a server to moving UE as already mentioned in the preceding subsection when the handover scenario. For a TCP traffic, the transmission speed of the TCP session determined by the (TCP) server is sensitive to the loss that occurs during the transmission path. Therefore, the packet loss of the wireless link leads to a very conservatively slow transmission rate of the server. As a result, as shown in the right of Figure 4-12, the end-to-end rate performance goes almost to zero between 6 and 8 seconds with an extensive loss of the wireless link. The proposed algorithm maintains TCP performance reliably in an environment in which "serving-SBS" changes due to UE mobility. The simulation results are shown in the left of Figure 4-12. Because of channel dynamics, TCP performance cannot maintain a certain percentage after the caching scheme

is applied. It is vital, in any case, that the transmission rate recognized by the UE does not drop to zero. This is because the server avoids situations where transmission is rapidly decreasing due to the inability to recognize the loss of radio sources, and the caching method also sends packets at that time under good channel conditions according to channel monitoring.

5 Interference Management

Unlike current wireless UAV connectivity technologies that rely on short-range communication range (e.g., Wi-Fi and Bluetooth), cellular-connected UAVs allow beyond line-of-sight control, seamless mobility, low latency, high mobile broadband data rate and large system capacity, and ubiquitous coverage. In essence, mobile networks offer wide area, high speed, and secure wireless connectivity, which can significantly enhance control and safety of drone operations. Such cellular-connected UAV-UEs will thus enable a myriad of applications ranging from real-time video streaming to surveillance. Despite the great potential, there are challenges in using existing mobile networks optimized for ground usage to provide drone connectivity. A main challenge in providing connectivity to the low altitude UAVs through existing cellular network arises due to the increased interference in the network, as illustrated in the figure below. As the height above ground level increases, the radio propagation becomes closer to that of line-of-sight free-space propagation. The increased altitude and favourable propagation condition cause UAVs to generate more interference to the neighbouring cells, and at the same time experience more interference from the downlink transmissions of the neighbouring base stations (BSs). The uplink interference problem may result in terrestrial UEs having degraded performance, whereas the downlink interference problem may make it challenging for a UAV to maintain connection with the network.

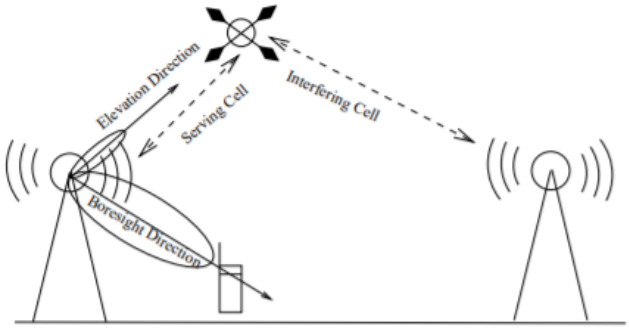

Figure 5-1: Illustration of connectivity for cellular-connected UAVs. [42]

In PriMO-5G, co-existence of aerial and ground UEs is essential in order to guarantee the latency and reliability requirements of different services in fire-fighting scenarios. The following sections present in detail the various technology components contributed by partners in this context. In particular, performance assessment for the co-existence of aerial and ground UEs is detailed. Moreover, new interference mitigation techniques that minimize the impact on the performance of terrestrial UEs while allowing mobile network operators to reuse existing deployed terrestrial networks for serving UAVs are proposed.

5.1 Performance Assessment for the Co-existence of Aerial and Ground Users

To illustrate the UAV interference problem in the uplink (UL) and downlink (DL), we show how interference level is increased when UAVs connect to the network compared to when only terrestrial UEs are in the network, as depicted in Figure 5-2. The blue curves represent interference over thermal noise (IoT) statistics when the network serves only terrestrial UEs. The red curves represent IoT statistics when the network serves both terrestrial UEs and UAVs according to a scenario defined in [43], where there are 10 terrestrial UEs and 5 UAVs per cell. The statistics are collected from all UEs in the network with a traffic load set to result in approximately 50% resource utilization (RU) in the network. From Figure 5-2, it can be seen that both UL and DL interference level increases when UAVs are served by the cellular network.

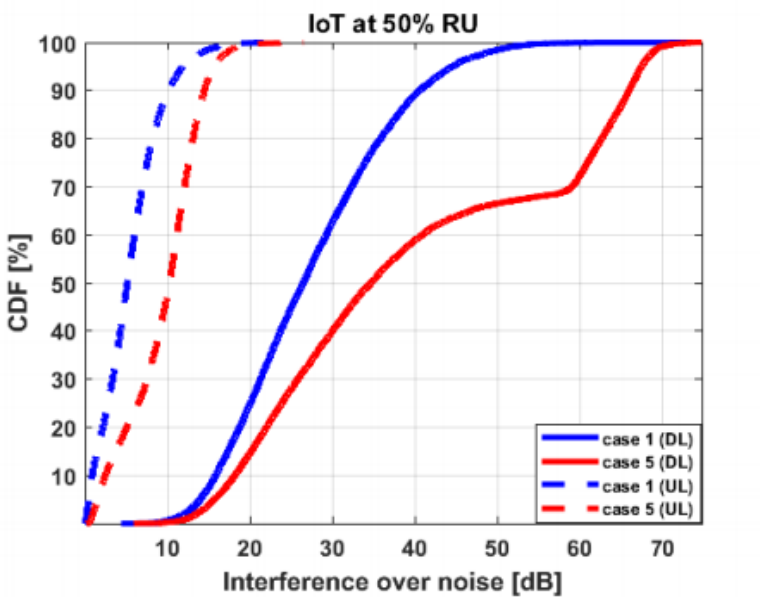

Figure 5-2: Interference over thermal noise (IoT) statistics for UL and DL at 50% resource utilization. Case-1 has only terrestrial UEs and case-5 is a hybrid deployment with 5 UAVs per cell [42]

In this subsection, we summarize and evaluate different co-existence techniques for mitigating the UL and DL interference problems that arise when cellular-connected UAVs are served by the cellular network.

5.1.1. Uplink Interference Mitigation

The uplink interference caused by the UAVs on the ground network can be addressed via uplink power control. The power control mechanism ensures that the transmit power of different uplink channels are controlled such that these channels are received at the BSs at appropriate power level. The power control procedure aims to control the received power to be just enough to demodulate the channel (target received power), at the same time the transmit power at UEs are not necessarily high as it could create interference to the other uplink transmissions. In many standards like LTE, the transmit power of the UE depends on the DL pathloss and target received power at the serving BS. Using the LTE Physical Uplink Shared Channel (PUSCH) as an example, a typical UE's UL power at subframe *i* can be expressed as:

$$P_{PUSCH}(i) = \min\left(P_{CMAX}, (10\log_{10}(M_{PUSCH}(i)) + P_0 + \alpha PL + \Delta_{TF}(i) + f(i))\right),$$

Where

- P_{CMAX} is the configured maximum UE transmit power in dBm,
- $M_{PUSCH}(i)$ is the bandwidth of the PUSCH resource assignment expressed in number of resource blocks valid for subframe *i*,
- P_0 is an open loop power control parameter in dBm composed of the sum of a cell specific component and a UE specific component,
- α is a fractional path loss compensation power control parameter,
- PL is the downlink pathloss estimate computed at the UE in dB,

- $\Delta_{TF}(i)$ is is an offset which can be used to ensure that the received SINR matches the SINR required for a given modulation and coding scheme (MCS) selected by the base station,
- $f(i)$ is the closed loop power control adjustment.

The above power control equation has two parts, an open loop part consisting of $10\log_{10}(M_{PUSCH}(i))+P_0+\alpha PL+\Delta_{TF}(i)$ and closed loop part consisting of $f(i)$.

5.1.1.1 Open Loop Power Control

One way to reduce the UL interference caused by UAVs on the ground network is to use smaller value of P0 and/or α. As mentioned earlier, P0 consists of a cell specific part and a UE specific part. The UE specific parameter can be tuned to adjust the transmit power of the UAVs. Another approach could be to add an additional power adjustment factor at BS, β, to the computed power based on the pathlosses to neighbour cells. For example, the transmit power can be adjusted by the BS based on the ratio between the serving cell pathloss and the n-th strongest neighbour cell pathloss, denoted as ΔPLn. If ΔPLn is low, then β can be adjusted to reduce the UL transmit power to reduce interference to neighbouring cells. For ΔPLn calculation, the transmit power of the neighbour cell is required at a UE. Alternatively, the ratio between the serving cell RSRP and the n-th neighbour cell RSRP may be used instead of ΔPLn.

5.1.1.2 Closed Loop Power Control

The closed loop power control part, f(i), can be expressed as follows:

- $f(i) = f(i-1)+ \delta_{PUSCH}\ (i- K_{PUSCH})$, if accumulation is allowed,
- else $f(i) = \delta_{PUSCH}(i - K_{PUSCH})$.

Where the variable $\delta_{PUSCH}\ (i- K_{PUSCH})$ denotes the transmit power control (TPC) command signaled to the UE at subframe $(i - K_{PUSCH})$. For convenience, TPC command, $\delta_{PUSCH}\ (i - K_{PUSCH})$, will be henceforth referred to as δ_{PUSCH}. The transmit power at UE, P_{PUSCH}, may be adjusted such that the received power at BS is equal to a predetermined target receive power. One or more TPC commands are sent to the UE by the BS to adjust its transmit power, P_{PUSCH}, to achieve the target received power at BS. Since UAVs are the main cause of interference, significant gains can be achieved by setting the target receive power individually based on the serving cell RSRP and the neighbour cell RSRP for UAVs, while keeping it same for all terrestrial UEs. In typical cellular networks, the open-loop power control compensates for the fractional path-loss (depending on choice of α) and the remaining path-loss is compensated based on the closed loop power control. Hence the total adjustment using closed loop power control is given by $Pcpc = (1 - \alpha)PL$.

5.1.2. Downlink Interference Mitigation

The power control-based technique presented in the previous section mainly addresses the uplink interference problems. In the downlink, due to favourable propagation condition, an UAV may experience strong inter-cell interference. A number of downlink physical channels/signals, e.g. Synchronization Channel (SCH) and Physical Broadcast Channel (PBCH), are used for cell acquisition. These channels are broadcast in nature as they need to be received by all UEs in the cell, and thus UE-specific beamforming or power control cannot be applied. For UAVs, the SINR for these channels may become lower than the normal coverage that an LTE network aims to achieve. Coverage extension (CE) is a feature set introduced in LTE Release 13. It was motivated for supporting machine type communications (MTC) which have stringent requirements on coverage. The LTE CE features however are not limited to MTC devices. For example, it can help UAVs complete cell acquisitions successfully in the presence of significant inter-cell interference. During cell acquisition, the UE needs to detect SCH,

get master information through PBCH and other system information through Physical Downlink Shared Channel (PDSCH). Cell acquisition is an essential step for supporting handover procedures. LTE coverage extension targets 155.7 dB maximum coupling loss (MCL). Rel-13 coverage extension is achieved mainly through repetitions. Repetitions give rise to higher signal energy which extends the coverage and help mitigate interference through a processing gain over the interfering signals. However, it is worth noting that such repetitions may result in higher latency. As CE achieves 155.7 dB MCL, it is guaranteed that UEs will have SINR higher than −14.3 dB and will be able to achieve cell acquisition.

5.1.3. Results and Analysis

In this subsection, we present results for the proposed uplink and downlink interference mitigation techniques. We consider the urban macro (UMa) scenario with case-5 deployment (5 UAVs and 10 terrestrial UEs per cell) as discussed in [43]. First, we present the results for the open loop power control where we configure the UAVs and terrestrial UEs with different P0 values denoted as P_{OA} and P_{OT} respectively, for six different combinations, as given in Table 5-1. Combination 1 is used as a baseline since the power control parameters for the UAVs are the same as those of the terrestrial UEs.

Table 5-1: The P0 values for terrestrial UEs and UAVs

Combination	P_{OT} [dBm]	P_{OA} [dBm]
1	-85	-85
2	-85	-86
3	-85	-87
4	-85	-88
5	-85	-89
6	-85	-90

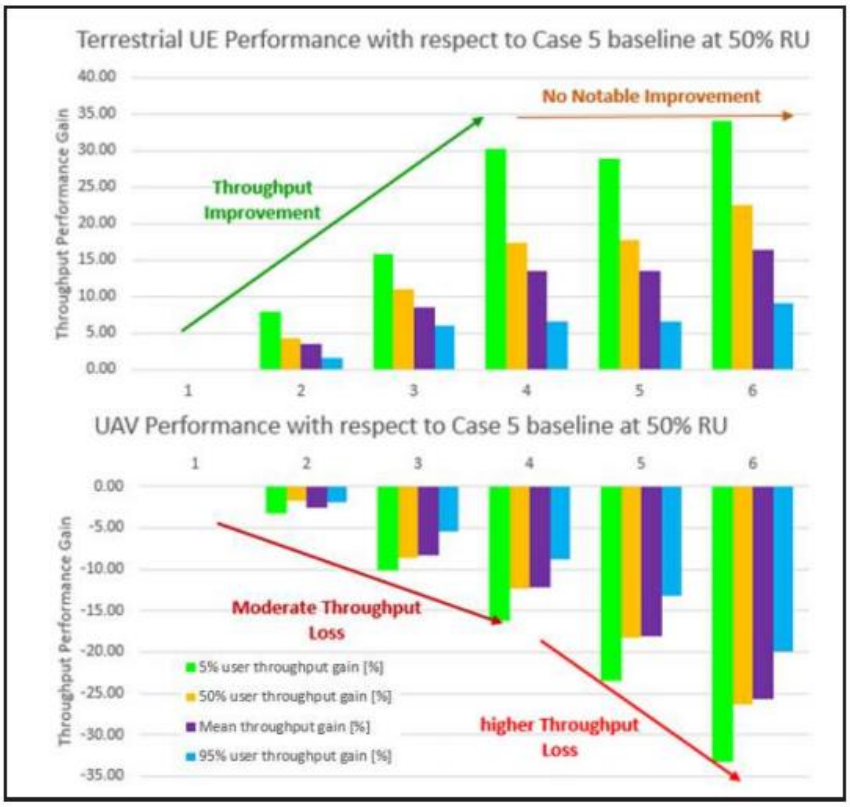

Figure 5-3: Uplink terrestrial UE and UAV throughput results with different P0 values for UAVs and terrestrial UEs considering 50% resource utilization. Baseline scheme is Combination-1 in Table 5-1 [42].

The terrestrial and UAV uplink throughput gains are shown in Figure 5-3 for the different combinations that were introduced in Table 5-1. From Figure 5-3, it is evident that the terrestrial UE throughput performance can be improved by configuring the UAVs with a lower P_{OA} value. The achieved improvement is significant as it can help in protecting the terrestrial users' throughput from increased interference from the UAVs. Also, notice that the decrease in transmit power of UAVs reduces the throughput of the UAVs. When P_{OA} is gradually reduced from −85 dBm to −88 dBm, moderate UAV throughput losses is observed. However, reducing P_{OA} even further results in higher UAV throughput losses without significant improvement to the terrestrial users.

For the closed loop simulations, we use the same deployment as in the open loop case (urban macro, case 5) and evaluate the performance for the two following combinations:

- Combination 1: P_{OT}= P_{OA}=-85dBm
- Combination 2: P_{OT}= -85dBm and P_{OA} adjusted individually based on serving cell RSRP and neighbour cell RSRP.

In the first combination, the closed loop parameters are kept the same for both terrestrial UEs and UAVs and is used as the baseline. Combination-2 uses the method described in subsection 5.1.1.2, where, for the UAVs, the target received power is individually adjusted based on the serving cell RSRP and the third strongest neighbour cell RSRP. Results are summarized in Figure 5-4. From this figure, it is evident that terrestrial UEs' and UAVs' mean, 50 percentile, and 95 percentile throughput performance are improved by the proposed solution. However, some cell edge throughput losses are seen for terrestrial UEs. One reason for this could be due to power limited terrestrial UEs not being able to reach

the target received power (P0 = −94 dBm).

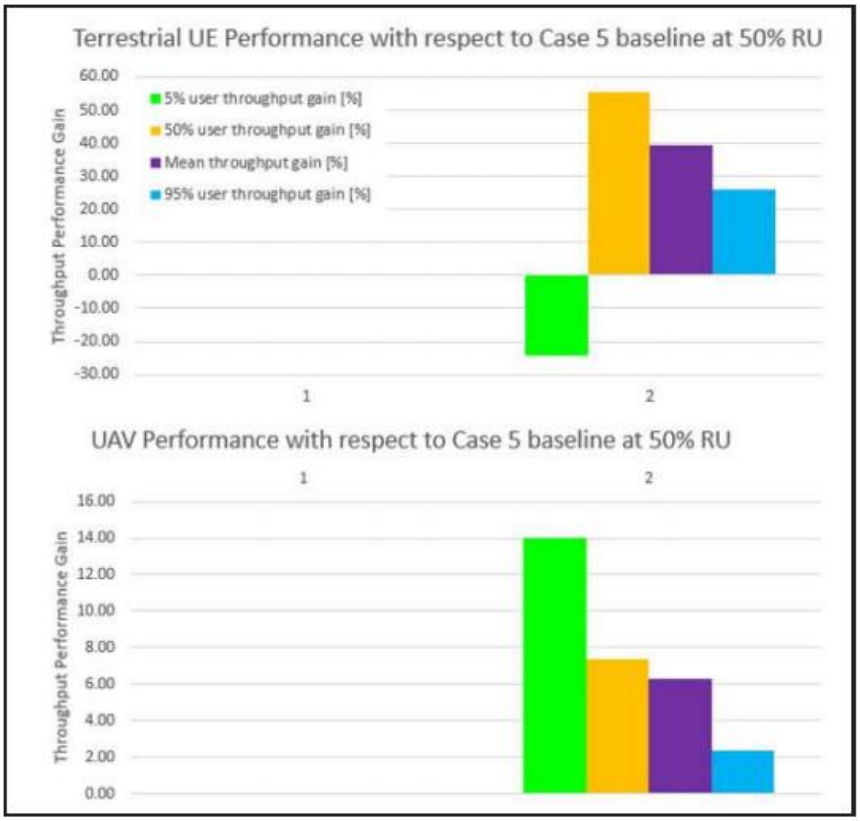

Figure 5-4: Uplink throughput results for terrestrial UEs and UAVs at 50% resource utilization [42].

Next, the effect of the DL interference on the performance of synchronization and cell acquisition experienced by UAVs is evaluated. For physical channels carrying unicast traffic, the level of inter-cell interference depends on the traffic load. However, for the synchronization and cell acquisition channels, the interference may not depend on the traffic load. One example for such is a system frame number (SFN) synchronized network, which is a possible network configuration when LTE features such as multicast-broadcast single-frequency network (MBSFN) and Positioning Reference Signal (PRS) are supported. In such scenarios, all the BSs may transmit SCH and PBCH at the same time. We study the downlink wideband SINR statistics experienced by the UAVs. To assess the UAVs' performance in the worst-case scenarios, the downlink wideband SINR statistics are obtained by assuming all the BSs in the network transmit at full power. We will also refer to this as DL geometry SINR. Figure 5-5 shows the DL geometry SINR collected from the UAVs for both RMa-AV and UMa-AV scenarios. Here, we see that the DL geometry SINR can be as low as −10.8 dB. However, this SINR value is still higher than the required SINR according to the LTE CE link budget.

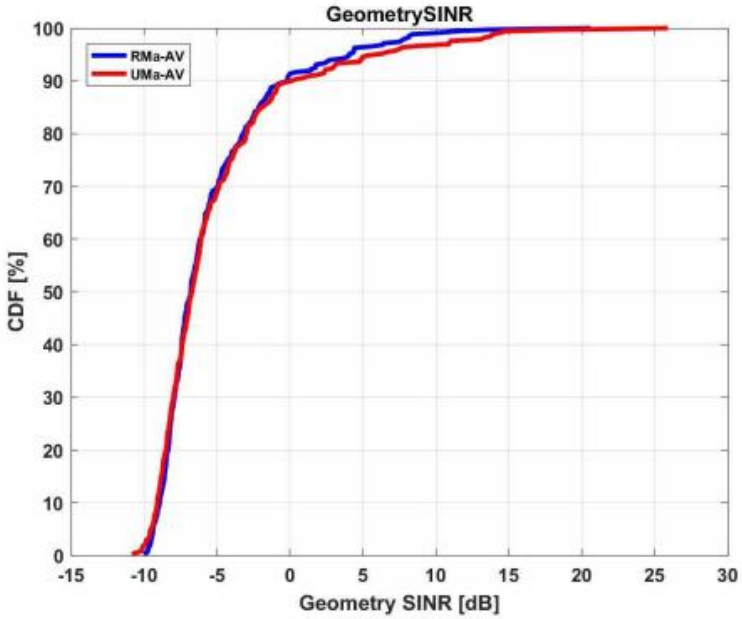

Figure 5-5: CDF of downlink geometry SINR experienced by UAVs [42].

One of the main challenges of re-using terrestrial cellular network for UAV connectivity is the high level of interference. In the uplink, UAVs are aggressors, which may generate interference to neighbouring cells due to potentially line-of-sight propagation conditions to many base stations. We showed that existing power control framework can be extended to mitigate uplink interference. Results show that for a scenario with mixed terrestrial UEs and UAVs as defined in 3GPP, the throughput gains for the terrestrial UEs can be improved by 30% to 50% using the proposed modifications. In the downlink, UAVs are victims of inter-cell interference. To maintain connectivity with the network, an UAV needs to be able to complete cell acquisition reliably so that potential handover target cells can be identified. LTE coverage extension solutions can be adopted to improve cell acquisition for UAVs. By using these tools, the outage probability of cell acquisition channels, e.g. SCH, PBCH, and PDSCH carrying system information, can be reduced to 0% from 33%-75%.

In summary, one can conclude that existing LTE networks can support initial drone deployments where UAVs may be served by the sidelobes of BS antennas due to down-tilted BS antennas. Enhancing solutions and 5G (LTE evolution and/or NR), such as beamforming, larger carrier bandwidth, and massive MIMO, will provide more efficient connectivity for wide-scale drone deployments.

5.2 Rouge Drone Detection

Due to the previously mentioned distinct features of cellular-connected UAVs, a network intruder can easily disrupt the operation of the ground network. In particular, a Subscriber Identity Module (SIM) card can be attached to a UAV generating excessive interference to the ground network and especially in regions in which flying a drone is not allowed by regulations such as near airports. In this regard, it is crucial for network operators to identify these rogue drones for protecting the performance of ground UEs from the potential interfering signals resulting from drone UEs and for security reasons. Moreover, for some scenarios, operators would want to have another subscription type for aerial users. That said, in this subsection, we propose a novel machine learning approach to identify rogue drones in the networks based on the radio measurement reports sent by the UEs to the BSs. We apply two classification machine learning models, Logistic Regression (LR), and Decision Tree (DT), using features from radio measurements to identify the rogue drones.

5.2.1. System Model and Simulation Scenario

We consider an urban scenario in which 19 macro cells, each having 3 sectors, are deployed with inter-site distance of 500 m, as depicted in Figure 5-6. Each BS has two cross polarized antennas at the height of 25 m with a transmit power of 46 dBm. The carrier frequency is 2 GHz with 10 MHz bandwidth. The detailed channel model description can be found in [44]. A mix of outdoor UAV-UEs and ground UEs (that can be located indoor or outdoor) is assumed - 19,000 UEs were simulated for 60 seconds; 25 percent of them being UAV-UEs at different height above ground-level (AGL) ranging from 15 m to 300 m; 65 percent being indoor ground UEs at different heights (modelling UEs located in high-rise buildings), and the rest of them being outdoor ground UEs at the height of 1.5 m. Both UAV-UEs and outdoor terrestrial UEs have a speed of 120 km/h, while the indoor terrestrial UEs have a speed of 3 km/h. The main event that determines handover is so-called event A3, which is a handover measurement report triggering event when a neighbour cell becomes better than the serving cell. Event A3 is triggered if a neighbour cell measurement minus A3 hysteresis is greater than the serving cell measurement plus A3 offset. Once event A3 is triggered, the UE will wait for a predetermined time before it sends measurement reports to the serving cell. The predetermined time is called time-to-trigger (TTT). With the measurement reports transmitted by the UEs with 40 ms periodicity, the network continuously predicts if a UE is a drone UE or not.

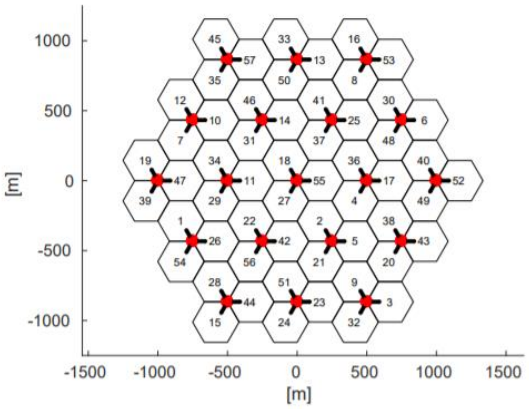

Figure 5-6: Simulation Scenario

5.2.2. Proposed Prediction Methodology

Our main objective is to approximate a mathematical function f(x) →p where f is the per cell machine learning model, x is the UE reported radio measurements, and p is the probability of UE being a UAV-UE. As such, measurement data is collected and divided into separate training and testing sets. The model f(·) is trained with known legitimate UAV-UEs and ground UEs with the assumption that there are no rogue drone UEs in the training data set. Evaluation was performed with different data containing a mixture of drone UEs and regular ground UEs. Note that the training phase requires measurement data from known legitimate UAV-UEs flying in the network. The training phase can hence take long time in areas where drones are less likely to operate. Fortunately, rogue drones may likely be less of a problem in these areas as well.

To select a convenient machine learning model, one would need to consider a trade-off between complexity and performance. A more complex model is likely to yield better performance if trained properly, but is also more resource consuming (time, memory, and computation resources). Depending on the problem at hand, a simple model may provide satisfactory performance while consuming much less resources. Here, we evaluate the following two basic classification machine learning models - logistic regression and decision tree. As for feature selection, four features are considered:

- RSSI: Received signal strength indicator
- RSRP-STD: Standard deviation of the eight strongest reference signals received powers (RSRP)
- RSRP-gap: Difference between the strongest RSRP and the second strongest RSRP
- Serving cell RSRP

Combinations of these features are used to evaluate the performance. However, it should be noted that the features and their combinations are not restricted to the above. The selection of these features is made based on the key observation that a UAV-UE operating at a high altitude is expected to have close to line of sight free-space propagation environment that leads to low variance of RSRPs of the strongest cells. RSSI statistics of UAV-UEs are different from those of ground UEs due to similar reason, e.g., a UAV-UE may receive signals from multiple cells with similar strengths.

In machine learning, the false positive rate (FPR), also known as false alarm rate, is the ratio of the number of incorrectly classified negatives (False Positives) to the total number of negatives (False Positives + True Negatives). In the context of this work, FPR > 0 means that some regular ground UEs are being identified as rogue drone UEs. Depending on how the networks deal with the UEs that are labelled as rogue drone UEs, the cost of false positives may be high since false positives may lead to unpleasant user experience. Therefore, one should try to achieve a very low FPR (ideally, zero FPR) during the classification. Aiming at zero FPR minimizes the number of occurrences that regular ground UEs are labelled as rogue drone UEs in our investigated test set of UEs. Therefore, the first metric studied in this work is the drone detection rate (i.e., true positive rate) at zero FPR, i.e., the ratio of the number of correctly classified positives to the total number of positives while ensuring no ground UEs are labelled as drone UEs in our test set. Note that this only guarantees that we have no ground UEs labelled as rogue drone in the test set of UEs. If a ground UE sends a measurement report different from the reports when building the model, there is a risk of classifying it as a rogue drone. This work also considers the receiver operating characteristic (ROC) and area under the curve (AUC) classification performance metric. The value of AUC lies in the range [0, 1]. The higher the AUC value, the better the prediction accuracy. For a model to be acceptable, AUC has to be greater than 0.5. An AUC of 1 represents a perfect classifier and the goal is to achieve an AUC as close to 1 as possible.

5.2.3 Results and Analysis

In this subsection, we summarize the main findings of the proposed rogue drone detection methodology. As mentioned earlier, the ROC AUC metric is a good accuracy indicator of the model prediction performance. The ROC AUC curves presented in Figure 5-7 show the prediction performance of both models (LR and DT) with several different combinations of the features. From Figure 5-7, it can be seen that the DT classifier with all the four extracted features provides the best performance.

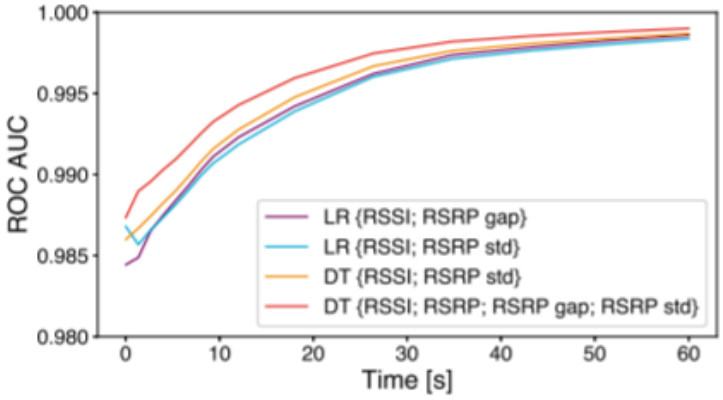

Figure 5-7: ROC AUC values as a function of simulation time [45]

We further analyse the feature importance by using the Gini importance metric which is based on the Gini impurity in the trained DT model [46]. The feature importance is plotted in Figure 5-8. As it can be seen from Figure 5-8, the RSRP-gap feature has the least amount of impact on the results. This suggests that replacing the RSRP-gap feature with a more important feature would likely yield better performance or removing the RSRP-gap feature can save resources while maintaining similar prediction accuracy.

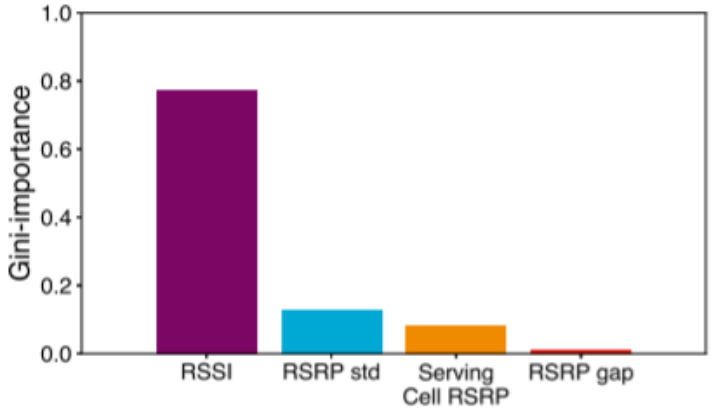

Figure 5-8: Feature Importance for the DT Classifier [45]

Figure 5-9 shows the percentage of detected drone UEs at each height above ground-level after 60 seconds using the DT classifier with RSSI and RSRP-STD as input features. It can be seen from Figure 5-9 that high drone UE detection rates can be achieved at the heights greater than 60 m. In contrast, only 5 percent of the drone UEs can be identified at 15 m while meeting the zero FPR target. The undetected drone UEs are at or below 60 m and they account for approximately 20 percent of all the drone UEs. In particular, for drone UEs above 60 m, their radio propagation environments are quite different from the radio propagation environment on the ground. As a result, high detection accuracy can be achieved for drone UEs above 60 m based on the radio measurements reported by the UEs. For drone UEs below 60 m, especially at the height of 15 m, the radio propagation environment of the drone UEs is similar to the radio propagation environment on the ground. As a result, it becomes challenging to distinguish these drone UEs from regular ground UEs solely based on the reported radio measurements.

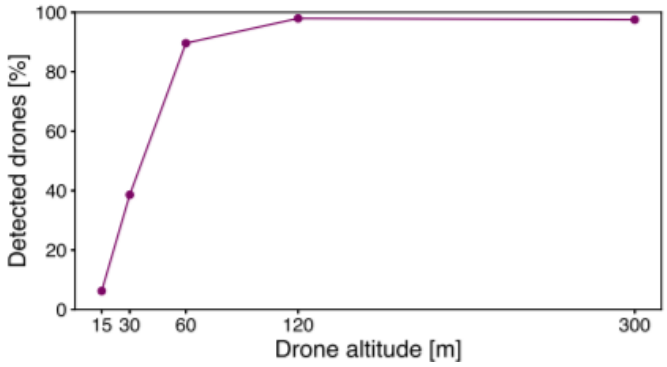

Figure 5-9: Percentage of detected drone per altitude after 60s using the DT classifier with features {RSSI, RSRP-STD} [39]

In this subsection, we proposed a novel machine learning approach to identify rogue drones in the mobile networks based on radio measurement reports. We have studied two classification machine learning models, logistic regression and decision tree, under different combinations of the four features: RSSI, RSRP-STD, RSRP-gap, and serving cell RSRP. Simulation results have shown that the proposed machine learning approach can achieve 100 percent detection rate for rogue drone UEs above 60 m height while meeting 0 percent false positive rate. The detection accuracy, however, degrades at lower heights: only 5 percent detection rate for rogue drone UEs at the height of 15 m to meet the 0 percent false positive rate. However, low altitude flying drones is less likely to create more interference than a regular UE and thus identification of them are less crucial from a network management point.

5.3 Full Duplex interference Management Scheme for Multicell Network

This section addresses the multicell Full Duplex (FD) network. FD network could double bandwidth efficiency over Half Duplex (HD) theoretically. The benefit of FD network gives us chance to upload high data rate streams, for instance, real-time high-quality video transmission. However, there are some issues to overcome in applying FD to the network. One of the most significant issues is interference. Two types of interference occur in the FD network which are called self-interference and user to user interference which both can severely affect to signal transmission. In this section, we focus on the uplink user to downlink user interference assuming self-interference is cancelled enough for communication.

The scheme for FD network is Code Division Duplex-Spatial Division Multiple Access (CDD-SDMA). The scheme eliminates interference from uplink to downlink and downlink to uplink by aligning the signals to different subspace by using code division and classify multiple access signals by spatial division. We first introduce the scheme for single cell case and expand it to the multi-cell network.

The system model consists of N RF-chains and M antenna elements and there are L number of cells to eliminate the interference. When the number of physical antennas at Full Duplex Base Station (FDBS) is, $M = 2LN$ and full channel states are assumed to be known at FDBS and constant over the $2L$ time slot.

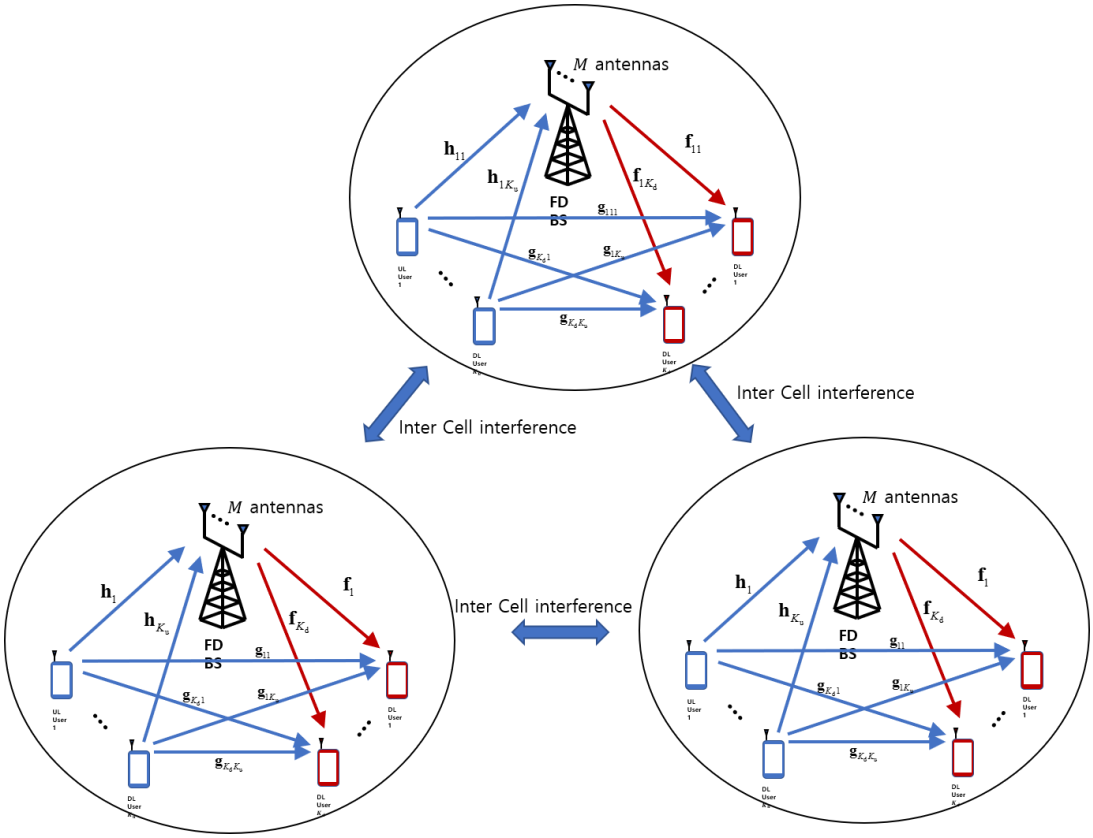

Figure 5-10: FD network System model

The goal of this scheme is to serve $2LN$ downlink and uplink users for the $2L$ time slot in each cell, while HD could serve total LN users consisting of uplink and downlink users in each cell. Let us first explain the scheme for single cell and expand it for multi-cell case.

For a single cell, FDBS serve $2N$ downlink and uplink users for 2-time slots. The process of the scheme is by two steps. Composing analog and digital precoder at FDBS and multiplying code at the user equipment. At first, FDBS construct analog and digital precoders for uplink and downlink users. For analog precoder, FDBS constructs $2N \times 2N$ orthogonal matrix **A** which is consisted of $2N \times N$ analog precoders for each time slots. Let us define $2N \times 2N$ channel matrix $\mathbf{F}$ which is consisted of each user's channel and find digital precoders for each user which eliminates all other users' signal. The digital precoder for each user is, the normalized result of each column of the pseudo-inverse of $\mathbf{F} \times \mathbf{A}$, and let us define digital precoder as $\mathbf{u}_{il}$ which satisfying $\|\mathbf{u}_{il}\|^2 = 1$ and $\begin{bmatrix} \mathbf{u}_{11} & \cdots & \mathbf{u}_{2N1} \\ \mathbf{u}_{12} & \cdots & \mathbf{u}_{2N2} \end{bmatrix} = \mathbf{\Psi}[\mathbf{F} \times \mathbf{A}]^{\dagger}$ where $\mathbf{\Psi}$ is diagonal matrix scaling each column**.** Then, at last, we construct 2×2 orthogonal matrix **C** which could align each signal to different subspace and let $\mathbf{c}_l = \begin{bmatrix} c_{l1} \\ c_{l2} \end{bmatrix}$ be the lth column of matrix **C**. The transmit signal for two-time slots at FDBS is $\mathbf{FA} \sum \begin{bmatrix} c_{11}\mathbf{u}_{i1} \\ c_{12}\mathbf{u}_{i2} \end{bmatrix} a_i$ where a_i is information for user i. And for the uplink user, the transmit signal for the two-time slot is $\mathbf{c}_2^T b_i$. Then if we multiply $\mathbf{c}_1^T$ to the total received signal for 2 timeslots, the uplink users' interference eliminated by their orthogonality $\mathbf{c}_1^T \times \mathbf{c}_2^T = 0$. Also, by the digital precoder, signals from other downlink users can be aligned to orthogonal subspace from the desired signal. For uplink signal, we can figure out the signal by doing the inverse as the downlink process at FDBS.

To expand this for multi-cell case, the number of physical antennas should be $2LN$. Also, the scheme is extended to $2L$ time slots. For other matrices, by the number of physical antennas changed, all matrices become $2LN \times 2LN$ and the matrix **C** become $2L \times 2L$ then, other process remains the same to eliminate interference.

5.4 OP-MAP based Flexible Hybrid Duplex

5.4.1 OP-MAP based Flexible Hybrid Duplex

The research that can flexibly transmit the signal based on the spectrum sensing and the opportunity mapping has shown the great potential to increase the data rates and reduce the latency in the sub-6GHz band [47]. However, in the mmWave band, there is a question as to whether this function can be applied and what benefits can be gained. In this section, we have briefly summarized the prior research and discussed why we do need a full duplex system in the mmWave band. Furthermore, we have organized several mathematical aspects that we applied opportunity map in the mmWave band with a directional antenna. Finally, we make some concluding remarks with a future work.

With growing spectrum scarcity, full duplex radio as well as dynamic spectrum access has been considered as one of the solutions in 5G communications. We proposed a new method that integrates full duplex and spectrum/spatial sensing in order to bring the maximum spectral efficiency. Figure 5-11 illustrates 3-step architecture of opportunity-map (OP-map) based flexible duplex system. Firstly, deployed sensors at fixed locations sense the interference level ceaselessly and deliver the data to a server at each time slot. The second step is to calculate the OP-map in the server in real-time and to transmit it to secondary users.

At the final step, each secondary user's node decides whether to transmit the data or not based on the OP-map. Note that OP is defined as the predicted transmission success probability of a typical secondary user when the interference level at its nearest sensor is given, i.e., OP :=P (SIR > theta | I), where theta and I represent an access threshold containing the constraint for primary network protection and the measured interference level at the nearest sensor, respectively. The communication system, including all node terms such as the primary node, the secondary node, and the sensor is implemented using LabVIEW system design software and an FPGA based PXIe SDR platform as shown in Figure 5-12.

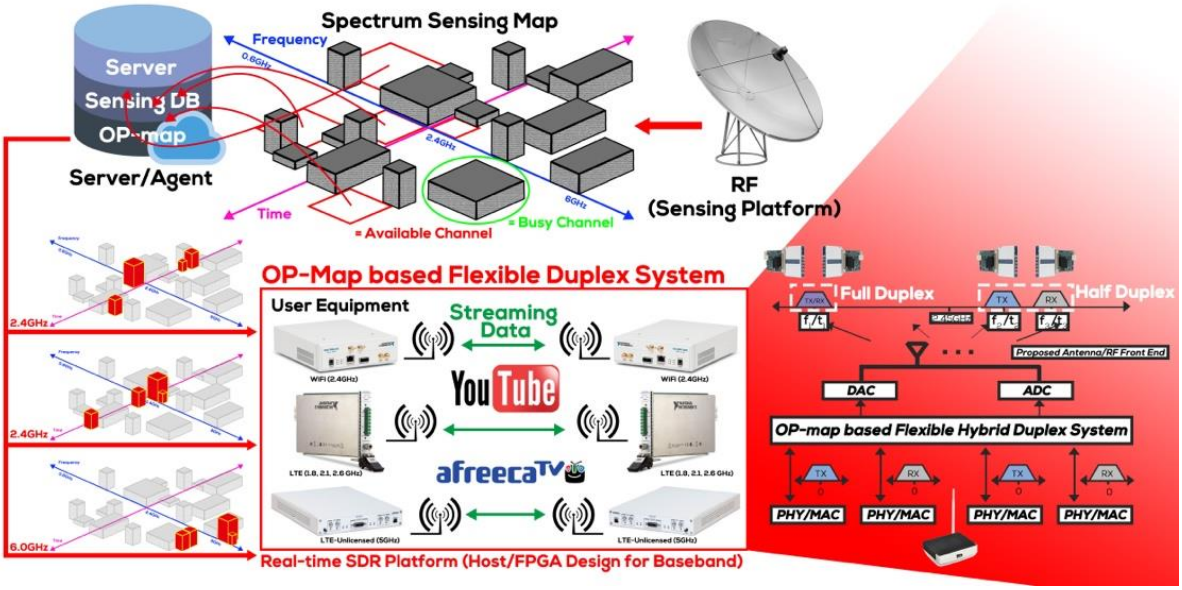

Figure 5-11 A Structure of OP-Map based Flexible Duplex System

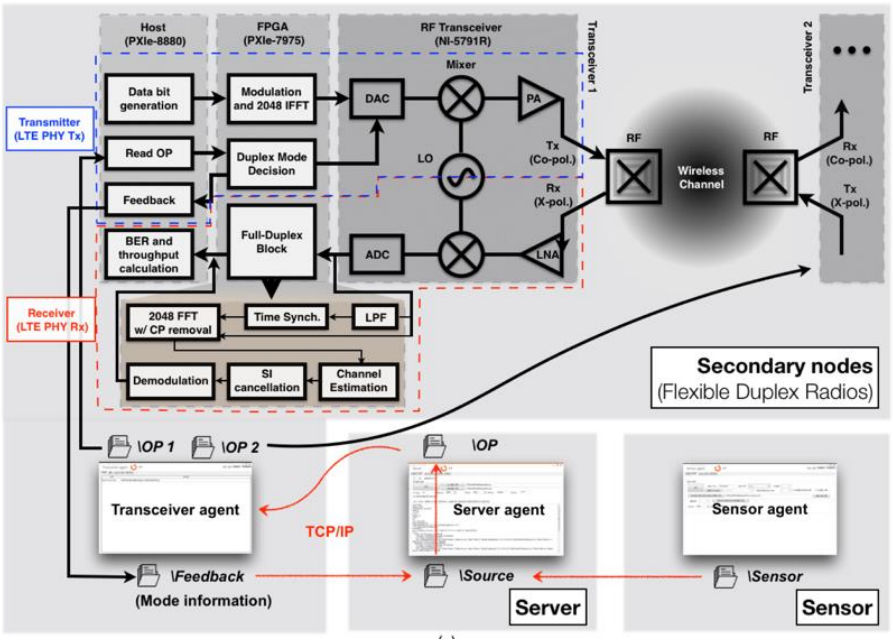

Figure 5-12 A block diagram of our proposed real-time testbed with the logic of the system with data exchanging through the agents.

In sub-6GHz, because of the insufficient frequency band, it is recommended to increase the spectral efficiency using full duplex to meet the requirement of 5G. In the case of the mmWave band, where the frequency band is abundant, however, one might argue about the value of using full duplex which needs complex technology. Since the mmWave band is sufficiently wideband, it may not be rational to double the spectral efficiency theoretically by using difficult technology. The following reasons, however, disprove it. First of all, one of the reasons that full duplex is challenging to commercialize is the lack of

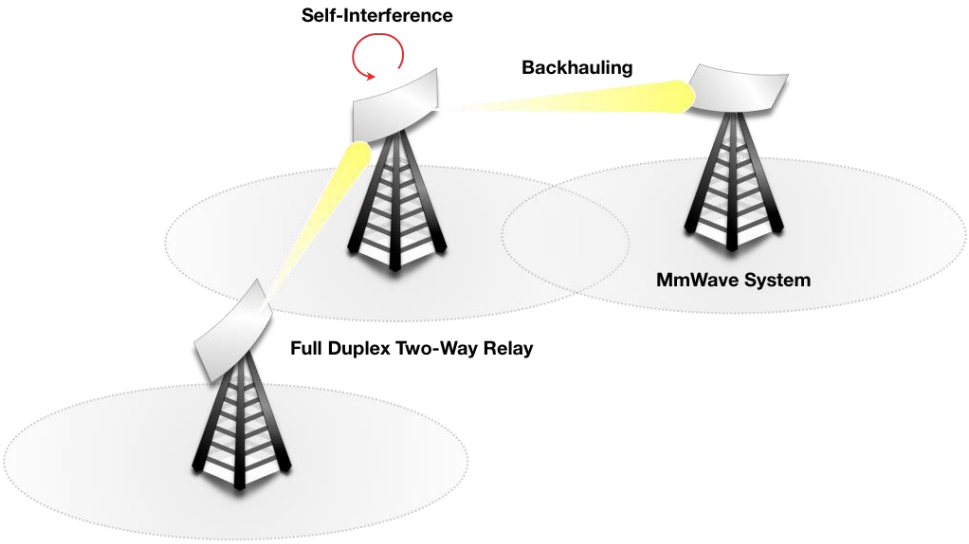

Figure 5-13: A basic concept of two-way relay full duplex system in the mmWave band

self-interference cancellation which is the key to enabling full duplex radio. By using the sharp beam using the proposed lens antenna, especially in the mmWave band, it is easier to separate the transmitted and received signal that makes the amount of the passive analog self-interference cancellation higher. Furthermore, it is useful to apply the full duplex system as an alternative to solve the backhaul problem in the mmWave band. The trend for dense deployment in future 5G mobile communication networks makes current wired backhaul infeasible owing to the high cost. To overcome

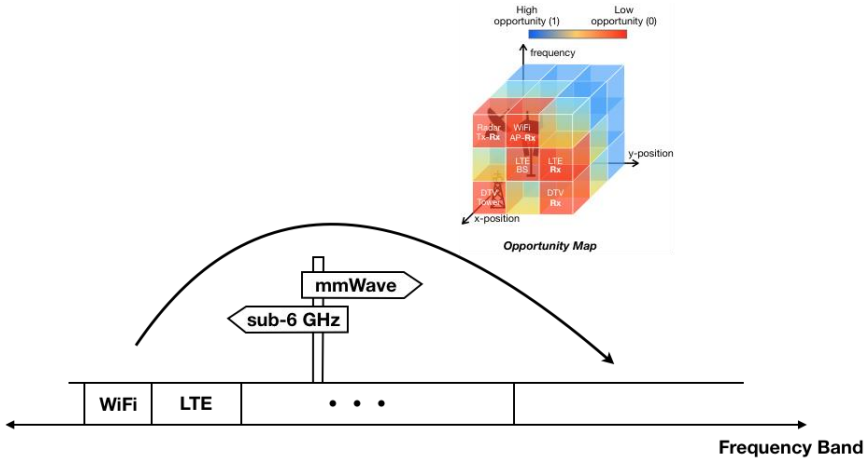

Figure 5-14: Opportunity Map in the mmWave band

this, wireless backhauling has been considered a feasible and effective way of obtaining end-to-end connectivity. The use of two-way relay full duplex system in wireless networks is recognized as one of the favorable architectures for the future wireless networks, specially mmWave networks as they can extend the coverage of the wireless link as shown in Figure 5-13. This combination of full duplex and mmWave can bring various benefits.

In the prior studies, we have considered the opportunity map in the sub-6GHz. From the perspective of the mmWave band, there are several changes to apply appropriately (See Figure 5-14). Also, in order to calculate the OP value based on stochastic geometry, it is essential to define the antenna beam

pattern and other properties. We exploited the dual-polarized antenna, which has the directivity that can be critical in OP calculating. From this point of view, we suggest a modified OP calculating algorithm that reflect the real-world better.

5.4.2 OP-MAP Reconstruction in the mmWave band

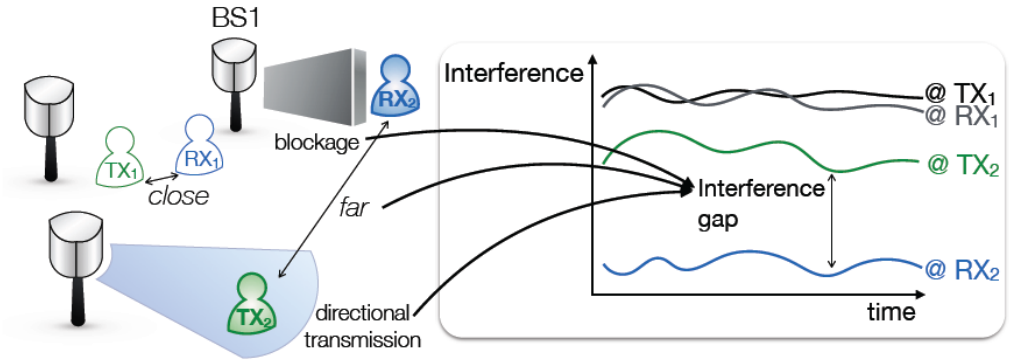

Figure 5-15: An illustration of opportunity detection problem caused by spatial difference, shadowing, and directional transmission effects.

Consider that there is a primary network composed of transmitters (TX) and receivers (RX) using licensed spectrum (e.g., a cellular network with base stations as a TX and mobile terminal as an RX when downlink communication is supposed). At the same time, it is assumed that there is a secondary network which desires to share the band when the channel is idle. Note that the opportunistic probability (OP) is closely related to the spatial interference correlation between secondary TX and secondary RX, attributable to (i) the distance between the TX and the RX; (ii) blockages; and (iii) directional signal transmissions (see Figure 5-15). We developed the spatial correlation in the form of a probability using stochastic geometry (SG), and use our result to obtain an accurate OP for both sub-6GHz and mmWave cases.

When building the opportunity map in the mmWave band, the first thing to do is to recalculate OP value which is computed by the legacy OP formula designed for the sub-6GHz spectrum. Unlike the sub-6GHz spectrum band, the mmWave band has several properties that must be considered in the calculation of OP, for example, blockage vulnerability or directional signal transmission. In order to cope with these features in calculating OP, two longstanding problems are considered, which are hidden/exposed node problems. From the definition of OP, the temporal interference correlation between the secondary transmitter and receiver decreases as the more hidden/exposed node problems are happened.

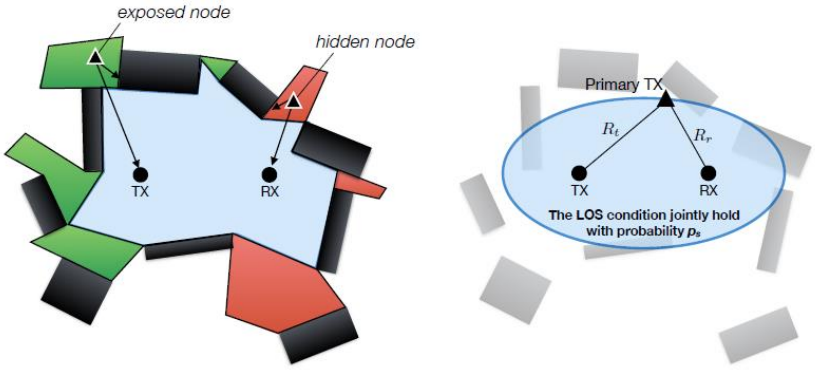

Figure 5-16: Illustration of hidden/exposed node problems (the left figure) and an approximated LoS ball (the ellipse in the right figure). The rectangles represent buildings that block signals from the

primary networks. Spatial interference correlation decreases along with the density of the number of the blockages.

The novel OP for above-6GHz (mmWave) includes the effects of the hidden/exposed problems with the aids of the LoS ball and the common interfering probability. First, the LoS ball is introduced to figure out the shadowing effect by approximating actual LoS regions to an ellipse ball as it is illustrated in Figure 5-16. Second, the common interfering probability is defined to reflect the effect of the directional signal transmission, which is necessary for mmWave scenarios. Besides the shadowing effects, the directional beam causes frequent hidden/exposed node problems because the primary network may not become a common interferer to both secondary transmitter and receiver. As depicted in Figure 5-17, the exposed node problem occurs when the primary transmitter interferes with the secondary transmitter, while the primary transmitter is not interferer to the secondary receiver. It is represented conditional probability with a beam width of the primary network. Its mathematical form and the detailed description is specified in [48].

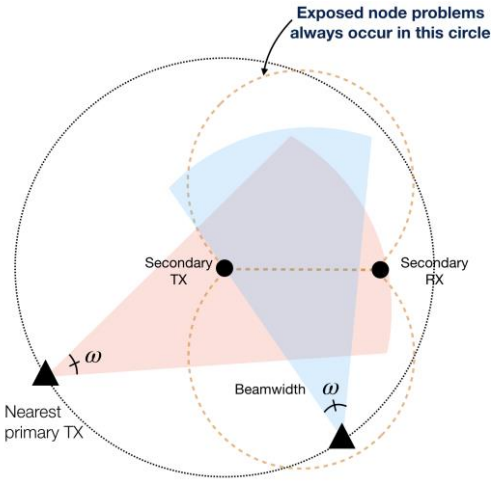

Figure 5-17: An occurrence of the exposed node problem. The red beam from the nearest primary TX interferes with both of the secondary TX and RX. On the other hand, The blue beam only interferes with the secondary TX. It causes the sub-6GHz OP calculation accuracy

In order to consider these two features, two new input parameters are introduced to yield OP in the mmWave band, which are the major axis length of the joint unblocked region and beam width of signals transmitted by the primary network.

6 Security management

6.1 Background on compressive sensing based authentication

In this section, we consider a unified approach for compression and authentication in 5G systems. Some wireless devices for 5G applications (e.g., smart grid) are urged to send sampled signals at a high rate for high quality services. Meanwhile, the signals have to be authenticated to prevent impersonation attacks. However, the security faces more challenges than conventional human-type communications because of limited hardware resources of a wireless device (e.g., small memory). Motivated by these problems, we study simultaneous compression and authentication for wireless signals in multicarrier systems, based on the notion of compressive sensing (CS). A CS based compression and authentication method uses a shared secret key, a measurement matrix in CS between legitimate parties. In particular, for authentication, the residual error of a received signal at the receiver is used as a test statistic for hypothesis testing, which determines whether the signal is a legitimate signal or an intrusion signal in the proposed approach. Through analysis and simulation results, we demonstrate that the CS based compression approach has good energy efficiency. In addition, it is shown that the proposed scheme can obtain a low authentication error probability under reasonable conditions.

CS has attracted considerable attention in electrical engineering, applied mathematics, statistics and computer science [49]. Recently, CS has been applied to the information security field in [50]-[65]. In particular, two aspects have been studied: the theoretical aspect and the application aspect [66]. In the theoretical aspect, CS based encryption, which uses a measurement matrix as a secret key, has been theoretically analyzed in [50]-[57]. In [50], CS based encryption was found to achieve computational secrecy, while it cannot provide perfect secrecy in terms of information security because of the linear property of measurements. To achieve perfect secrecy, some unfeasible assumptions used in [53] have to be made. In addition, CS based encryption is analyzed in terms of robustness and security in [51]. Particularly, as shown in [54], CS cannot guarantee the security of cryptographic standards, but may provide a useful built-in data obfuscation layer. In the application aspect, CS has been applied to various applications (e.g., image, biometric data) for security [57]-[65]. Particularly, image encryption methods using the notion of CS have been studied to enable simultaneous image compression and encryption in [57]-[60]. Furthermore, an image authentication scheme based on CS is considered in [65]. In [65], a CS based authentication mechanism that uses a tag signal for image authentication is presented, but the study does not provide any theoretical basis. In particular, a threshold for hypothesis testing and theoretical performance analysis is not given in [65].

In wireless communication systems, authentication techniques have been studied mostly in network and application layers [67]-[69]. However, these techniques may not be suitable for some wireless devices with limited resources such as low computational capability and limited bandwidth due to high complexity. To address this issue, physical layer authentication methods based on the dynamic physical characteristics (e.g., channel, analog front-end (AFE)) have been considered. Channel based physical layer authentication [70] uses the time-variant channel state information (CSI). In addition, the phases of multicarrier channels are used for secure physical-layer challenge-response authentication with a shared secret key in multicarrier systems [71]. In [72], channel coding is employed to mitigate the difference between the two estimated channels, which are used for physical-layer challenge-response authentication. The hardware imperfection of AFE which causes input and output (I/O) imbalance, phase offset error, carrier frequency offset error can be used for physical layer authentication [73]. However, if the characteristics of AFE and channel for an intrusion node are close to those of a legitimate transmitter, the authentication techniques may result in relatively poor authentication performance. In [74], a tag signal is concurrently transmitted for a stealth authentication with a message signal.

6.2 Proposed approach

We present a physical layer authentication scheme that enables simultaneous compression and authentication based on the notion of CS. In the CS based authentication, a measurement matrix is

used as a secret key. In general, linear feedback shift registers (LFSRs) which are typically used for a low-complexity implementation of a pseudo-random generator can be employed to generate the measurement matrix for security. In this case, an initial vector in the LFSRs becomes a secret key to generate the measurement matrix. We consider the following scenario for the physical layer authentication:

- The legitimate receiver performs an initial authentication by using conventional cryptography-based authentication.
- The legitimate receiver generates a measurement matrix as a secret key by using LFSRs.

By using a physical layer security scheme [75] based on CSI between the legitimate receiver and the legitimate transmitter, the legitimate receiver securely transmits an initial vector of LFSRs to generate measurement matrix.

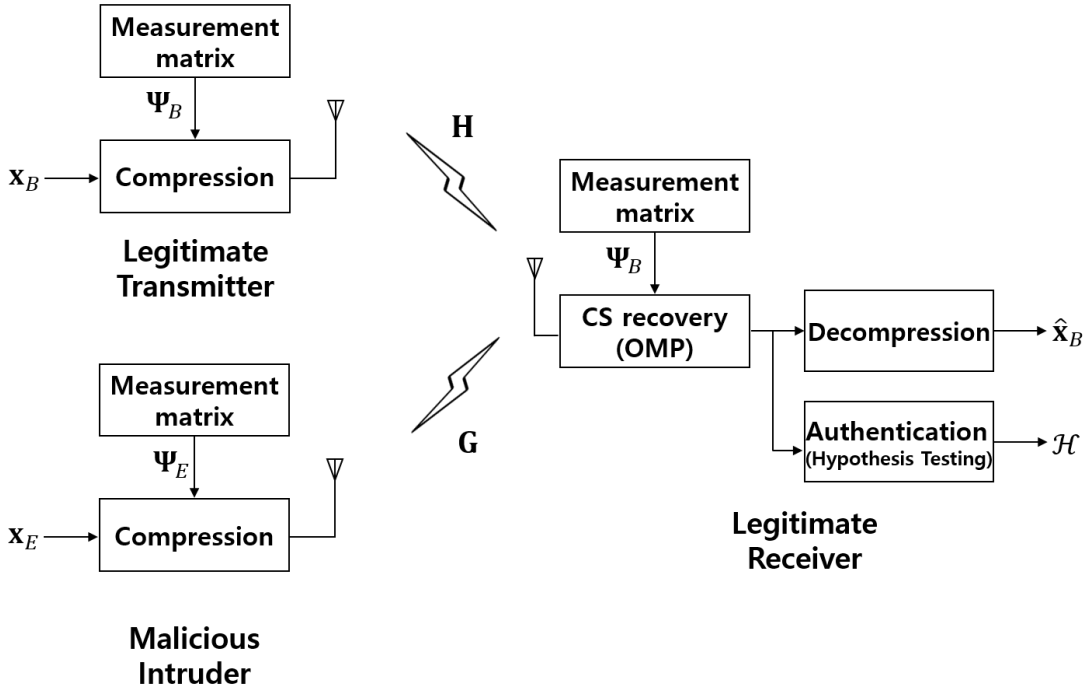

Figure 6-1: System model of a proposed approach

Based on the shared measurement matrix, the legitimate receiver determines whether or not a received signal is from the legitimate transmitter by using the CS based authentication.

As mentioned earlier, we consider a physical layer security scheme in [75] to share a measurement matrix between a legitimate receiver and a legitimate transmitter. As [75], subcarriers are interleaved according the sorted order of their channel gains in time division duplex (TDD) mode. Then, based on the channel reciprocity, the legitimate transmitter can derive the interleaving pattern initiated by the legitimate receiver, while the interleaving pattern is unknown to the intruder. Then, the legitimate receiver can securely send an initial vector which is used to generate the measurement matrix to the legitimate transmitter. Based on the scenario, the CS based authentication between the legitimate receiver and the legitimate transmitter is considered in the presence of the intruder.

We consider a multicarrier system for transmissions from a legitimate transmitter to a legitimate receiver with L subcarriers. Throughout this section, the legitimate transmitter sends a block of signals denoted by $\mathbf{x}_B$ over L subcarriers, where $\mathbf{x}_B$ contains a message of wireless device data. We also consider the

case that an intruder transmits a forged signal block, denoted by $\mathbf{x}_E$, over L subcarriers with the aim at impersonating the legitimate transmitter.

We assume that information signals can be transformed into sparse signals with a proper representation matrix (e.g., HWT). It means that information signals can be compressed using the notion of CS. Meanwhile, for the authentication, we can design an authentication matrix, $\mathbf{\Phi}_B$ which has to be shared between the legitimate transmitter and the legitimate receiver as a secret key for the authentication. As mentioned earlier, we consider that the legitimate receiver transmits an initial vector used to generate the measurement matrix to the legitimate transmitter based on a physical layer security scheme [75]. Then, the authentication matrix is unknown to the intruder, while the representation matrix, $\mathbf{\Psi}$, is known. Let $\mathbf{x}_B = \mathbf{\Phi}_B \mathbf{\Psi} \mathbf{s}_B$ and $\mathbf{x}_E = \mathbf{\Phi}_E \mathbf{\Psi} \mathbf{s}_E$, where $\mathbf{s}_B$ and $\mathbf{s}_E$ are the sparse signals at the legitimate transmitter and intruder, respectively, and $\mathbf{\Phi}_B$ and $\mathbf{\Phi}_E$ are the authentication matrices for the legitimate transmitter and the intruder, respectively. Then, the received signal at the legitimate receiver is given by

$$\mathbf{y} = \begin{cases} \mathbf{H}\mathbf{\Phi}_B \mathbf{\Psi} \mathbf{s}_B + \mathbf{n}, & \text{if the legitimate transmitter transmits} \\ \mathbf{G}\mathbf{\Phi}_E \mathbf{\Psi} \mathbf{s}_E + \mathbf{n}, & \text{if the intruder transmits} \end{cases}$$

Here, $\mathbf{\Phi}_B$ used as a secret key is known to the legitimate receiver, while $\mathbf{\Phi}_E$ is unknown to the legitimate receiver. Meanwhile, the legitimate receiver should know the channels to detect the transmitted signals. To this end, the wireless devices transmit pilot signals before the information signals. Throughout the section, we assume that the channels for the legitimate transmitter and intruder are perfectly estimated, respectively. For the legitimate transmitter, the intruder which performs impersonation attacks also transmits a pilot signal to estimation channels between the legitimate receiver and the intruder. Then, as shown in [75], the channel estimation errors which can be influenced by noises can sufficiently be reduced by using channel estimation techniques based on denoising strategies. So, the channels can be estimated with negligibly small error. For convenience, let $\mathbf{D}$ be the estimated channel at the legitimate receiver, i.e., $\mathbf{D} = \mathbf{H}$ or $\mathbf{G}$ if the legitimate transmitter or intruder transmits, respectively. Then, a legitimate receiver can detect an intrusion signal via hypothesis testing using residual errors as test statistics.

The measurement matrix which is unknown to the intruder can be estimated by the intruder's known plaintext attacks [76] due to the linear property of CS. Therefore, as [76], if an artificial noise is used, it makes the attacks difficult. To minimize the performance degradation at the legitimate receiver, the artificial noise is selectively transmitted in the frequency domain based on known CSI. It becomes difficult for the intruder to perform attack with a fraction of the received signals due to artificial noise [76]. Then, it ensures a guarantee of secrecy in terms of a probability of successful attack under certain conditions. For example, if SNR = 8dB, $L = 64$, a successful attack probability, denoted by P_{SA}, can be as low as $P_{SA} \approx 10^{-12}$. In this section, the method using artificial noise is not studied.

6.3 Exemplary performance evaluation

We evaluate performances by using numerical simulations (MATLAB). In simulations, the proposed scheme is applied to smart grids but could be extended to 5G security management in PriMO-5G use cases.

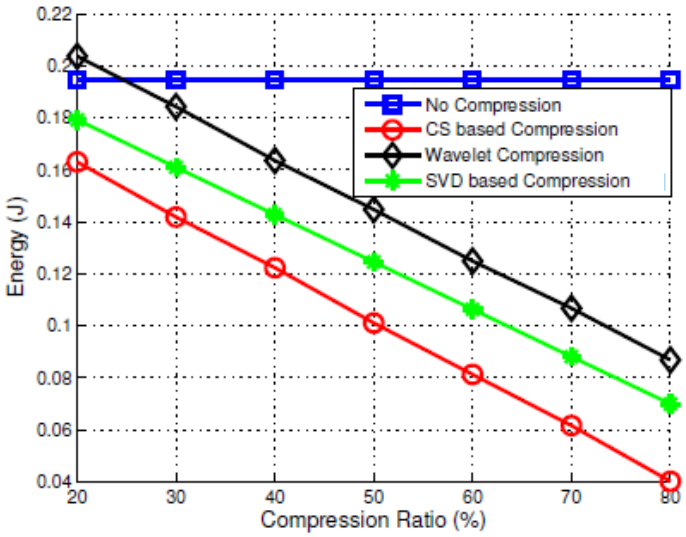

Figure 6-2: Energy consumption for compression and transmission over the compression ratio

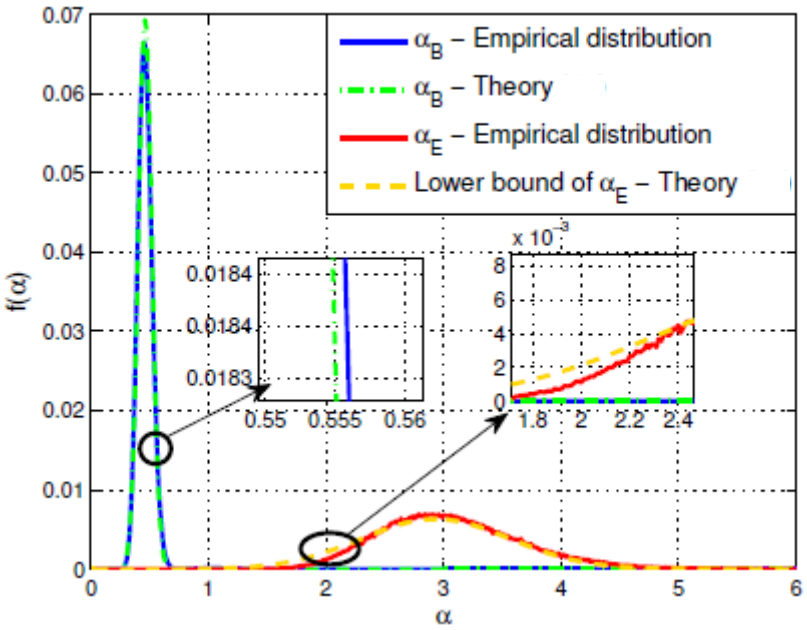

Figure 6-3: Comparison of the probability density functions between the legitimate transmitter and the intruder

For a low compression ratio (i.e., CR < 20%), the case of 'wavelet compression' has poorer energy efficiency than that of 'no compression' because of energy consumption for compression, while the case of 'CS based compression' has a high energy efficiency regardless of the compression ratio. In Figure 6-2, it is shown that the proposed CS based compression scheme is suitable for smart meters that have limited hardware resources (e.g., low computational capability) with large energy efficiency.

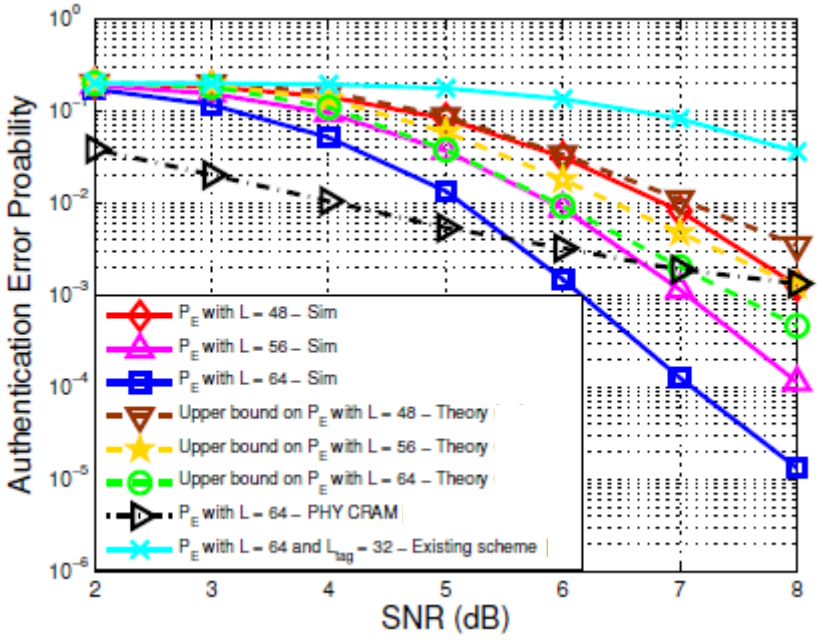

Figure 6-4: Total packet transmission latency as a function of packet size

From Figure 6-3, we can see that the distribution of a legitimate transmitter's residual errors is different with that of an intruder. This means that the difference between authentication matrices of the legitimate receiver and intruder induces a sufficiently large residual error in the proposed scheme. Then, we can find that if we set a proper threshold for the hypothesis testing in the proposed scheme, the signal from the intruder can be detected with a high probability.

In Figure 6-4, the authentication error probabilities are shown, in which a low authentication error probability can be obtained for a high SNR and a large L. In summary, although a target detection probability is high, the proposed scheme can guarantee good authentication performance (e.g., $P_E \leq 10^{-4}$) with a moderate SNR (e.g., 8dB) and L (e.g., 64).

As a final remark, we emphasize that the proposed approach using the notion of CS which enables simultaneous compression and authentication can reduce the burden of computational complexity for low-cost wireless devices in 5G systems. Furthermore, from the simulation results, we showed that the power reading signal can be authenticated under reasonable conditions.

7 Conclusions

The main objective of this deliverable is to provide an intermediate status report about the work that has been conducted as part of work package mmWave radio technologies. In section 2 we started with a recap of the main PriMO-5G use case about smart firefighting which is described in deliverable D1.1 in more detail. Here we focused specifically on the required mmWave link and the UAVs which are part of the firefighting scenario. This is followed by an analysis about the 5G NR standardization with respect to mmWave frequencies as well as the beam management. Furthermore, in this section we also provided a first overview about the intended mmWave link architecture which shall be used for the PriMO-5G demonstration. In section 2.1 we described the initial work for seamless connectivity starting with an analysis about reducing the access delay for mmWave based wireless networks when beamforming is used. Afterwards a novel beam-based positioning algorithm is presented that can be used for UAV positioning. This is followed by an investigation of hand-over management in cell-free architectures in ultra-dense networks. In section 4 the mobility management is discussed which is important for the drone support. First, an investigation about the support of drone connection using conventional cellular networks is provided followed by an approach for a grant free resource management which significantly reduces the latency. Furthermore, techniques for mobility caching are discussed for device-to-device communication as well as mmWave networks. In section 5 interference management with focus on UAVs is discussed. This includes a detailed analysis of interference that is caused by an UAV to the ground users. This interference can also be used for a drone detection which is described subsequently. Moreover, in this section an interference management scheme for full duplex networks is shown that could be used to increase the system throughput. In this context also the application of the full duplex technology to mmWave transmission is investigated with a comparison to sub-6 GHz networks. Finally, in section 6 a new physical layer authentication approach based on compressed sensing is presented that can be applied to 5G networks.

Reference

[1] 3GPP TS 38.300, NR and NG-RAN Overall Description, V15.4.0

[2] ITU Resolution 238, https://www.itu.int/dms_pub/itu-r/oth/0c/0a/R0C0A00000C0014PDFE.pdf

[3] 3GPP TS 38.104, Base Station (BS) radio transmission and reception, V15.5.0.

[4] 3GPP TR 38.913, Study on Scenarios and Requirements for Next Generation Access Technologies, V15.0.0

[5] 3GPP TS 38.211, Physical channels and modulation, V15.5.0

[6] 3GPP TS 38.306, User Equipment (UE) radio access capabilities, V15.4.0

[7] 3GPP TS 38.213, Physical layer procedures for control, V15.5.0

[8] 3GPP TS 38.912, Study on New Radio (NR) access technology, V15.0.0

[9] 3GPP TS 38.214, Physical layer procedures for data, V15.5.0

[10] Erik Dahlman Stefan Parkvall Johan Skold, “5G NR: The Next Generation Wireless Access Technology“, 2018

[11] Shehzad Ali Ashraf, Torsten Dudda, 5G for latency-critical IoT applications, https://www.ericsson.com/en/blog/2017/7/5g-for-latency-critical-iot-applications

[12] Younsun Kim, “NR Physical Layer Design: NR MIMO”, https://www.3gpp.org/ftp/workshop/2018-10-24_25_WS_on_3GPP_subm_tw_IMT2020/Docs/RWS-180008.zipbnb

[13] NI Software Defined Radio Website, http://www.ni.com/en-us/innovations/wireless/software-defined-radio.html

[14] Introduction to the NI mmWave Transceiver System Hardware, http://www.ni.com/product-documentation/53095/en/bnbn

[15] 5G NR Development and Releases, OAI Website, https://gitlab.eurecom.fr/oai/openairinterface5g/wikis/5g-nr-development-and-releases

[16] Selecting a USRP Device Ettus Websize, https://kb.ettus.com/Selecting_a_USRP_Device

[17] OpenAirInterface 4G Feature Set, OAI Website, https://gitlab.eurecom.fr/oai/openairinterface5g/blob/master/doc/FEATURE_SET.md

[18] “SCF calls for industry to adopt open RAN interfaces to prevent 5G fragmentation, SCF Website: https://www.smallcellforum.org/press-releases/scf-calls-for-industry-to-adopt-open-ran-interfaces-to-prevent-5g-fragmentation/

[19] 3GPP TS 23.501, System Architecture for the 5G System, V16.0.2

[20] H. Q. Ngo, A. Ashikhmin, H. Yang, E. G. Larsson and T. L. Marzetta, "Cell-Free Massive MIMO: Uniformly great service for everyone," 2015 IEEE 16th International Workshop on Signal Processing Advances in Wireless Communications (SPAWC), Stockholm, 2015, pp. 201-205. doi: 10.1109/SPAWC.2015.7227028.

[21] X. Gelabert, C. Qvarfordt, M. Costa, P. Kela and K. Leppänen, "Uplink reference signals enabling user-transparent mobility in ultra dense networks," 2016 IEEE 27th Annual International Symposium on Personal, Indoor, and Mobile Radio Communications (PIMRC), Valencia, 2016, pp. 1-6. doi: 10.1109/PIMRC.2016.7794816.

[22] B. Hu, Y. Wang, C. Wang and L. Wang, "A user-centric clustering method for mobility management in ultra-dense networks," 2017 ninth International Conference on Wireless Communications and Signal Processing (WCSP), Nanjing, 2017, pp. 1-5. doi: 10.1109/WCSP.2017.8170946.ghgh

[23] Y. Yang, H. S. Ghadikolaei, C. Fischione, M. Petrova, and K. W. Sung, "Reducing Initial Cell-search Latency in mmWave Networks," in Proc. IEEE INFOCOM Workshop mmSys, Honolulu, Hawaii, USA, April 16 2018.

[24] Y. Yang, H. S. Ghadikolaei, C. Fischione, M. Petrova, and K. W. Sung, "Fast and Reliable Initial Access with Random Beamforming for mmWave Networks," arXiv, https://arxiv.org/abs/1812.00819 2018.

[25] H. S. Ghadikolaei, Y. Yang, M. Petrova, K. W. Sung, and C. Fischione, "Fast and Reliable Initial Cell-search for mmWave Networks," in Proc. ACM Mobicom Workshop mmNets 2018, New Delhi, India, October 29 2018.

[26] M. Giordani, M. Mezzavilla and M. Zorzi, "Initial Access in 5G mmWave Cellular Networks," IEEE Communications Magazine, vol. 54, no. 11, pp. 40-47, November 2016.

[27] S. Sun, et al, “Propagation path-loss models for 5G Urban Micro- and Macro-Cellular Scenarios”, VTC 2016

[28] Shahmansoori, Arash et al. “Position and Orientation Estimation Through Millimeter-Wave MIMO in 5G Systems.” *IEEE Transactions on Wireless Communications* 17 (2018): 1822-1835

[29] Menta. E, Malm. N, Jäntti. R, Ruttik. K, Costa. M and Leppänen. K, 2019, 'On the Performance of AoA based Localization in 5G Ultra Dense Networks' *IEEE Access*, vol. 7, 8662565, pp. 33870-33880. https://doi.org/10.1109/ACCESS.2019.2903633

[30] X. Lin, R. Wiren, S. Euler, A. Sadam, H. Maattanen, S. Muruganathan, S. Gao, Y. Wang, J. Kauppi, Z. Zou, and V. Yajnanarayana, “Mobile Networks Connected Drones: Field Trials, Simulations, and Design Insights”, arXiv:1801.10508, Jan. 2018.

[31] 3GPP TS 36.331, “Radio resource control (RRC); Protocol specification (Release 15)”, V15.2.2, June 2018.

[32] 3GPP TR 36.839, “Mobility enhancements in heterogeneous networks (Release 11)”, V11.1.0, December 2012

[33] GSMA, “Mobile-enabled unmanned aircraft,” white paper, February 2018. Available at https://www.gsma.com/iot/wp-content/uploads/2018/ 02/Mobile-Enabled-Unmanned-Aircraft-web.pdf

[34] S. Euler, H. Maattanen, X. Lin, Z. Zou, M. Bergström, and J. Sedin, “Mobility Support for Cellular Connected Unmanned Aerial Vehicles: Performance and Analysis”, in Proc. of IEEE Wireless Communications and Networking Conference (WCNC), Marrakech, Morocco, April 2019.

[35] M. M. Kassem et al., “Future Wireless Spectrum below 6 GHz: A UK Perspective,” Proc. IEEE DySPAN, Sept. 2015, pp. 59–70

[36] 3GPP TSG RAN WG1 Meeting 87, November 2016

[37] Popovski, “Ultra-reliable communication in 5G wireless systems,” in 1st Int. Conf. on 5G for Ubiquitous Connectivity (5GU). IEEE, 2014, pp. 146–151.

[38] X. Foukas, G. Patounas, A. Elmokashfi, and M. K. Marina, “Network slicing in 5g: Survey and challenges,” IEEE Communications Magazine, vol. 55, no. 5, pp. 94–100, 2017.

[39] 3GPP TS 36.300 V11.2.0, “Evolved Universal Terrestrial Radio Access (E-UTRA) and Evolved Universal Terrestrial Radio Access Network (EUTRAN), Overall Description,” June 2012.

[40] D. Fooladivanda and C. Rosenberg, “Joint resource allocation and user association for heterogeneous wireless cellular networks,” IEEE Trans. Commun., vol. 12, no. 1, pp. 248–257, Jan. 2013.

[41] Minho Kim, Seung-Woo Ko, Hyesung Kim, Seunghwan Kim, and Seong-Lyun Kim. "Exploiting Caching for Millimeter-Wave TCP Networks: Gain Analysis and Practical Design." *IEEE Access, vol.6,* 2018, pp. 69769-69781

[42] V. Yajnanarayana, Y. Wang, S. Gao, S. Muruganathan, and X. Lin, “Interference Mitigation Methods for Unmanned Aerial Vehicles Served by Cellular Networks”, arXiv:1802.00223, Feb. 2018.

[43] 3GPP TR36.777, “Study on enhanced LTE support for aerial vehicles,” Mar 2017.

[44] 3GPP, “Enhanced LTE support for aerial vehicles”, Technical report (TR) 36.777, 3rd Generation Partnership Project (3GPP), 03 2018. Version 15.0.0.

[45] H. Ryden, S. Bin Redhwan, and X. Lin, “Rogue Drone Detection: A Machine Learning Approach”, in Proc. of IEEE Wireless Communications and Networking Conference (WCNC), Marrakech, Morocco, April 2019.

[46] S. Marsland, Machine Learning: An Algorithmic Perspective. Chapman & Hall/CRC, 1st ed., 2009.

[47] J. Kim, S.-M. Kim, H. Cha, J. Choi, S.-W. Ko, C.-B. Chae, and S.-L. Kim, 'Opportunism in Dynamic Spectrum Access for 5G: A Concept and Its Application to Duplexing,' submitted to IEEE Wireless Communications

[48] Seunghwan Kim, Han Cha, Jeemin Kim, Seung-Woo Ko, and Seong-Lyun Kim: Sense-and-Predict: Harnessing Spatial Interference Correlation for Cognitive Radio Networks. CoRR abs/1802.01088 (2019)

[49] Y. C. Eldar and G. Kutyniok, Compressed Sensing: Theory and Applications. Cambridge University Press, 2012.

[50] Y. Rachlin and D. Baron, “The secrecy of compressed sensing measurements,” in Communication, Control, and Computing, 2008 46th Annual Allerton Conference on, pp. 813–817, IEEE, 2008.

[51] A. Orsdemir, H. O. Altun, G. Sharma, and M. F. Bocko, “On the security and robustness of encryption via compressed sensing,” in Military Communications Conference, 2008. MILCOM 2008. IEEE, pp. 1–7, IEEE, 2008.

[52] S. A. Hossein, A. Tabatabaei, and N. Zivic, “Security analysis of the joint encryption and compressed sensing,” in Telecommunications Forum (TELFOR), 2012 20th, pp. 799–802, IEEE, 2012.

[53] M. R. Mayiami, B. Seyfe, and H. G. Bafghi, “Perfect secrecy via compressed sensing,” in 2013 Iran Workshop on Communication and Information Theory, pp. 1–5, IEEE, 2013.

[54] T. Bianchi, V. Bioglio, and E. Magli, “Analysis of one-time random projections for privacy preserving compressed sensing,” IEEE Transactions on Information Forensics and Security, vol. 11, no. 2, pp. 313–327, 2016.

[55] R. Dautov and G. R. Tsouri, “Establishing secure measurement matrix for compressed sensing using wireless physical layer security,” in Computing, Networking and Communications (ICNC), 2013 International Conference on, pp. 354–358, IEEE, 2013.

[56] V. Cambareri, M. Mangia, F. Pareschi, R. Rovatti, and G. Setti, “On known-plaintext attacks to a compressed sensing-based encryption: A quantitative analysis,” IEEE Transactions on Information Forensics and Security, vol. 10, no. 10, pp. 2182–2195, 2015.

[57] P. Lu, Z. Xu, X. Lu, and X. Liu, “Digital image information encryption based on compressive sensing and double random-phase encoding technique,” Optik-International Journal for Light and Electron Optics, vol. 124, no. 16, pp. 2514–2518, 2013.

[58] J. Lang and J. Zhang, “Optical image cryptosystem using chaotic phase-amplitude masks encoding and least-data-driven decryption by compressive sensing,” Optics Communications, vol. 338, pp. 45–53, 2015.

[59] N. Zhou, S. Pan, S. Cheng, and Z. Zhou, “Image compression–encryption scheme based on hyper-chaotic system and 2D compressive sensing,” Optics & Laser Technology, vol. 82, pp. 121–133, 2016.

[60] Y. Zhang, J. Zhou, F. Chen, L. Y. Zhang, D. Xiao, B. Chen, and X. Liao, “A block compressive sensing based scalable encryption framework for protecting significant image regions,” International Journal of Bifurcation and Chaos, vol. 26, no. 11, 2016, Art. no. 1650191.

[61] S.-Y. Chiu, H. H. Nguyen, R. Tan, D. K. Yau, and D. Jung, “JICE: Joint data compression and encryption for wireless energy auditing networks,” in 2015 12th Annual IEEE International Conference on Sensing, Communication, and Networking (SECON), pp. 453–461, 2015.

[62] L.-b. Zhang, Z.-l. Zhu, B.-q. Yang, W.-y. Liu, H.-f. Zhu, and M.-y. Zou, “Medical image encryption and compression scheme using compressive sensing and pixel swapping based permutation approach,” Mathematical Problems in Engineering, vol. 2015, 2015.

[63] C. Wang, B. Zhang, K. Ren, J. M. Roveda, C. W. Chen, and Z. Xu, “A privacy-aware cloud-assisted healthcare monitoring system via compressive sensing,” in INFOCOM, 2014 Proceedings IEEE, pp. 2130–2138, IEEE, 2014.

[64] I. Orovic and S. Stankovic, “Combined compressive sampling and image watermarking,” in ELMAR, 2013 55th International Symposium, pp. 41– 44, IEEE, 2013.

[65] T. Wu and C. Ruland, “An improved authenticated compressive sensing imaging,” in Semantic Computing (ICSC), 2018 IEEE 12th International Conference on, pp. 164–171, IEEE, 2018.

[66] Y. Zhang, L. Y. Zhang, J. Zhou, L. Liu, F. Chen, and X. He, “A review of compressive sensing in information security field,” IEEE Access, vol. 4, pp. 2507–2519, 2016.

[67] M. M. Fouda, Z. M. Fadlullah, N. Kato, R. Lu, and X. S. Shen, “A lightweight message authentication scheme for smart grid communications,” IEEE Transactions on Smart Grid, vol. 2, no. 4, pp. 675–685, 2011.

[68] H. Nicanfar, P. Jokar, and V. C. Leung, “Smart grid authentication and key management for unicast and multicast communications,” in 2011 IEEE PES Innovative Smart Grid Technologies, pp. 1–8, IEEE, Nov 2011.

[69] H. Li, R. Lu, L. Zhou, B. Yang, and X. Shen, “An efficient Merkle-tree based authentication scheme for smart grid,” IEEE Systems Journal, vol. 8, no. 2, pp. 655–663, 2014.

[70] L. Xiao, L. J. Greenstein, N. B. Mandayam, and W. Trappe, “Using the physical layer for wireless authentication in time-variant channels,” IEEE Transactions on Wireless Communications, vol. 7, no. 7, pp. 2571–2579, 2008.

[71] X. Wu and Z. Yang, “Physical-layer authentication for multi-carrier transmission,” IEEE Communications Letters, vol. 19, no. 1, pp. 74– 77, 2015.

[72] J. Choi, “A coding approach with key-channel randomization for physical-layer authentication,” IEEE Transactions on Information Forensics and Security, vol. 14, no. 1, pp. 175–185, 2019.

[73] W. Hou, X. Wang, J.-Y. Chouinard, and A. Refaey, “Physical layer authentication for mobile systems with time-varying carrier frequency offsets,” IEEE Transactions on Communications, vol. 62, no. 5, pp. 1658–1667, 2014.

[74] L. Y. Paul, J. S. Baras, and B. M. Sadler, “Physical-layer authentication,” IEEE Transactions on Information Forensics and Security, vol. 3, no. 1, pp. 38–51, 2008.

[75] H. Li, X. Wang, and J.-Y. Chouinard, “Eavesdropping-resilient OFDM system using sorted subcarrier interleaving,” IEEE Transactions on Wireless Communications, vol. 14, no. 2, pp. 1155–1165, 2015.

[76] J. Choi, “Secure transmissions via compressive sensing in multicarrier systems,” IEEE Signal Processing Letters, vol. 23, no. 10, pp. 1315–1319, 2016.